Hydroxylamine-Containing Ligands:

Synthesis and Reactions with Copper Ions


Nooshin Sheibany


A Thesis

in

The Department

of

Chemistry and Biochemistry


Presented in Partial Fulfillment of the Requirements

For the Degree of Master of Science (Chemistry) at

Concordia University

Montreal, Quebec, Canada


April 2017

CONCORDIA UNIVERSITY
School of Graduate Studies

This is to certify that the thesis prepared

By:      Nooshin Sheibany

Entitled:  Hydroxylamine-Containing Ligands: Synthesis and Reactions with Copper Ions

and submitted in partial fulfillment of the requirements for the degree of

Master of Science in Chemistry

complies with the regulations of the University and meets the accepted standards with respect to originality and quality.

Signed by the final examining committee:

Dr. Judith Kornblatt                          Chair

Dr. Pat Forgione                              Examiner

Dr. John Oh                                   Examiner

_____             Examiner

Dr. Xavier Ottenwaelder                       Supervisor

Approved by:     _____
                 Chair of Department or Graduate Program Director

                 _____
                 Dean of Faculty

Date:     April 7th, 2017

# ABSTRACT

## Hydroxylamine-Containing Ligands: Synthesis and Reactions with Copper Ions

Nooshin Sheibany

Organic hydroxylamine (*C*-NHOH) and nitroso (*C*-NO) species are reactive compounds that find application in organic synthesis, for example in C–N or C–O bond formation. These groups are redox active, interconverting via reduction or oxidation amidst the series of organic nitrogen substituents: $NH_2$, NHOH, NO, and $NO_2$. In order to expand the synthetic potential of hydroxylamine and nitroso species, an understanding their reactivity in the presence of a metal-based catalyst is required. In this thesis, we are studying how copper ions influence the reactivity of a NHOH group tethered to a coordinating ligand. This tethering strategy allows for controlled reaction and a precise characterization of the reaction products.

Chapter 1 introduces the redox chemistry of nitrogen groups, current organic applications of nitroso compounds, as well as current methods to convert a nitro group into a hydroxylamine moiety.

Chapter 2 covers design and synthesis of different ligands with a pendant $NO_2$ group to provide a NHOH moiety by partial hydrogenation. The optimization of reduction reactions using zinc and ammonium formate helped us to obtain several NHOH-containing ligands in high yields.

Chapter 3 studies the interaction of the ligands with copper(II) ions. Spectroscopic titrations provided insight into the stoichiometry of complexation. In particular, reaction of a NHOH-containing ligand with copper(II) acetate yielded a neutral complex with a *C*-NO moiety that is N-bonded to Cu. The complex was analyzed by crystallography, NMR, magnetic measurements, electrochemistry and DFT calculations. The electronic structure is consistent with a strongly antiferromagnetically coupled Cu(II)-(nitrosyl anion) formulation. Therefore, copper(II) has transformed a NHOH group into a $1e^-$-reduced NO moiety, *C*-$(NO^-)$, adding to redox versatility of the organic NO linkage.

# ACKNOWLEDGEMENTS

# TABLE OF CONTENT

# LIST OF FIGURES

# LIST OF TABLES

# LIST OF ABBREVIATIONS

$^1$H-NMR: Proton Nuclear Magnetic Resonance

ACN: Acetonitrile

BDE: Bond Dissociation Energy

BDNBS: 3,5-dibromo-4-nitrosobenzene sulfonic acid

DCM: Dichloromethane

DFT: Density Functional Theory

DMSO: Dimethylsulfoxide

EDTA: Ethylenediaminetetraacetic acid

EPR: Electron Spin Resonance

ESI-MS: Electrospray Ionization Mass Spectrometry

Et$_3$N: Triethylamine

gCOSY: Gradient-Selected Correlation Spectroscopy

HDVV: Heisenberg-Dirac-Van Vleck

HOMO: Highest Occupied Molecular Orbital

LUMO: Lowest Unoccupied Molecular Orbital

MHz: Megahertz

MNP: 2-methyl-2-nitrosopropane

PhNHOH: Phenylhydroxylamine

PhNO: Nitrosobenzene

RNO: Organic nitroso compound (R−N=O)

SQUID: Superconducting Quantum Interference Device

TBP: Trigonal bi-pyramidal

*t*Bu: *tert*-Butyl

THF: Tetrahydrofuran

TLC: Thin-Layer Chromatography

TMAC: Tetramethylammonium chloride

TMPD: *N,N,N',N'*-tetramethylpropylenediamine

TMS: Tetramethylsilane

TPP: Tetraphenylporphyrin

UV-Vis: Ultraviolet-Visible spectroscopy

VT-NMR: Variable-Temperature Nuclear Magnetic Resonance

XoRG: Xavier Ottenwaelder Research Group

# Chapter 1.  Organic nitrogen groups and their redox chemistry

**1.1 Redox Versatility of Inorganic Nitrogen Compounds**

Nitrogen belongs to Group 15 of the periodic table, also known as pnictogens, and exists as a colorless and odourless diatomic ($N_2$) gas under normal pressure and temperature. Being intrinsically inert, $N_2$ is a useful blanketing gas to create an inexpensive inert environment where moisture and oxygen need to be avoided in laboratory and industry settings.[1,2,3] Liquid nitrogen with a boiling point of -196ºC (77 K) is extensively used as refrigerant both in the laboratory (e.g. superconducting magnets or X-ray detectors[4]) and in the industry (e.g. quick freezing food, food transportation, freeze grinding or cryosurgery).[1,2,3]

As part of compounds, the nitrogen atom can have different oxidation states ranging from -3 to +5 (Figure 1.1).[1] Nitride ($N^{3-}$) is a highly charged ionic species formed by reaction of lithium (Li) with $N_2$ or group-2 elements with liquid ammonia.[1,2] They are good ligands for d-block metals as they are both potent σ- and π- donors. The azide anion ($N_3^-$) possesses nitrogen atoms in +1 (central) and –1 (peripheral) formal oxidation states. Sodium and heavy metal salts of azides are detonated upon shock creating dinitrogen gas and are therefore used as a propellant in car air bags or detonators.[1,2] Lower oxidation states of nitrogen occur in hydrides (e.g. ammonia ($NH_3$) and hydrazine ($N_2H_4$)) and hydroxylamine ($NH_2OH$) having –3, –2 and –1 oxidation states respectively. Higher oxidation states +1 to +5 are achieved in oxides or oxoanions (Figure 1.1).[1]

Possible Oxidation States of Nitrogen

| -3 | -2 | -1 | 0 | +1 | +2 | +3 | +4 | +5 |
|----|----|----|----|----|----|----|----|----|
| $NH_3$ | $N_2H_4$ | $NHOH$ | $N_2$ | $N_2O$ | $NO$ | $HNO_2$ | $NO_2$ | $N_2O_5$ |
| $NH_4^+$ | | | | | | $NO_2^-$ | $N_2O_4$ | $HNO_3$ |
| $NH_2^-$ | | | | | | | | $NO_3^-$ |

Figure 1.1. Various oxidation states of nitrogen in ions and molecules.

Many of these compounds have prolific application in different sections of the industry. For example, nitric acid ($HNO_3$) with N(+5) is used in the production of ammonium nitrate by

1

neutralization with ammonia in the synthesis of fertilizers and explosives.[1,5] Nitric acid is also used for the production of phosphate fertilizers such as ammonium hydrogen phosphates, $NH_4H_2PO_4$ and $(NH_4)_2HPO_4$.[1,5] Nitrate ($NO_3^-$) is an oxidizing agent and also is consumed in the production of fertilizers.[1,2] Nitrogen dioxide ($NO_2$) a brown gas, with N(+4) is an intermediate in the synthesis of nitric acid.[1] Nitrous acid ($HNO_2$) with N(+3) is a powerful oxidizing agent and can be utilized in the preparation of diazonium salts widely applied in the dye industry for the production of azo dyes.[1,5] Nitric oxide (NO) with N(+2) is an odd-electron paramagnetic gas, with many biological roles as neurotransmitter, cell signaling agent and vasodilation agent.[1] In inflammatory or infectious diseases, NO is produced by macrophages, a type of white blood cell, showing cytotoxic activity towards bacteria, parasites, tumour cells, fungi, etc.[6] Nitrous oxide ($N_2O$) with N(+1) is well known as "laughing gas", was used as a general anesthetic and is currently used as analgesic as 1:1 mixture with dioxygen for medical needs including labour pain relief or pre-hospital care, and dental care.[1,7]

## 1.2 ACTIVATION OF DINITROGEN

### 1.2.1 Electronic structure of $N_2$

The nitrogen atom is one of the major constituents of the biosphere and biological molecules as in amino acids, purine and pyrimidine building blocks of nucleic acids, proteins and enzymes.[1] Although $N_2$ is a readily available reservoir of nitrogen, incorporating it into nitrogen-containing compounds requires cleavage of the strong N-N triple bond (Bond Dissociation Energy, BDE, of 945 kJ mol$^{-1}$).[1,8] Therefore, reactions using $N_2$ as nitrogen source and its reactions are quite slow in ambient conditions and often require harsh conditions.[1] Carbon monoxide (CO) isoelectronic to $N_2$ molecule, even with a higher BDE (945 kJ mol$^{-1}$), takes part in many reactions under milder conditions.[8] CO is a classic ligand in organometallic chemistry, having lone pair on C atom serving as a σ-donor to the metal and energy-accessible π* orbitals that confer CO with strong π-accepting properties. Electron delocalization from the metal to a π*(CO) weakens the CO bond and thus it can undergo reactions easier than free CO.[1] Therefore, a strong BDE is not the only reason why $N_2$ is an inert molecule. The orbital energy diagram of the $N_2$ provides a justification for this inertness (Figure 1.2).[8] There is a large gap between the Highest Occupied Molecular Orbital (HOMO) and the Lowest Unoccupied Molecular Orbital (LUMO) in dinitrogen. The low energy of HOMO (–15.6 eV) makes $N_2$ a poor σ-donor and high

energy LUMO (−7.3 eV) makes $N_2$ a poor π-acceptor.[8,9] This large gap also rationalizes the difficulty in oxidizing and reducing dinitrogen.[9] Other factors also can be attributed to the inertness of $N_2$, including a lack of dipole moment, a high ionization energy (1402 kJ mol$^{-1}$, 15.58 eV), and a small electron affinity (−7 kJ mol$^{-1}$, −1.8 eV).[8,10]
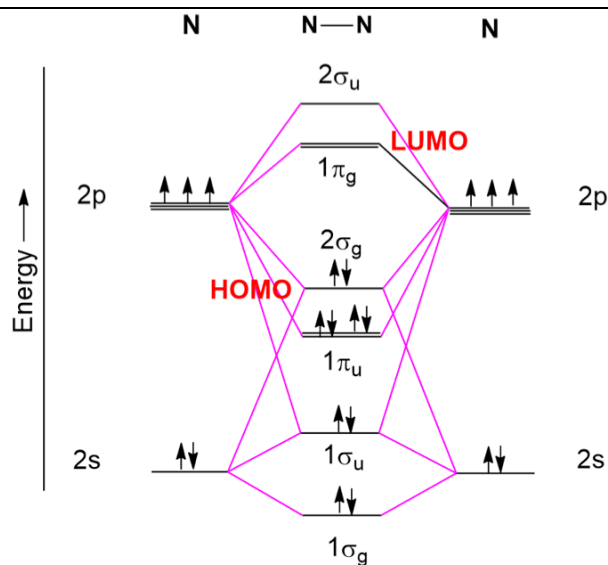
Figure 1.2. Orbital energy level diagram for $N_2$ (adapted and modified from reference 1).

## 1.2.2   Activation of Dinitrogen in Biosphere: Nitrogen Fixation

In the biosphere, nitrogen fixation is a part of the biochemical "Nitrogen Cycle", where inorganic nitrogen is interconverted to its different oxidation forms in reactions that are exclusively enzyme-catalyzed (Figure 1.3).[1] In nitrogen fixation, unreactive $N_2$ is converted to the accessible reduced form of nitrogen, ammonia, which can subsequently be used in important biosynthetic pathways to form organic molecules such as amino acids, protein and nucleotides.[1] This process is carried out only by microorganisms, prokaryotes, and a very effective nitrogen fixation emerges from symbiosis interaction of soil bacteria (rhizobia) residing in root nodules of higher plants, legumes.[1,11]
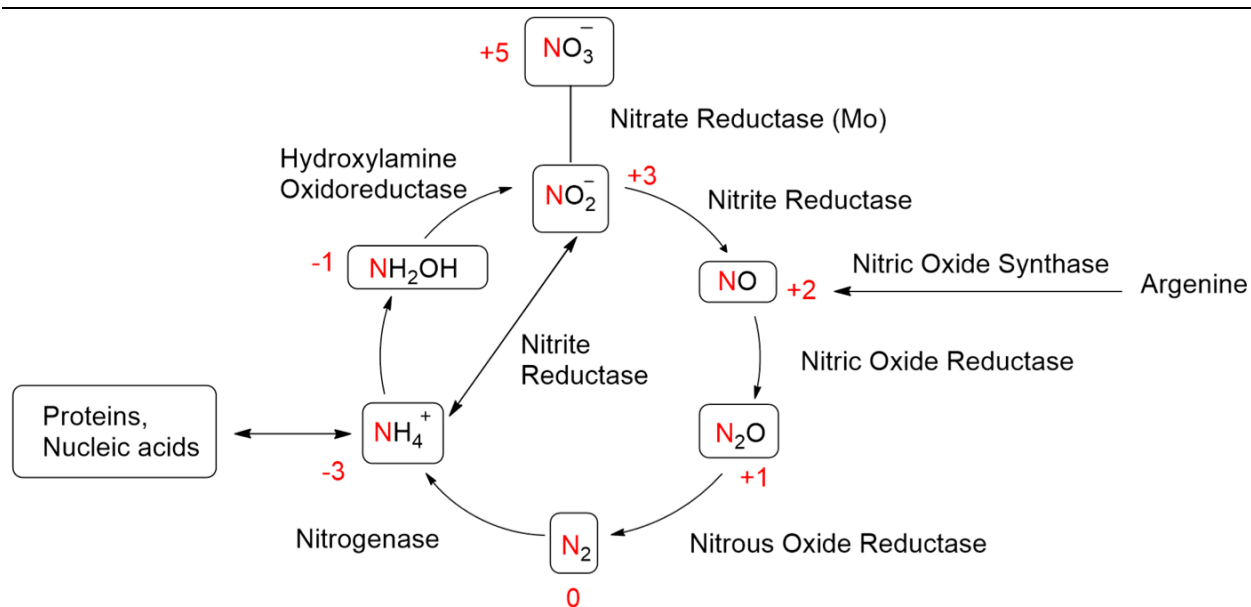
Figure 1.3. Biological nitrogen cycle (adapted and modified from reference 1).

Nitrogenase, a metalloenzyme that catalyzes the formation of ammonia, affords activation of $N_2$ by the contribution of metals in its active site known to be iron (Fe), molybdenum (Mo) and a non-metal element sulfur (S).[1] In nitrogenase, FeMo-cofactor, [7Fe-Mo-9S-Homocitrate-X], is proposed to be the site of binding, activation and reduction of dinitrogen (Figure 1.4).[12]
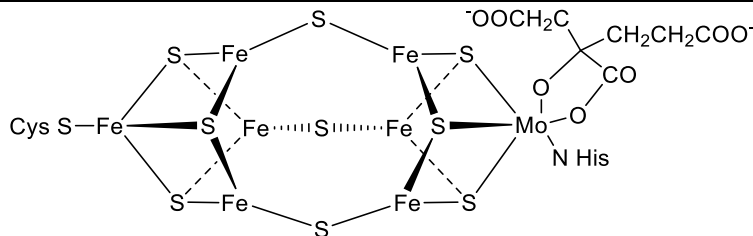


Figure 1.4. Scheme of FeMo-cofactor of the nitrogenase (adapted from reference 13).

For end-on coordinated dinitrogen metal complexes, both σ-donation and π-backdonation contribute to the bonding (Figure 1.5).[13] As the electron populates $\pi^*(N_2)$ orbitals, The N-N bond order decreases. Discovery of the exact binding site of $N_2$ is still unknown.[1] Computational analysis suggested the possibility of different substrate binding sites at Mo, one or two Fe atoms located on the waist part and the combination of Fe, S, and Mo.[12] Fe atoms coordinate atom X at one corner which electron density map is effective to accept N, C or O yet to be proved.[1,12]

4

Figure 1.5. End-on metal coordinated $N_2$ complexes, showing σ-donation from $N_2$ to the metal ion and backbonding from the metal ion into $\pi^*(N_2)$ orbitals (adapted from reference 13).

Proposed nitrogen fixation mechanisms begin by considering similar process (nitrogen fixation) carried out by inorganic mononuclear Mo-complexes and then implement it in the FeMo-protein's Mo centre in the mechanism called "Distal" (**D**). In this mechanism, the distal nitrogen is repetitively reduced and protonated, while each intermediate is still connected to the metal centre. After transferring $3e^-$ and $3H^+$ to this single nitrogen, the N-N bond is cleaved and ammonia is released. The remaining nitrido complex is consecutively reduced and protonated by additional $3e^-$ and $3H^+$ and the second ammonia molecule is produced. The second, "Alternating" (**A**), mechanism is proposed where the binding site is changed from Mo to Fe. Each two N atoms are alternatively reduced, protonated and cleavage of N-N bond happens only after the addition of the fifth electron followed by a protonation of the hydrazine-metal intermediate with releasing first ammonia (Figure 1.6).[12,14]
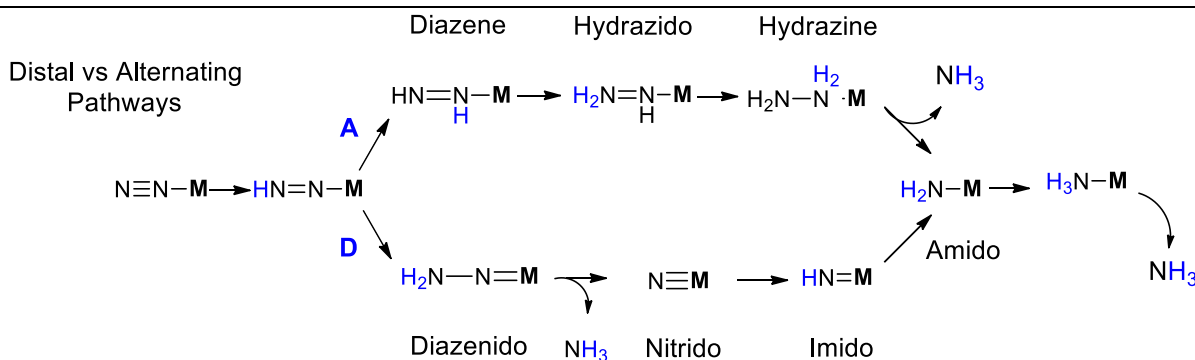


Figure 1.6. Proposed pathways for $N_2$ reduction by nitrogenase (adapted and modified from references 12 and 14).

### 1.2.3  Activation of Dinitrogen in Industry: Haber-Bosch Process

By contrast with these biological conditions, activation of dinitrogen in the industry still struggles with the intrinsic inertness of $N_2$. The industrial Haber-Bosch process produces ammonia in a million-ton scale annually with major application in synthesizing fertilizers and numerous organonitrogen commercial compounds.[1,8,9] This process requires the direct treatment

of one equivalent of nitrogen gas with three equivalents of hydrogen gas over promoted Fe (iron) or Ru-(ruthenium)/C heterogeneous catalysts.[8,13] Although the formation of ammonia is thermodynamically favourable in ambient conditions ($\Delta H° = -46.2$ kJ mol$^{-1}$ for the formation of one mole NH$_3$),[13] the high activation energy required to cleave dinitrogen requires high temperature (400-550 °C) and high pressure (100-300 atm).[8] While the catalyst accelerates the reaction, the need for high temperature is, however, detrimental to the reaction conversion due to a strongly negative entropy of reaction ($\Delta S° = -99.3$ J K$^{-1}$ mol$^{-1}$). Therefore, a high pressure is required to push the equilibrium in favour of ammonia. Obviously, these conditions are much harsher than those under which nitrogenase operates, highlighting the difficulty of performing this transformation outside of a well-tailored protein environment.

## 1.3 REDOX POTENTIALS AND REACTIVITY OF ORGANIC NITROGEN-CONTAINING FUNCTIONAL GROUPS

As nature uses enzymes containing transition metals to manipulate the oxidation state of nitrogen atoms, we are interested in studying how a transition metal affects the redox properties of nitrogen-containing functional groups on organic substrates. Nitrogen moieties are versatile in their redox properties and can interconvert by formal electron donation (reduction) or removal (oxidation). Consecutive two-electron reductions of nitro (R−NO$_2$) moieties results in the formation of nitroso (R−N=O or RNO), hydroxylamine (R−NH−OH) and finally amine (R−NH$_2$) groups. Reversibly, R-NH$_2$ can successively be oxidized to its equivalent R−NO$_2$ group (Figure 1.7). *C*-Nitroso structures, i.e. when the nitroso function is attached to a carbon, are highly reactive and undergo various reactions, making them potential tools for organic synthesis.[15,16,17] The production of unwanted side-products due to high reactivity, however, currently restricts their synthetic potential.[16] These compounds can also react with starting materials and reagents or they may isomerize.[15] Isomerization occurs for primary or secondary nitrosoalkanes to R$_2$C=N−OH (oxime), therefore influencing the choice of solvent in the preparation of nitroso compounds.[15,18] In equilibrium with its monomeric form in liquid or solid state, *C*-nitroso compounds can create two distinct *Z*-azodioxy (cis)- or *E*-azodioxy (trans) dimers.[19] While aliphatic *C*-nitroso compounds have a high predisposition to form dimers, the dimerization of aromatic nitroso compounds depends on the concentration, substitution on the ring and temperature.[17] At a concentration of about 0.1 M and at low temperature, dimers are mostly present.[17] Dimerization is favoured in *ortho*-substituted nitrosoarenes, yet steric effect may

6

exclusively control dimerization. Very bulky substituents at the 2 or 2,6 *ortho* positions can repress dimerization.[19] During the reduction process, high reactivity results in condensation reaction between aromatic nitro group and aromatic hydroxylamine creating $RN=N^+(O^-)R$ (azoxy) compounds.[20]
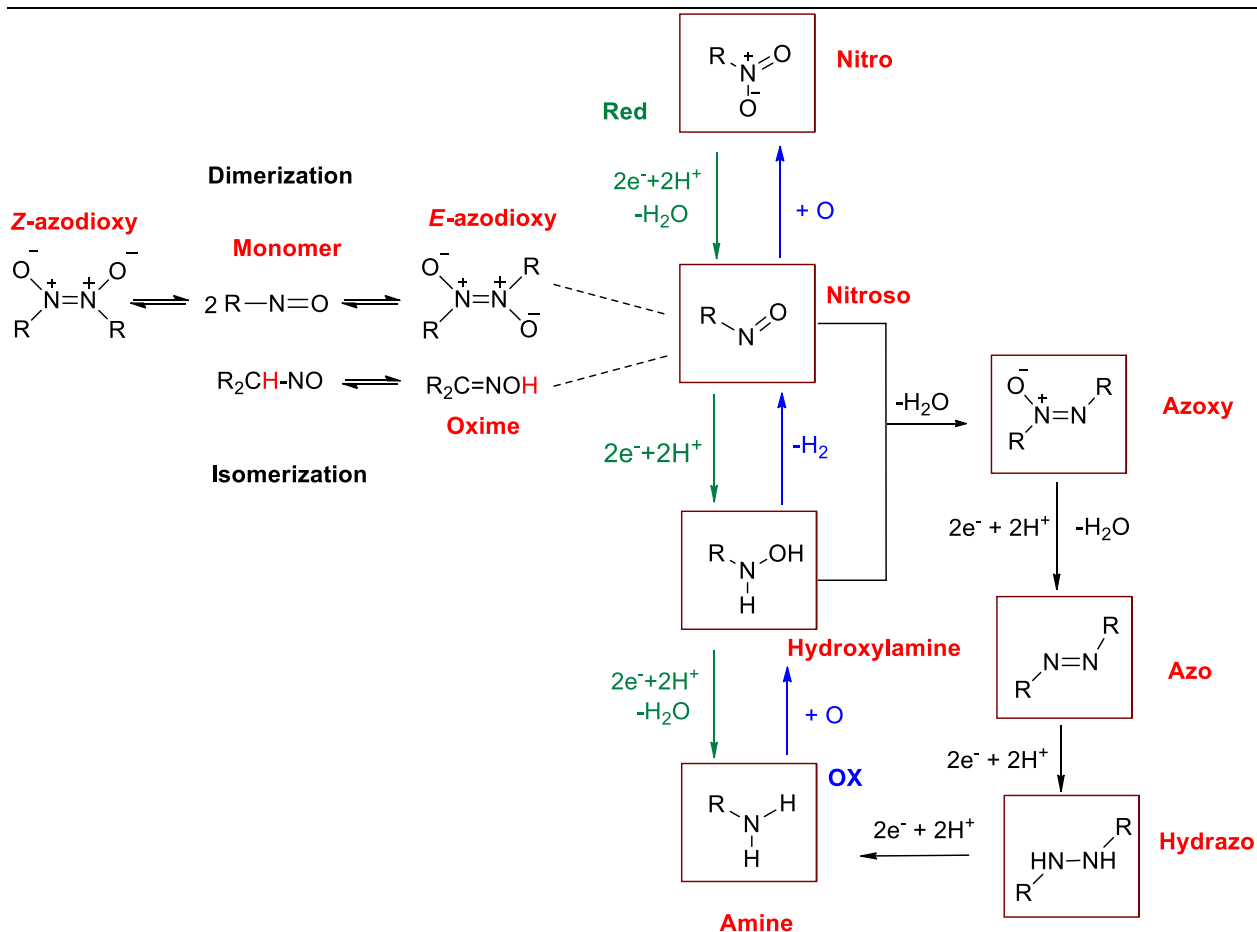


Figure 1.7. Redox, dimerization and tautomerisn profiles of organic nitrogen-containg functional groups.

## 1.4 APPLICATIONS OF *C*-NITROSO COMPOUNDS IN ORGANIC SYNTHESIS

The nitroso group having polarized N=O bond and low LUMO energy reacts as a potent electrophile that can undergo many addition reactions with nucleophiles.[16,17] Some of their organic synthetic applications is summarized in Figure 1.8.
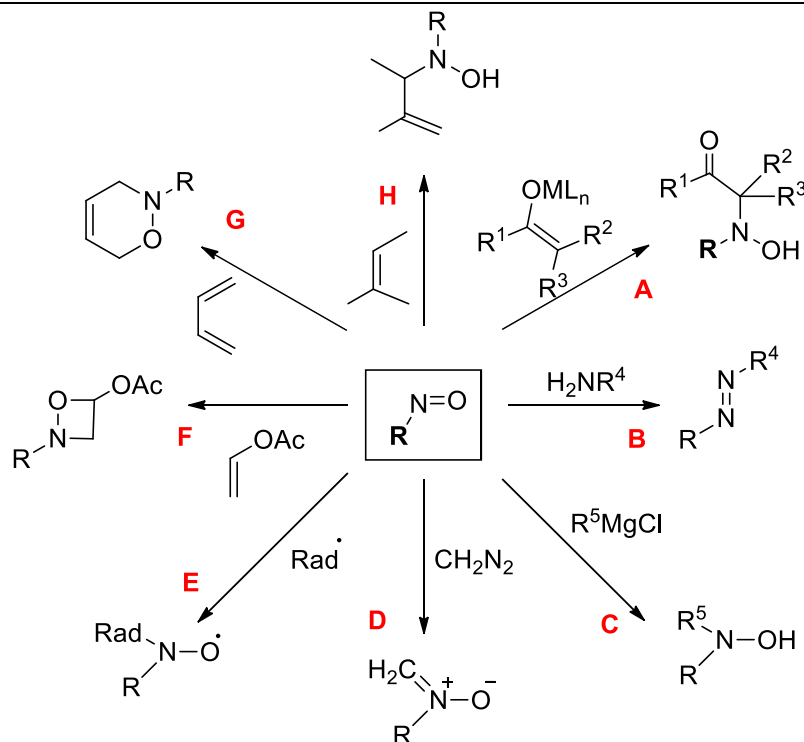
Figure 1.8. Application of nitroso compounds in organic synthesis (adapted from reference 16).

Nitroso groups react with enolates in the nitroso aldol reaction (Figure 1.8 **A**), producing α-hydroxyamino carbonyl compounds.[16] Yamamoto et al. reported a general, high-yielding method for the reaction of aromatic nitroso compounds with tin and alkali metal enolates, resulting in the formation of α-hydroxyamine carbonyl compounds. Reaction of different tin enolates with nitrosobenzene showed high yield and significant regioselectivity of 99 to 1 for the N-adduct vs. the O-adduct. Although lithium enolate produced a hydroxyl amino ketone, silyl enol ester in the presence of lewis acid catalyst afforded α-aminooxy ketone (Figure 1.9).[21] Azo groups, secondary hydroxylamines, and nitrone are created in the reaction of nitroso with amines,[17] Grignard reagents and diazomethane, respectively (Figure 1.8 **B,C,D**).[16] Some nitroso compounds are used as spin traps in Electron Spin Resonance (EPR) spectroscopy, facilitating the detection of mostly carbon-centred radical species.[22] They will trap the desired radical sample by forming detectable and stable nitroxide radicals adducts (Figure 1.8 **E**). 2-methyl-2-nitrosopropane (MNP) and 3,5-dibromo-4-nitrosobenzene sulfonic acid (BDNBS) are examples of nitroso spin traps.[22] Nitroso compounds participate in [2+2] and [4+2] hetero Diels-Alder cycloadditions as enophiles and dienophiles respectively (Figure 1.8 **F,G**).[16] Nitroso-ene

reactions are economical ways for nitrogen functionalization of allylic substrates, forming N-allyl hydroxylamines, using readily accessible alkene compounds (Figure 1.8 **H**).[16]
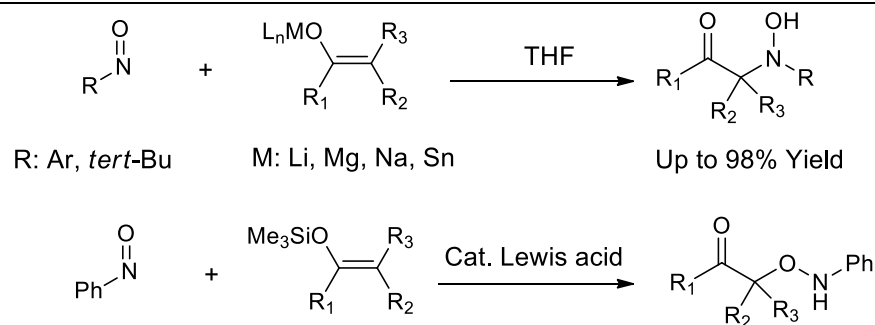


Figure 1.9. Nitroso-aldol reaction of aliphatic/aromatic nitroso compounds with alkali or tin enolates (Top); Lewis acid catalyzed nitroso aldol reaction afforded α-aminooxy ketones (bottom).[21]

## 1.5  BINDING MODES OF *C*-NITROSO COMPOUND WITH A METAL CENTRE

Several of these aforementioned reactions are catalyzed by a metal-containing species. In particular, the interaction of active species such as RNO or RNHOH with a transition metal species enables the synthesis of many organic adducts (see below). The classic hydrogenation of $RNO_2$ to $RNH_2$ is also performed with a transition-metal catalyst (e.g. Pd or Ni). In this section, we introduce known binding modes of *C*-nitroso species with metals and examples of these interactions in organic reactions and reduction processes of nitro groups to hydroxylamine/amine groups.

### 1.5.1   Metal complexes with *C*-nitroso species

RNO species can bind to a metal centre through nine main binding modes, all of which have been verified by single-crystal X-ray crystallography. These modes are categorized into sole *N*-binding ($\kappa$-*N*), sole *O*-binding ($\kappa$-*O*) and *N,O*-binding ($\eta^2$-*N,O*) modes (Figure 1.10). Different R groups, nature and number of existing metal centres have a major impact on the pattern of the binding mode in R-NO species.[23] **Sole *N*-binding** is the most abundant binding fashion characterized for RNO-metal coordinated species and nitrogen may bind in mono- or bi-nuclear manner (Figure 1.10 **A** and **B**). In monometallic non-porphyrin compounds, the N-O bond length is in the range of 1.209-1.296 Å. For instance, in *t*BuNO complexes of W, Fe, and Pt the bond length are 1.24-1.234 Å and 1.21-1.22 Å, respectively. This small increase in the bond length compared to the monomeric aliphatic N=O bond length (1.1-1.22 Å) is attributed to

backdonation of metal d-electrons to $\pi^*$(NO) orbitals.[23] Greater affinity of hemoglobin for nitrosobenzene than for $O_2$ was an incentive for the preparation of heme-model complexes.[24] The binding mode of a RNO species to a metalloporphyrin has a major influence on the chemical reactivity of this group. *N*-binding is the most common mode in metalloporphyrin models.[23]

**N-Binding**
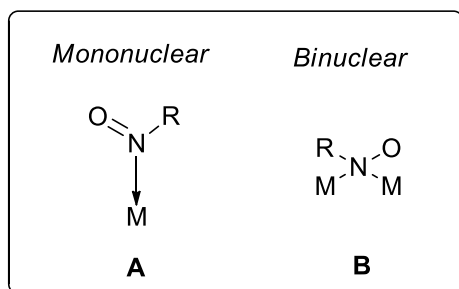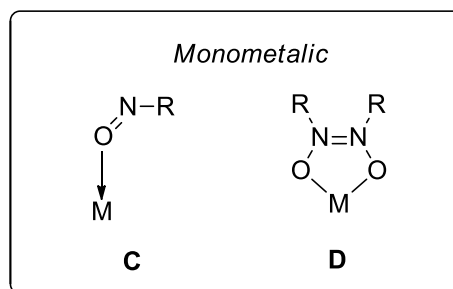
**O-Binding**
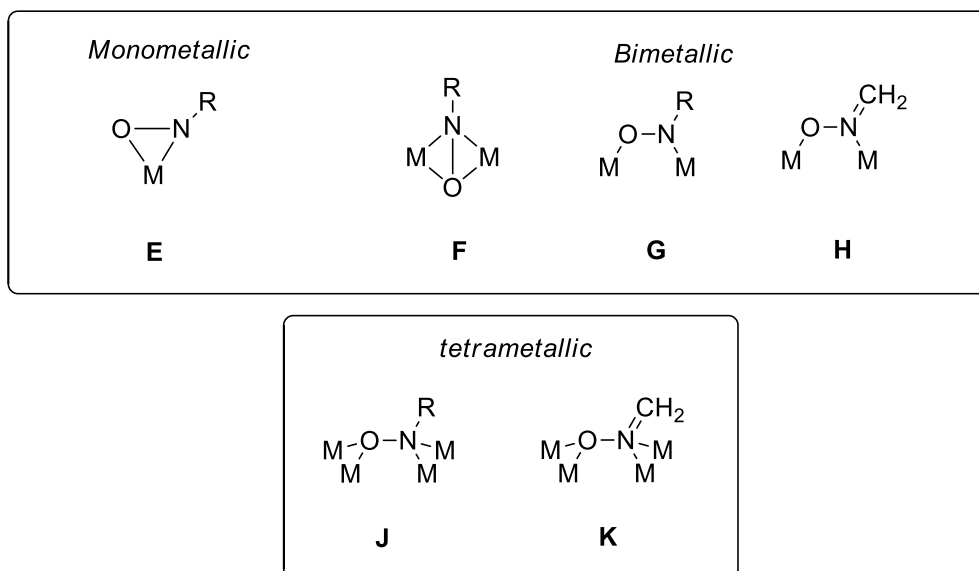


Figure 1.10. Crystallographically verified metal-RNO binding modes (adapted from reference 23).

Metalloporphyrins complexes of Co, Zn, Fe, Mn, Os, and Ru bearing RNO ligands are reported.[23] The X-ray structure of (TPP)Fe(PhNO)$_2$ (TPP= tetraphenylporphyrin) reveals $\kappa$-*N* binding to Fe[II] on the two faces of the porphyrin.[25] However, Fe[III] and Mn[III] porphyrins show *O*-binding, suggesting that a higher oxidation state would favour binding to the harder O atom (Figure 1.11).[23] (PMe$_3$)$_3$Pt$_2$(PhNO)$_3$ is the only characterized bimetallic RNO/metal complex (Figure 1.10 **B**). It shows an elongated N-O bond, with more of a single bond character.[23]
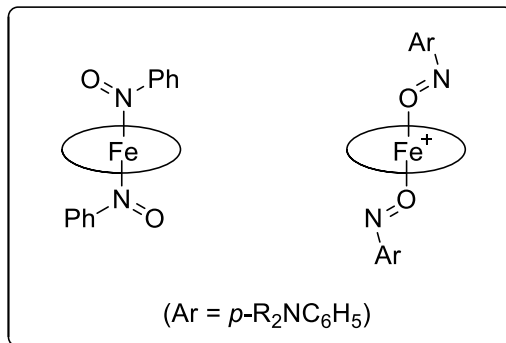
Figure 1.11. $\kappa^1 N$ binding in $Fe^{II}$ porphyrin complexes (left); $\kappa$-$O$ binding in $Fe^{III}$ porphyrin complexes (right).[25]

**Sole _O_-binding** is much less abundant than _N_-binding. In $Fe^{III}$-porphyrin complexes of [(TPP)Fe(ONC₆H₄NEt₂)₂], dipolar resonance contribution of _p_-substituted nitrosoarene plays an important role in stabilizing the $\kappa$-$O$ binding mode (Figure 1.12).[25] With softer $Fe^{II}$, $\kappa$-$N$ binding is observed, while $\kappa$-$O$ binding is observed with harder $Fe^{III}$.[25] Therefore, the metal oxidation state is one of the factors affecting RNO binding in Fe-porphyrins complexes.[23] $\kappa$-$O$ mode is also characterized for $Mn^{III}$-complex in [(TPP)Mn(ONC₆H₄NEt₂)₂].[25] Prior to characterization of these two complexes, this less common _O_-binding mode, was characterized only for main group 10 (monomeric complexes of Zn and Sn) and for polymeric complexes of Pb.[23] There is only one example of _O_-binding mode **D** characterized, for the {Fe[Ph(O)NN(O)Ph]₃}[FeCl₄] complex. These triazodioxide complexes having RNO dimers as ligands are active species in allylic-amination of alkenes (section 1.6.1, iron catalyst).[23]
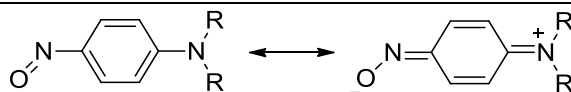


Figure 1.12. Dipolar resonance contribution of _p_-amino-substituted nitrosoarenes for $\kappa$-$O$ binding.[25]

**_N,O_-binding** occurs when both nitrogen and oxygen of RNO are bonded to the metal centre ($\eta^2$-NO) which leads to an increase in the N-O bond distance and a decrease in bond order. Side-on metallooxaziridine structure **E**, displays N-O bond lengths of 1.386-1.432 Å. Molybdooxaziridine complex generates required free PhNO in the allylic amination reaction of alkenes (section 1.6.1, manganese catalyst) An increase in bond length is observed for structures **F** (1.422-1.500 Å) and **G** and **H** (1.30-1.498 Å). Only one example for Fe-tetrametallic complex of type **J** is known.[23]

## 1.5.2  Interaction of redox-active metal complexes with RNO and RNHOH

Nitrosobenzene, PhNO, and phenylhydroxylamine, PhNHOH, are the *N*-substituted structure of their parents, nitroxyl (HNO) and hydroxylamine (NH$_2$OH).[24,26] HNO is a very reactive species that can readily undergo irreversible dimerization (rate: $8 \times 10^6$ M$^{-1}$s$^{-1}$) to hyponitrous acid (H$_2$N$_2$O$_2$) followed by dehydration to nitrous acid and water.[26,27] In biological systems, PhNO and PhNHOH can be endogenously synthesized by reduction of nitro aromatics or oxidation of aromatic amines.[26] Being more stable analogues, PhNO and PhNHOH are used as models to understand the reactivity of their more reactive parents when interacting with metal centres.[26,28]

Herein are introduced a few examples of studied models on the effect of using transition metals in ArN=O bond activation. The coordination environment around the metal centre influences the nature of the NO binding mode and metal-NO interaction. The symmetrical coordination of two *β*-diketiminato fragments, [Me$_2$NN]Ni, to the ArN=O moiety, forms monovalent Ni complex **A** (Table 1.1). The greater N-O bond length (1.440(4) Å) compared to the free monomeric nitrosoarene with N-O distance of 1.13-1.29 Å indicates N-O bond order reduction and activation.[24] Compared with monometallic complexes, the bimetallic complexes display a higher degree of NO bond activation. The copper(I) complex **B**, has shorter N-O bond distance (1.333(4) Å) than the formally characterized mononuclear $\eta^2$-NO "metalloxaziridine" mode of binding with N-O distance of 1.386(3)-1.432(6) Å.[23,24] Reactivity studies on complex **A** and **B** upon interaction with anaerobic NO gas shows the formation of diazeniumdiolate species, [Me$_2$NN]**M**($\eta^2$-O$_2$N$_2$Ar-$\kappa^2$*O,O'*), via NO incorporation into the already coordinated ArNO ligand, indicating the ability of the complexes to perform *oxidative* nitrosylation.[24] The formation of these "NONOate" ligands from ArNO precursors suggests similar reactivity patterns for their less stable parent HNO or even NH$_2$OH.

Table 1.1. Activation of arylnitroso compounds with Cu(I) and Ni(I) complexes.

| Complex | N-O Binding Mode | N-O bond length (Å) | Complex Reactivity Studies |
|---|---|---|---|
| **A**  Ar = 2,6-Me$_2$C$_6$H$_3$ Ar'= 3,5-Me$_2$C$_6$H$_3$ | $\mu$-$\eta^2$:$\eta^2$-N,O | 1.440(4) | **A** $\xrightarrow{\text{2 NO}}$ [Me$_2$NN]Ni($\eta^2$-O$_2$N$_2$Ar-$\kappa^2$O,O') + [Me$_2$NN]Ni(NO) |
| **B**  Ar = 2,6-Me$_2$C$_6$H$_3$ Ar'= 3,5-Me$_2$C$_6$H$_3$ | $\eta^2$-N,O | 1.333(4) | **B** $\xrightarrow{\text{NO}}$  |
| **C**  Ar = 2,6-Me$_2$C$_6$H$_3$ | $\eta^2$-N,O | 1.330(4) | [Cu](NCMe) + PhNHOH $\longrightarrow$ [Cu](ONPh) + PhNH$_2$ + H$_2$  [Cu](ONPh) + NO $\longrightarrow$ [Cu]  |
| **D**  | $\kappa$-N | 1.250(6) 1.236(7) | **C** [Cu] = [Me$_2$NN$_{F6}$]Cu **D** [Cu] = $^{iPr2}$TpCu |
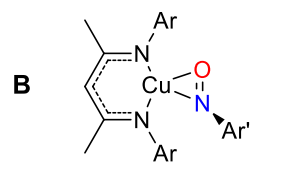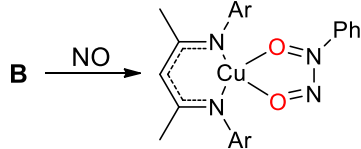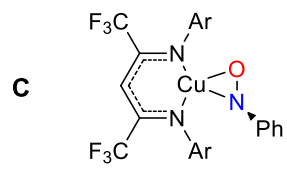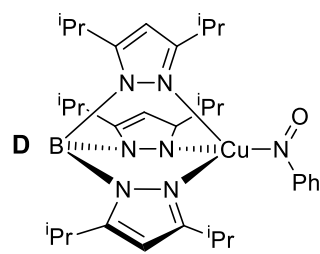
Reaction of the Cu(I) complex of a more electron-deficient $\beta$-diketiminate ligand, [[Me$_2$NN$_{F6}$]Cu(NCMe)], with PhNO forms complex **C** (Table 1.1) having a N-O bond length of 1.330(4) Å. The lower $\nu_{NO}$ stretching frequency (1122 cm$^{-1}$) compared with $\nu_{NO}$ (1506 cm$^{-1}$)[23] in free nitrosobenzene foreshadows backbonding from Cu to $\pi$*(NO) orbitals.[26] A sterically

hindered Cu(I) complex, [iPr$_2$TpCu(CNMe)], makes $\eta^2$-$N,O$ binding mode rather challenging and treatment with PhNO gives complex **D** with $\kappa$-$N$ binding mode ($\nu_{NO}$ = 1358 cm$^{-1}$).[26] Two independently characterized structures of this complex show N-O bond length of 1.250(6) Å and 1.236(7) Å, proving bond activation in comparison with the monomeric nitrosobenzene (N-O distance of 1.22 Å in aqueous solutions). The DFT calculations and lower $\nu_{NO}$ reflect a stronger backdonation in $\eta^2$-$N,O$-bonded complex **C** compared with $\kappa$-$N$-bonded complex **D** for which backdonation is not sterically available.[26] The treatment of complexes **C** and **D** with NO forms Cu(II) square-planar diazeniumdiolate Cu($\eta^2$-O$_2$N$_2$Ph-$\kappa^2O,O'$) complexes, suggesting similar reactivity patterns of HNO and NH$_2$OH on a copper centre in the presence of NO.[26]

Complexation of the Ni(I) complex of the more electron-deficient $\beta$-diketiminate ligand with PhNO leads to the formation of square planar Ni(II) complex, [iPr$_2$NN$_{F6}$]Ni($\eta^2$-ONPh), and reduction of PhNO ligand to PhNO$^{\bullet/-}$, i.e. an nitrosyl (or aminoxyl) anion (Figure 1.13). Two independently characterized X-ray structures show elongated N-O bond lengths of 1.3270(19) Å and 1.323(2) Å, close to the 1.333(4) Å NO bond length in complex **B** but longer than 1.440(4) Å in complex **A** (Figure 1.10).[24,28]
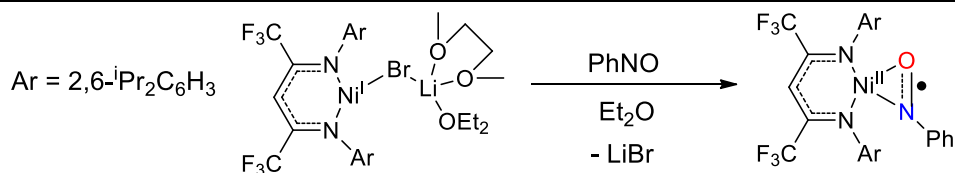


Figure 1.13. Formation of [$^{iPr2}$NN$_{F6}$]Ni($\eta^2$-ONPh) complex (adopted from reference[28]).

One-electron reduction of the complex occurs on the PhNO$^{\bullet/-}$ moiety and creates PhNO$^{2-}$ square-planar Ni(II) complex, [$^i$Pr$_2$NN$_{F6}$]Ni$^{II}$($\mu$-$\eta^2$:$\eta^2$-ONPh)K[18C6]. This process is substantiated by longer N-O bond length 1.382(3) Å compared to 1.3270(19) Å and 1.323(2) Å of PhNO$^{\bullet/-}$ complex (Figure 1.14).[28]
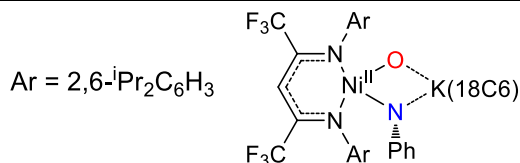


Figure 1.14. One-electron reduction of [iPr$_2$NN$_{F6}$]Ni($\eta^2$-ONPh) leads to [$^i$Pr$_2$NN$_{F6}$]Ni$^{II}$($\mu$-$\eta^2$:$\eta^2$-ONPh)K[18C6].[28]

Upon reaction of $[Ni(II)](\eta^2\text{-PhNO}^{\bullet/-})$ with NO gas, a near-planar Ni(II) diazeniumdiolate complex with $\kappa^2\text{-}O,O'$ coordination is formed through the radical coupling between free NO and N-centred spin of $\eta^2\text{-PhNO}^{\bullet/-}$. The diazeniumdiolate species can also form by reaction between $[Ni(II)](\eta^2\text{-PhNO}^{2-})$ with $[NO^+]BF_4^-$ as NO source (Figure 1.15).[28]
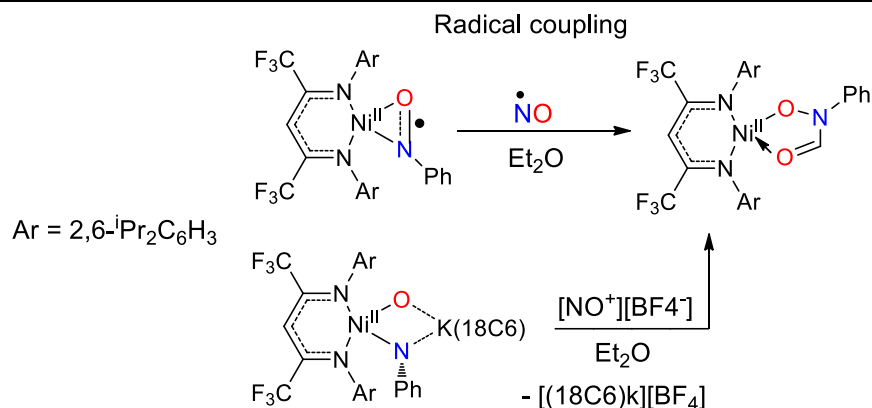


Figure 1.15. Reaction of Ni(II) complexes $[Ni(II)](\eta^2\text{-PhNO}^{\bullet/-})$ and $[Ni(II)](\eta^2\text{-PhNO}^{2-})$ with NO sources.[28]

Extreme cases of bond order reduction (four-electron reduction of ArNO) is reported in the case of $\{[Me_2NN]Co^{III}\}_2(\mu\text{-}O)(\mu\text{-}NAr)\}$ (Ar = 3,5-Me$_2$C$_6$H$_3$) complex with complete cleavage of PhNO bond by a Co(I) precursor (Figure 1.16).[28]
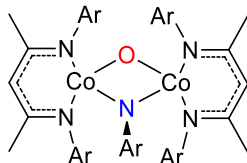


Figure 1.16. Four-electron reduction of PhNO in $\{[Me_2NN]Co\}_2(\mu\text{-}O)(\mu\text{-}NAr)\}$ (Ar = 3,5-Me$_2$C$_6$H$_3$) complex.[28]

## 1.6 METAL-CATALYZED NITROSO-ENE REACTIONS

Metal-nitrosoarene complexes not only serve as models for understanding the reactivity of nitroso derivatives, but also play roles in the catalytic cycles of metal-catalyzed allylic amination of different alkenes (section 1.6.1, copper catalyst).[24,26] The nitroso-ene reaction indeed performs nitrogen functionalization (C−N bond formation) of different types of olefins from a nitroso precursor and is often catalyzed by a metal complex.[16] Two distinct methodologies are widely studied, whereby the nitroso is formed *in situ* from a hydroxylamine (oxidative catalytic amination) or from a nitro precursor (reductive catalytic amination).[16]

### 1.6.1  Allylic amination approach 1: oxidative catalytic amination

In this procedure, the molybdenum, iron or copper catalysts acts as redox-active agents. Their role is to first oxidize PhNHOH to PhNO, which will undergo the nitroso-ene reaction with an alkene, and the second is to reduce the hydroxylamine-ene interemediate to the allylamine product while regenerating the catalytic oxidant.[16]

**Molybdenum Catalyst**. At the beginning of the cycle (Figure 1.17), $L_nMo(VI)O_2$, **A**, oxidizes PhNHOH to produce molybdenaoxaziridine complex **B,** which then dissociates and forms PhNO and $L_nMo(IV)O$.[29] Produced PhNO undergoes the nitroso-ene reaction with an alkene and the reduced $L_nMo(IV)O$ catalyst then reduces the hydroxylamine-ene product to the corresponding allylamine. The oxidized $L_nMo(VI)O_2$ complex re-enters the catalytic cycle.[16]
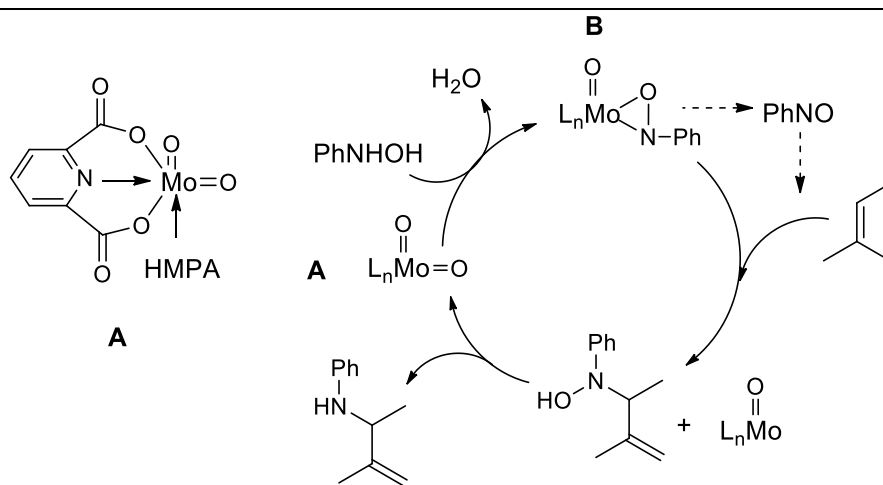


Figure 1.17. Molybdenum-catalyzed nitroso-ene reaction.[16,29]

**Iron Catalysts**. There is yet no definite catalytic cycle for iron-catalyzed nitroso-ene reactions.[16] Nicholas et al. reported the formation of an iron-triazodioxide complex (bearing C-nitroso dimer ligands) using a Fe(II)/(III) chloride catalyst.[16,30,31] This complex, {Fe[Ph(O)NN(O)Ph]₃}[FeCl₄], is isolated and characterized by X-ray crystallography and proved to be the active amination species.[31] One of their many different proposed mechanistic pathways is de-chelation of one azo dioxide ligand (arm opening), leaving space for coordination of an alkene to produce a five coordinate iron complex. Allyhydroxylamine forms by transferring the R-NO agent intramolecularly to the coordinated alkene but exact details are still unknown. Fe(II) reduces allylhydroxylamine to the allylamine product and the active catalytic complex regenerates (Figure 1.18).[31]
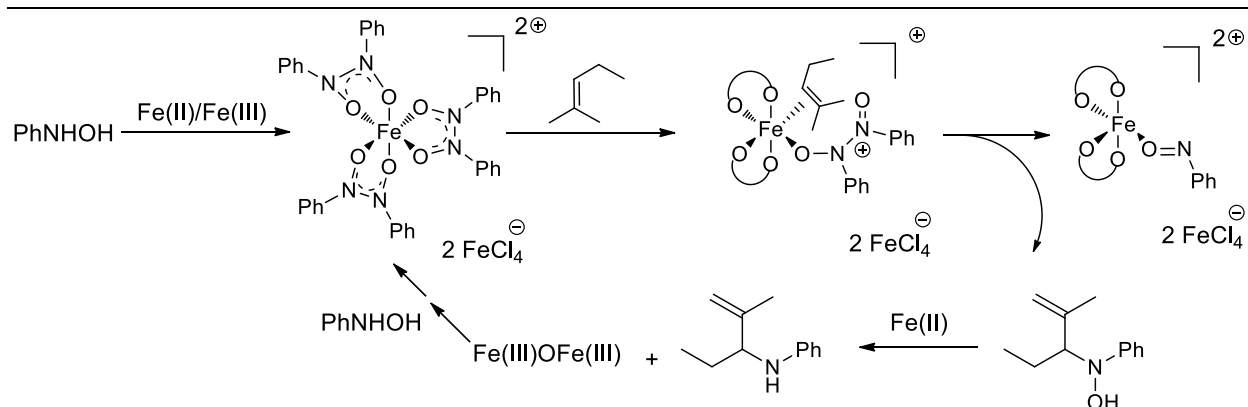
Figure 1.18. Proposed mechanism for nitroso-ene reaction using iron salts catalyst (adapted and modified from references [16,31]).

Jørgensen et al. proposed off-metal nitroso-ene reaction mechanism in iron phthalocyanine ($Fe^{II}Pc$)-catalyzed allylic amination where free PhNO acts as an aminating agent (Figure 1.19). At the beginning of the cycle, iron leads to disproportionation of PhNHOH and formation of free PhNO and $PhNH_2$ products. PhNO reacts with the alkene in nitroso-ene reaction to form the allylhydroxylamine which is further reduced by $Fe^{II}Pc$ to allylamine. The generated high-valent $Fe^{IV}O$ species oxidizes both hydroxylamine and aniline to the corresponding nitroso species. The role of iron in the nitrose-ene reaction is still unknown and it may act as both disproportionation/oxidation catalyst in allylic amination reaction.[32]
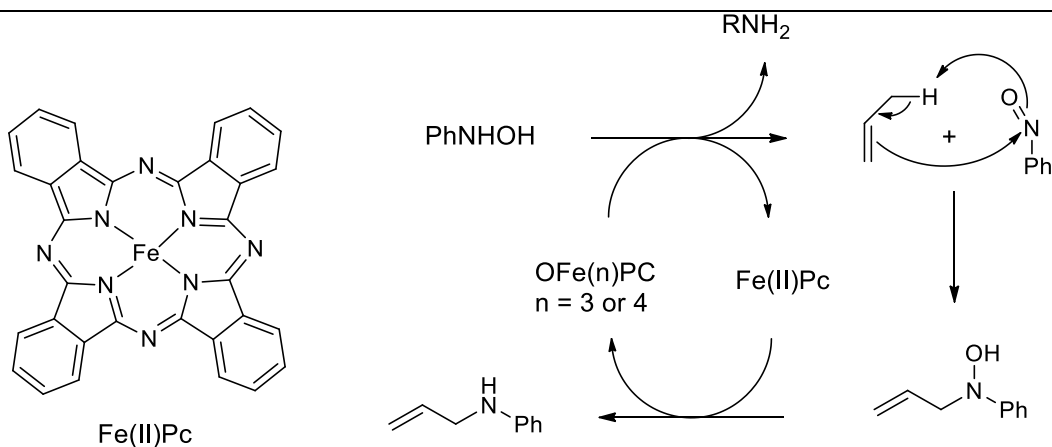


Figure 1.19. Proposed mechanism using Fe(II)Pc catalyst for nitroso-ene reaction (adapted and modified from references [16,32]).

17

**Copper Catalysts**. In allylic amination using $[Cu^I(CH_3CN)_4](PF_6)$ as pre-catalyst, Cu(I)-ArNO-coordinated complexes are considered to be the active aminating agents, in contrast with Mo and $Fe^{II}Pc$ catalysts where the ene-reaction is proposed to occur from free ArNO. The mechanistic route suggests that at the beginning of the cycle the Cu(I) catalyst reduces PhNHOH to the corresponding amine and Cu(II) (Figure 1.20). Cu(II) then oxidizes PhNHOH to PhNO to form a Cu(I)-nitroso complex. This complex further undergoes metal-mediated ene-reaction and creates allylhydroxylamine. This product will be further reduced to allyamine by Cu(I), and Cu(II) re-enters the cycle.[33,34]

Ho et al. reported the use of $CuCl_2 \cdot 2H_2O$ as precatalyst and PhNHOH as nitrogen fragment donor for moderate yield and highly regioselective allylic amination. It was proposed that Cu(II) is a redox agent that first oxidizes PhNHOH to free PhNO, which then reacts with allylic species to produce allylhydroxylamine (like the mechanisms of Mo and $Fe^{II}Pc$ catalysts). Cu(I) reduces the product to allylamine and oxidized Cu(II) returns to the cycle. $PhNH_2$ is one of the reaction side products, which is proposed to form by Cu(I) deoxygenation of PhNHOH. Oxidation and disproportionation of PhNHOH by Cu(II) is proposed to produce 60% and 40% of PhNO in the reaction, respectively. The disproportionation of PhNHOH by copper was suggested to be the key factor affecting the yield of the final product (Figure 1.21).[30]
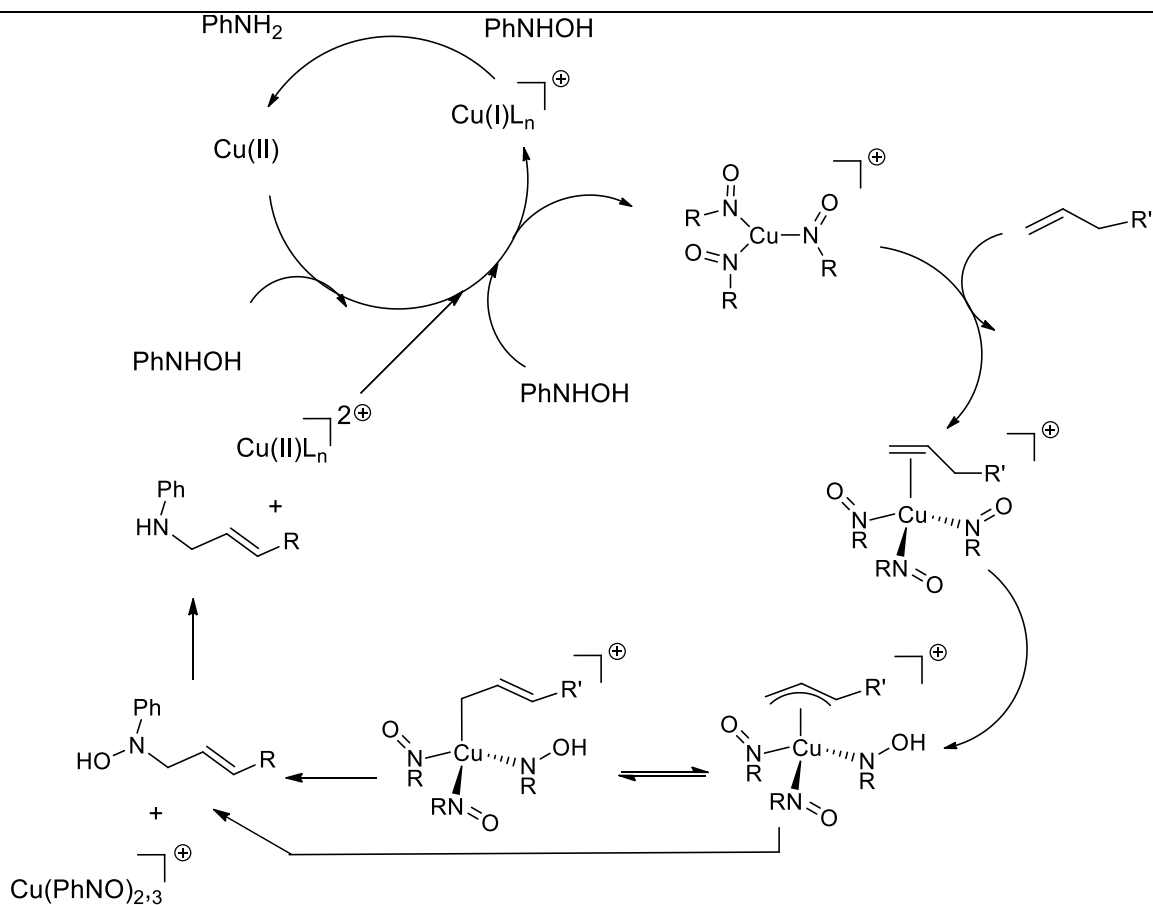
Figure 1.20. Proposed mechanism for the Cu(I)-catalyzed allylic amination (adapted from reference 34).
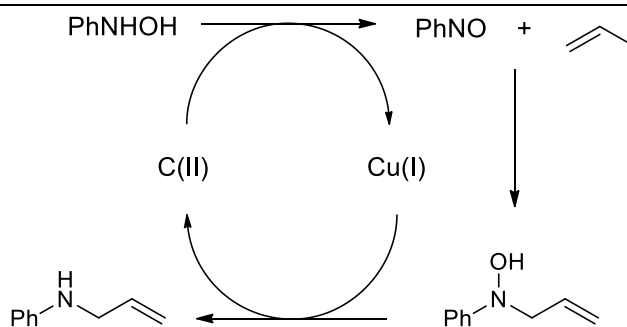


Figure 1.21. Proposed mechanism for the allylic amination using CuCl$_2$.2H$_2$O (adapted from reference 30).

## 1.6.2 Allylic amination approach 2: reductive catalytic amination

Reductive catalytic amination is a new method of metal-catalyzed allylic amination. Nitroarene used as nitrogen fragment donor with carbon monoxide as reducing agent (Figure 1.22).[35] Ru$_3$(CO)$_{12}$/DIAN-Me, [CpFe(CO)$_2$]$_2$ and [Cp*Fe(CO)$_2$]$_2$ are catalysts for this reaction.

Nicholas et al. reported that with [CpFe(CO)$_2$]$_2$ and [Cp*Fe(CO)$_2$]$_2$, amination on unsymmetrical alkenes occurs regioselectively on the less substituted vinylic carbon typical of ene-type reactions. They proposed a metal coordinated organonitrogen could bet the active aminating agent.[36,37] For [Cp*Fe(CO)$_2$]$_2$ catalysts, a cyclic carbamoyl complex in the resting state is structurally characterized but pathways leading to its formation are still unknown (Figure 1.22 B).[37] So far very scarce information about the catalyst cycles is known.[16]
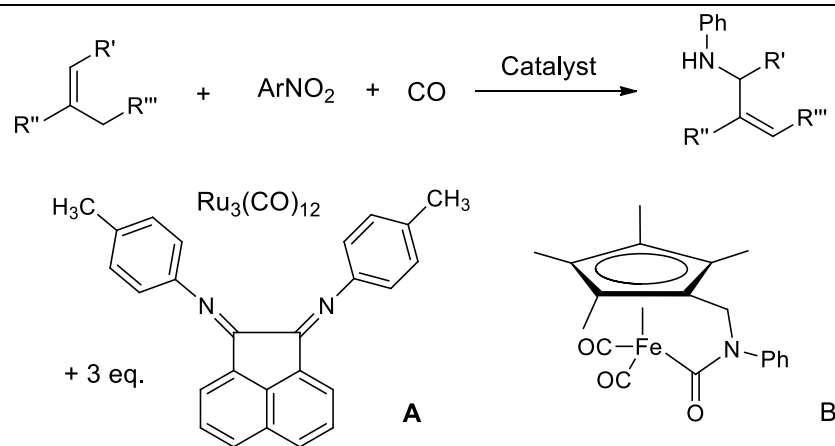


Figure 1.22. Metal-catalyzed amination using CO as reducing agent (top)[16], catalyst Ru$_3$(CO)$_{12}$/DIAN-Me (A[16,35]), Active aminating agent species proposed for [Cp*Fe(CO)$_2$]$_2$ catalyst.[16,37]

*C*-Nitroso species are not the only reactive species in these reactions, allylhydroxylamine, the product of allylic amination can undergo many *in situ* side reactions such as elimination, disproportionation, oxidation, condensation and leading to the formation of amine, azoxy, nitrone, nitroxide, and imine compounds.[16] Controlling the reactivity of these groups is an indispensable factor that challenges their application in organic synthetic chemistry.

## 1.7 ARYL NITROSO-COPPER COMPLEX: CONTROLLED NITRENE TRANSFER

We are interested in studying the reaction of versatile ArNO with L-Cu(I) complexes enabling us to study different inner-sphere electron transfer reactions. In case of LCu/O$_2$ chemistry, using electron rich Cu(I) reduces oxygen to superoxide or peroxide moieties. Particularly, we are interested in ones with $\mu$-$\eta^2$:$\eta^2$-peroxodicopper(II) moieties that are similar to Cu/O$_2$ structure in the active site of tyrosinase. However, because of stability issues (these species are typically stable at $-80$ °C), it is difficult to prepare Cu/O$_2$ complexes. Studies done by Mohammad S. Askari et al. in the XoRG, showed reaction of *p*-nitrosonitrobenzene with TMPD-

Cu(I) ligand (TMPD = *N,N,N′,N′*-tetramethylpropylenediamine) yields a green complex stable in an inert atmosphere (Figure 1.23 **B**) that envisions reactivity similar to product **A**.[38] Therefore, ArNO groups are a practical substitute for $O_2$, giving adducts that are stable at room temperature to be used in further reactions. As a result, reaction of compound **B** with 2,4-di-*tert*-butyphenolate forms TMPD-Cu(I)-iminoquinone diamagnetic complex (product **2**) in which the *ortho* position of the phenol is replaced by a nitrene fragment coming from the activated ArNO moiety. The product is isolated and structurally characterized. Further reductive workup on this product produces novel 2-aminophenol (product **3**).[38]
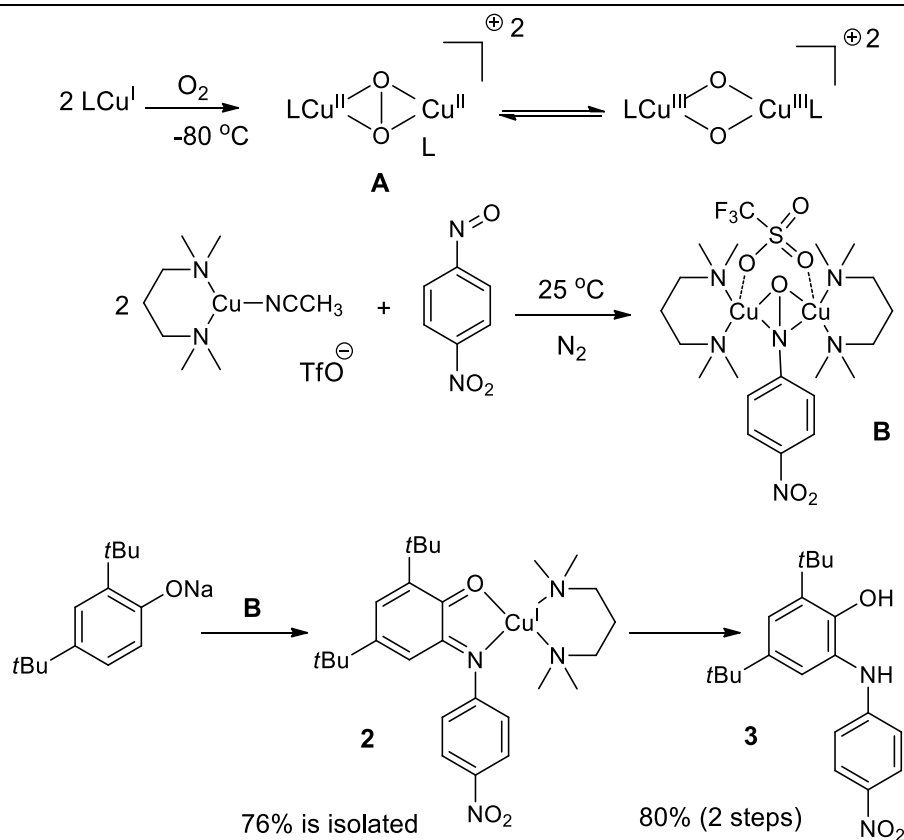


Figure 1.23. Analogy between the Cu/$O_2$ (top) and Cu/ArNO (middle) reaction with TMPD-Cu(I) complex, and ensuing nitrene transfer to sodium 2,4-di-*tert*-butylphenolate (bottom).[38]

## 1.8 METAL-PROMOTED REDUCTION OF AROMATIC NITRO GROUPS

### 1.8.1 Catalytic hydrogenation of nitro compounds

Reduction of nitroarene (ArNO$_2$) group to the corresponding amine (ArNH$_2$) is through intermediate states including ArNO and ArNHOH compounds. These transformations require

reduction by two electrons in each step. Catalytic hydrogenation reduction of $ArNO_2$ compounds follows the similar electrochemical reduction pathways proposed by Haber in more than 100 years ago (1898) by either "direct route" or "condensation route".[20,39] In the "direct route", reduction of $ArNO_2$ to ArNO and further to ArNHOH, are very fast and both $ArNO_2$ and ArNHOH are highly adsorbed on the catalyst surface during the course of reaction.[20] However, reduction of ArNHOH to the final amine product is slow since it requires cleavage of the N-O bond and is considered to be the rate-determining step.[20,39] This slow reaction results in accumulation of ArNHOH and also the creation of unwanted side products.[20] Ar-$NH_2$ can even be produced by disproportionation of ArNHOH in a process called "catalytic by-pass".[20,40] In the "condensation route" ArNHOH reacts with ArNO, creating an azoxy compound, which in consecutive steps reduces to azo, hydrazo and finally to Ar-$NH_2$.[39] Since all of the intermediates proposed by Haber are proved to exist, these two routes are generally the accepted catalytic reduction pathways of $ArNO_2$ compounds (Figure 1.24).[20]
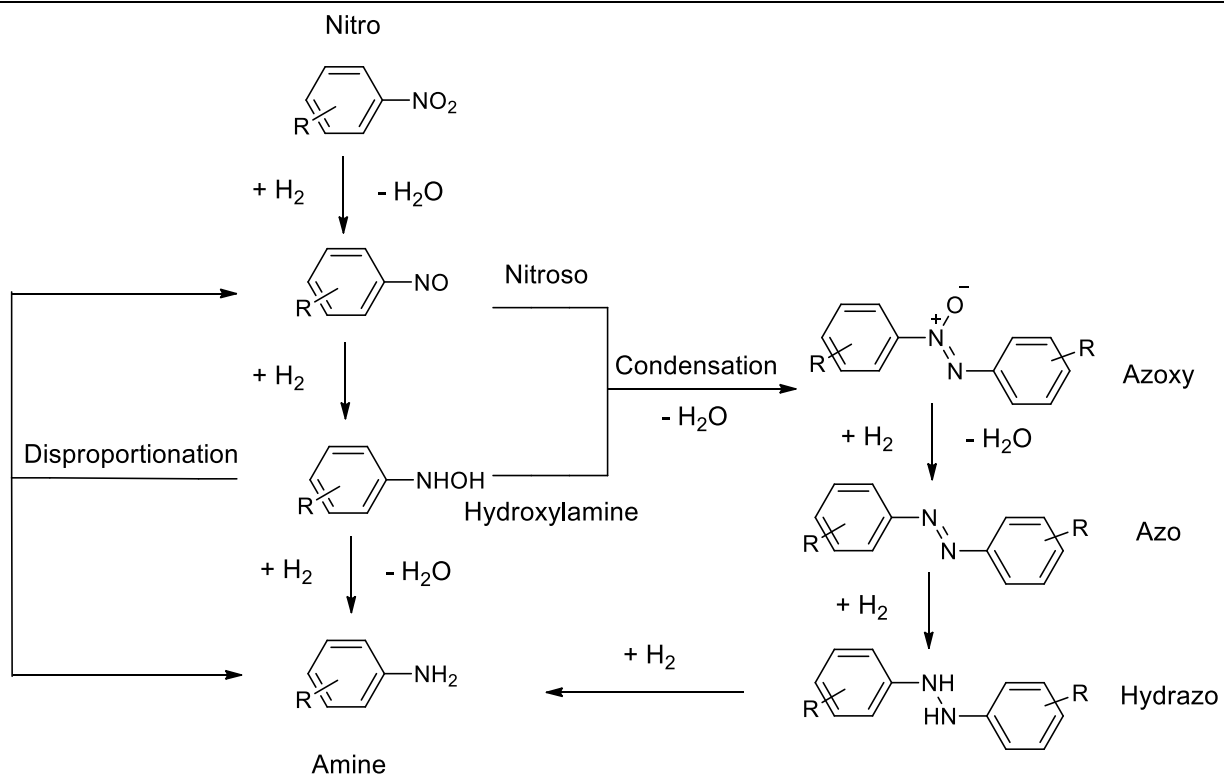


Figure 1.24. Proposed pathways for reduction of aromatic nitro compounds.[20]

22

Catalytic hydrogenation is a well-known reduction method for nitro compounds.[41] The reaction proceeds by the adsorption of hydrogen gas and the desired nitro compound on the surface of the catalytic amount of transition metal. Sometimes transition metal oxides and halides are used as heterogeneous catalyst instead of using expensive transition metals on a supporter. Heterogeneous catalysts are adsorbed or admixed to supporters that are basically inert compounds including calcium sulfate ($CaSO_4$), barium sulfate ($BaSO_4$), carbon supporter for palladium (Pd) or platinum (Pt) black and alumina mostly for rhodium catalysts. Although supporters alone could minimize catalytic reactivity, poisons and modifiers can change the surface structure of the catalyst. Poisons can bind to catalytically active sites, hence preventing adsorption of either hydrogen or the organic substrate and lowering the reactivity/selectivity. Divalent sulfur compounds, carbon dioxide, carbon monoxide, phosphine, amine, and $Hg^0$ are famous examples of poisons.[41] For nitro compounds, hydrogenation normally occurs in ambient conditions with less than 10 mol % of catalyst per mole of the substrate [(5% Pd/C (4-8%), $PtO_2$ (1-5%)] or higher amounts of Raney nickel (10-80%). In all of these reactions amine is the final product.[41]

## 1.8.2   Selective hydrogenation of nitro compounds

Selective hydrogenation of substituted aromatic nitro compounds using transition metals is challenging since they are prone to cleave bonds as in halogens or reduce bonds as in olefin (C=C), and carbonyl (C=O) functional groups.[20,40,42] The catalysts such as palladium, platinum and nickel are highly reactive but very unselective towards hydrogenation of functionalized aromatic nitro compounds.[20] Due to the difficulty in selective reduction of these compounds, a non-catalytic method is usually applied (using reducing reagents stoichiometrically).[39]

Zinc and ammonium formate/chloride are widely used for the synthesis of aromatic and aliphatic amine compounds from nitro groups.[43] There are procedures for fast, cheap, selective and in good yield production of amine derivatives having substituents including halogens and carbonyl groups, using activated zinc and ammonium formate/formic acid in methanol (or other solvents) in a few minutes and at room temperature (Figure 1.25).[43]

X: halogen, -OH, OCH$_3$, -CHO, -COCH$_3$, -COC$_6$H$_5$, -COOH, -COOC$_2$H$_5$, -CONH$_2$, -CN, -CH=CH-COOH, -NHCOCH$_3$, and R=alky group
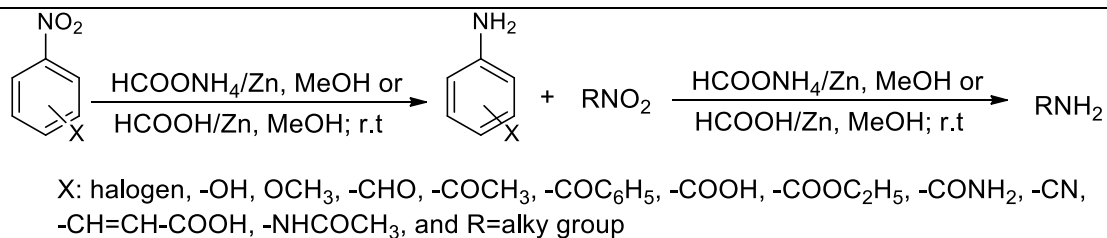
Figure 1.25. Reduction scheme of aromatic nitro groups to aromatic amine.[43]

Zinc dust/ammonium chloride is also used for reduction of nitrobenzene to aniline in presence of water at 80 °C and short reaction time. This reaction can be considered as environmentally benign since it proceeds without using organic solvents or harsh reaction conditions such as concentrated HCl or NaOH (20% aq.), less expensive metallic starting material, and producing high yields of aniline compounds even when potentially reactive groups such as halide, ester, and amide are present.[44] Since functionalized aniline products are important intermediates in pharmaceutical, polymers, herbicide, dyes and pigments, creating chemoselective hydrogenation catalyst for such aromatic nitro compounds are valued.[20,40,42]

Catalyst selectivity towards nitro compounds having reducible substituents is achieved by using surface modifiers (phosphorus, sulfur, nitrogen or halogen containing modifiers), which modify the adsorption abilities of the metal catalyst.[20,42] By reducing the catalytic activity, however, the reduction is incomplete, generating a substantial amount of hydroxylamine, which needs to be further reduced by addition of promoters, mainly vanadium salts.[20,40]

Two commercially new heterogeneous catalysts are designed to selectively reduce nitro groups in the presence of C=C, C≡C, C≡N and iodide functions.[40] The first is Pb-modified Pt catalyst having an irreversibly adsorbed thin Pb over-layer on Pt surface.[20,40] This layer plays an important role in reactivity and selectivity of Pt-catalyst by allowing adsorption and dissociation of small hydrogen molecules but not nitro or other functional groups. 5%Pt-1%Pb-CaCO$_3$ catalyst shows high activity and significant selectivity for reduction of aromatic nitro with olefin substitutes at 120 °C and in polar solvents. Formation of azoxy and hydrazo side products as the result of hydroxylamine accumulation lowers the yield of the final product. This problem can be avoided by using iron (II) chloride (FeCl$_2$) with tetramethylammonium chloride (TMAC) as promoters to increase the rate of hydrogenation and selectivity towards the aniline product.[40]

The second catalyst is hypophosphorous acid (H$_3$PO$_2$)-modified Pt/C that among many other phosphorus-based modifiers (e.g. H$_3$PO$_3$, (PhO)$_2$P(O)H, HPPh$_2$) shows significant selectivity.

For example, Pt/C-H$_3$PO$_2$ keeps C≡C bonds intact while Pb-modified Pt systems did not.[40] Although, these are efficient chemoselective catalytic systems, controlling their selectivity and reactivity by modifiers results in the accumulation of hydroxylamine, therefore consumption of metal salt promoters for further reduction of hydroxylamine is required.[42]

Chemoselective gold nanoparticles supported on TiO$_2$ and Fe$_2$O$_3$ can perform hydrogenation under milder conditions without accumulation of hydroxylamine and addition of metal salts.[39,42] Although gold is reported to be a catalyst in hydrogenation of carbonyl and olefin bonds, this is the first example where it is used in the reduction of the aromatic nitro compounds.[20]

### 1.8.3 Partial reduction of nitro compounds

Our group is interested in the partial reduction of ArNO species to their corresponding ArNHOH moieties. Placing a transition metal in the vicinity of a hydroxylamine group on the ligand would allow to study the interaction between two redox-active centres, the metal ion and the hydroxylamine moiety. Chemical reductions of nitro to hydroxylamine groups include using stoichiometric amount of reductants such as tin, aqueous suspensions of zinc with ammonium chloride/ammonium formate,[45] silicon hydride, boron hydride and hydrazine.[46]

Kamm O. reported the first reduction of ArNO$_2$ in an aqueous suspension of zinc dust and ammonium chloride at temperature ranges of 60-65 °C.[47] However, common problems in traditional zinc reductions are high quantity consumption of ammonium chloride and waste production.[48] Ung et al. reported the advantage of using ultrasonic activation in reduction of ArNO$_2$ to hydroxylamine using 2.1 M equivalent of zinc (solvent/water 9:1 mixture) and ammonium chloride at room temperature in short reaction time (5 min.) (Figure 1.26). This method is highly selective for hydroxylamine without the formation of overly reduced by-products.[49]
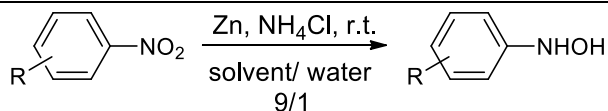


Figure 1.26. Reduction scheme of aromatic nitro groups to aromatic hydroxylamine.[49]

A method of ultrasonic activation (zinc/CO$_2$/H$_2$O system) for selective reduction of ArNO$_2$ to PhNHOH without using ammonium chloride is reported by Liu et al. (Figure 1.27).[48] The optimized conditions lead to 98% conversion and 93% yield of hydroxylamine. Using ultrasonic

systems leads to better selectivity and better yield in shorter reaction times than traditional mixing techniques.[48]
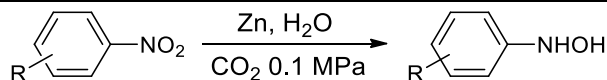


Figure 1.27. Reduction scheme of aromatic nitro groups to aromatic hydroxylamine.[48]

Metal-catalyzed hydrogen transfer is another method of reducing nitro to hydroxylamine groups. Nitroarene with *para*-substituted electron withdrawing groups are reduced to arylhydroxylamine using a catalytic amount of selenium (Se) and sodium borohydride ($NaBH_4$) in methanol solution at room temperature (under argon) but strong electron donating substitutes are inactive toward reduction reaction.[50] Similar to Se, a catalytic amount of tellurium (Te, 10mol%) in a solution of sodium borohydride in methanol at room temperature reduces *p*-nitroarenes to their corresponding hydroxylamines in good yields.[51]

Application of chemical methods for large-scale industrial reduction of aromatic nitro compounds to arylhydroxylamines is problematic. Due to making large quantities of chemical waste, they are not environmentally safe or economically advantages methods.[45,52] However, selective catalytic hydrogenation applies benign catalysts for the partial reduction of nitroarene, produces no harmful by-product (water) and consume inexpensive reductant ($H_2$).[52]

Takenaka, Yasuda et al. reported a highly selective hydrogenation method for $ArNO_2$ compounds using silica-supported Pt catalyst (5% $Pt/SiO_2$), small quantities of DMSO and amine additives (Figure 1.28). The existence of both additives is crucial for achieving high selectivity and very good catalytic activity with up to 99% yield at room temperature and atmospheric pressure.[52]
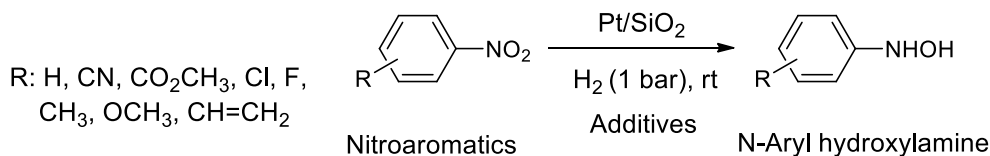


Figure 1.28. Partial reduction of nitroarenes using platinum supported on $SiO_2$.[52]

Patented Pt/C and Pd/C catalysts are impractical systems for selective hydrogenation, having disadvantages including large consumption of organic additives, difficulty in separation or

purification of the hydroxylamine and low hydroxylamine yields. Therefore, finding selective catalysts for partial hydrogenation of $ArNO_2$ compound to ArNHOH group without using organic additives is still a vibrant domain of research.[45]

Silica-supported Pd catalysts without additives are also used for highly selective catalytic hydrogenation of $RNO_2$ to high yield RNHOH at ambient temperature and pressure, with the benefit of reusing the catalyst for a minimum of five times.[46] Pt/C synthesized by colloid method is a highly active catalyst for conversion of $ArNO_2$ compounds with substituted electron-withdrawing groups to the corresponding hydroxylamine final product.[53] Although this method requires no organic additives, its application is limited to $ArNO_2$ with electron-withdrawing substituents.[45]

## 1.9 SCOPE OF THE THESIS

In order to study the redox chemistry of hydroxylamine-containing ligands near a copper centre, we first focused on the design of ligands with pendant nitro moieties that can be then converted to hydroxylamine moieties by partial reduction. The design is based on salen-ligand family, famous for making stable complexes with d-block transition metals. Substitutions on the aromatic ring provide different steric and electronic environment.

In Chapter 2, we introduce nitro-containing ligands that were previously synthesized in the XoRG. These ligands possess either imine (I) and amine (A) moieties on the linker backbone along with substitution on the aromatic rings ($L^{I/A}_R-NO_2$, R = H, $t$Bu). Previous work using a hydrogenation method on poisoned Pd/C has shown that the imine ligands, $L^I_R-NO_2$, get reduced to their corresponding hydroxylamine, but are also further reduced to amine structures, including reduction of the imine function. In addition, attempts to separate and purify the products failed due to decompositions of compounds on column chromatography. Therefore, we focused instead on the more resilient amine-based ligands ($L^A_R-NO_2$). This chapter relates reduction experiments using zinc and ammonium formate and provide and optimized procedures to selectively obtain the hydroxylamine-containing ligands ($L^A_R-NHOH$, R = H, $t$Bu). The benefit of this procedure is to use non-toxic zinc, simple mechanical stirring, low solvent consumption and a simple work-up method. These procedures allow having $L^A_R-NHOH$ ligands in high yield (70-80%) and high purity (>85%).

In Chapter 3, we studied the interaction of the nitro-containing ligands with Cu(II) ions. Previously characterized square-pyramidal Cu(II) complex of $L^I_H-NO_2$ showed a 1:1 ligand-to-

Cu stoichiometry. UV-Vis titrations of all synthesized $NO_2$ and NHOH ligands with Cu(II) salts provided insight into the ligand-field strength of the ligands and the stoichiometry of complexation. The titration of $L^A_R$-NHOH (R = H, $t$Bu) ligands with Cu(II) proved the existence of the reaction not following the expected one-to-one stoichiometry and complications on the stability and the intractability of the complexes formed. Therefore, I moved to another hydroxylamine-containing ligand based on a bis(picolyl)amine coordinating moiety, $Lpy_2$-NHOH, previously designed and studied by Maryam Habibian in the XoRG. Reaction of $Lpy_2$-NHOH with Cu(II) acetate leads to the formation of a neutral complex of formula $Lpy_2$-NO-Cu. Its crystal structure as well as its paramagnetic ^{1}H-NMR spectra suggested the existence of a paramagnetic compound, proposing the electronic structure of a Cu(II)-nitrosyl radical species, $Lpy_2$-NO$^{\bullet/-}$-Cu(II). Solid-state SQUID measurements were silent, suggesting a very strong antiferromagnetic coupling between the spins of Cu(II) and NO$^{\bullet/-}$. VT-NMR experiments allowed to evaluate a coupling constant $J$ (singlet-triplet gap) of ca. $-420$ cm$^{-1}$, confirming a strong antiferromagnetic coupling. The complex is very stable at high temperature (tested up to 90 °C in DMSO). Cyclovoltammetry shows a reversible oxidation wave at low potential ($-187$ mV vs. Fc$^{+/0}$) and a reversible reduction wave at very low potential. Further studies are underway to better characterize this complex and gain more insight regarding the redox properties of a NO group near the copper centre.

# Chapter 2. Design and synthesis of hydroxylamine-containing ligands

## 2.1 LIGAND DESIGN

One of the essentials for studying the redox chemistry of hydroxylamine and nitroso functional groups is to finely position them in close proximity to a metal centre. In order to do so, we chose to work with famous salen-type ligands (Figure 2.1 **A**), which form stable, well-defined complexes with many different transition metals.[54] Salen-type ligands can coordinate to the metal ion via their two imine nitrogen and two phenol oxygen (deprotonated upon coordination), forming a tetradentate ligand.[55] These ligands are easily synthesized and structurally manipulated, which makes them ideal for catalysis, including asymmetric versions.[55,61] Most famously, Jacobsen et al. reported the synthesis of a chiral Mn(III)-salen complex (Figure 2.1 **B**) being a highly efficient enantioselective catalyst for the epoxidation of simple ununctionalized cis-olefins.[56,57] Salen-complexes with Ti, V, Mn, Fe, Co and Ru have been studied as potential oxygenation catalysts for a number of substrates including aromatic amine, organic sulfide, and sulfoxide.[55]
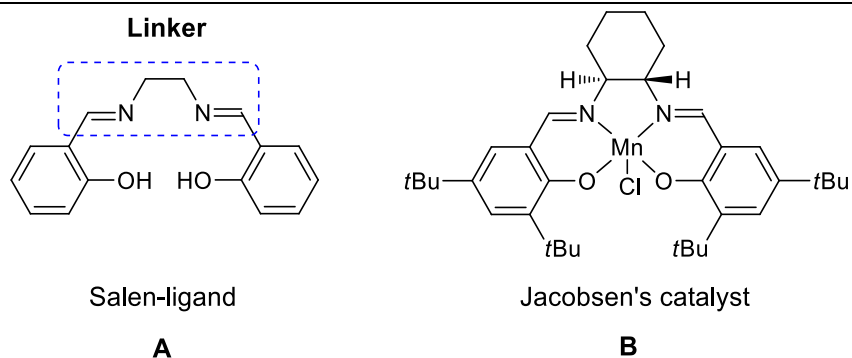


Figure 2.1. A) Salen ligand[54], B) Jacobsen's Mn(III)-salen complex catalyst for epoxidation of cis-olefin.[56,57]

Our ligand design consists of using half a salen moiety while the other half is modified to introduce the *N*-functional group. Salen ligands are generally synthesized by imine condensation of ethylenediamine and salicylaldehyde. Substitutions on the ethylene moiety and/or on

29

salicylaldehyde aromatic ring afford various structurally and electronically modified salen-type ligands. Complying to our research purpose, we structurally functionalized the diamine backbone to create asymmetric salen-type ligands, bearing one salicylimine moiety and one *ortho*-nitrogen-containing aromatic moiety (Figure 2.2). The multi-chelating nature of these ligands is an important factor to improve the complex stability. The sulfonamide-modified arm places the nitrogen-containing functional group close to the metal atom, enabling coordination in the case of the hydroxylamine and nitroso groups, the nitro and aromatic $NH_2$ groups are usually not coordinating with the first-row transition metal we intend to use.

Following the work of past XoRG undergraduate members Fei Chen,[58] Klervi Dalle, Maëlle Mosser and Pierre-Étienne Rouet, two different types of ligands containing imine or amine sulfonamide functionalized backbones with/without substitution on the aromatic ring were synthesized (Figure 2.2). Nitro functional groups on these ligands are non-coordinating, therefore deprotonation of sulfonamide and phenol moieties leaves a di-anionic, tridentate ligand. Our approach is to obtain ligands with the other *N*-functional groups via partial hydrogenation of the nitro group.
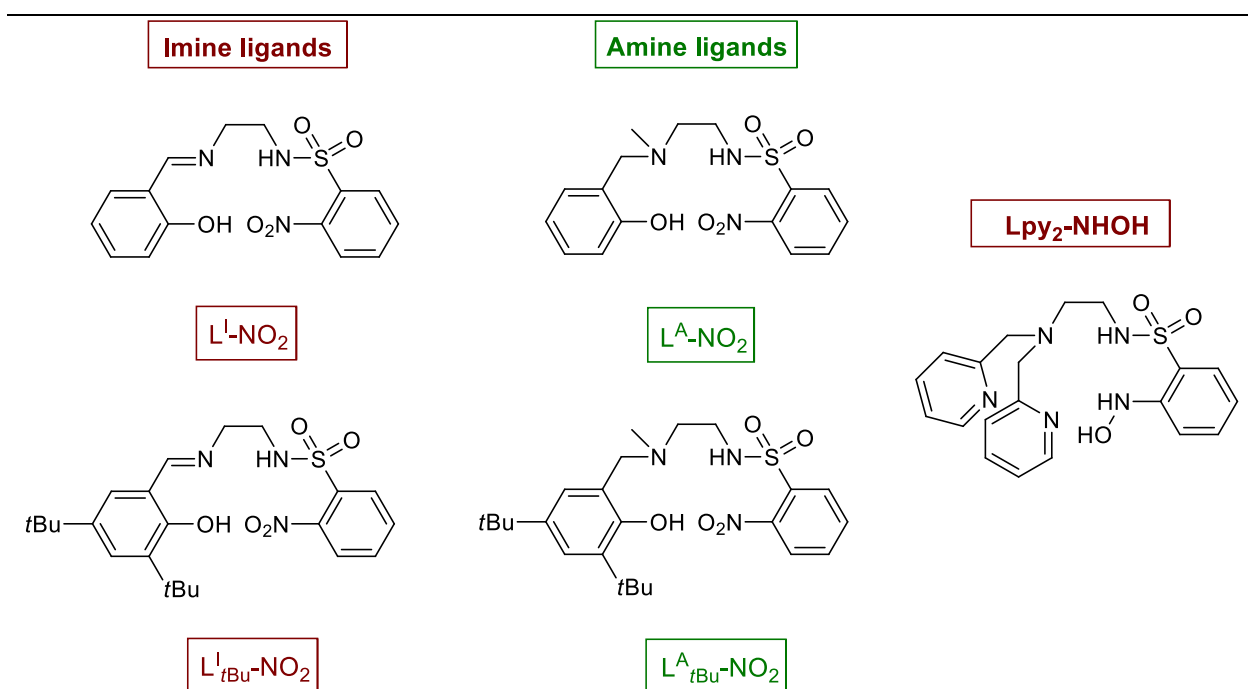


Figure 2.2. Synthesized imine and amine ligands used in this thesis.

The synthesis of the asymmetric salicylimine-sulfonamide ligands generally proceeds in two steps (Figure 2.3). The first step is the formation of the mono-sulfonamide via reaction of ethylene diamine with 2-nitrobenzenesufonyl chloride. Formation of the bis-substituted ligand is prevented by cooling down reaction temperature with dropwise addition of dilute 2-nitrobenzenesufonyl chloride onto a large excess of ethylenediamine. Protonation of the half-ligand with concentrated hydrochloric acid (12 M HCl) made it soluble in water and left the bis-substituted ligand as a precipitate. Excess ethylenediamine before adding HCl is removed by the rotary evaporator. The second step is to condense protonated half-ligand with salicylaldehyde or 3,5-di-*tert*-butylsalicylaldehyde to retrieve the imine-containing ligands $L^I$-$NO_2$ and $L^I_{tBu}$-$NO_2$ in 65% and 84% yields, respectively.
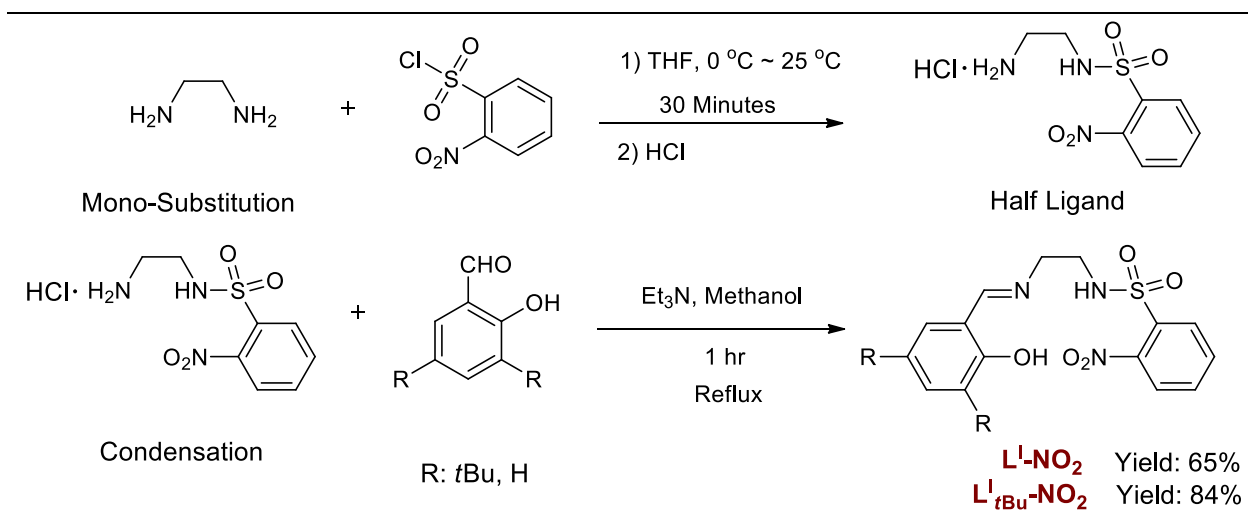


Figure 2.3. General synthesis scheme for $L^I$-$NO_2$[58] and $L^I_{tBu}$-$NO_2$ ligands.

Following this initial work, I have repeated and optimized the procedures to obtain the $L^I$-$NO_2$ and $L^I_{tBu}$-$NO_2$ ligands with 77% and 84% yields, respectively. The synthesis of $L^A$-$NO_2$ proceeds best via a one-step, one-pot reductive methylation of $L^I$-$NO_2$ in 74% yield (Figure 2.4 top). The synthesis of $L^A_{tBu}$-$NO_2$, however, affords good yields only when performed in two steps (but still in one pot). Thus, the imine is first reduced with sodium cyanoborohydride to form the secondary amine ligand, which is then methylated into $L^A_{tBu}$-$NO_2$ by reductive amination of formaldehyde with a 98 % overall yield. As a note, the ligand with the secondary amine group can be isolated after the first step in 69% yield by Maëlle Mosser, but it is not used in the present thesis and will not be mentioned further.
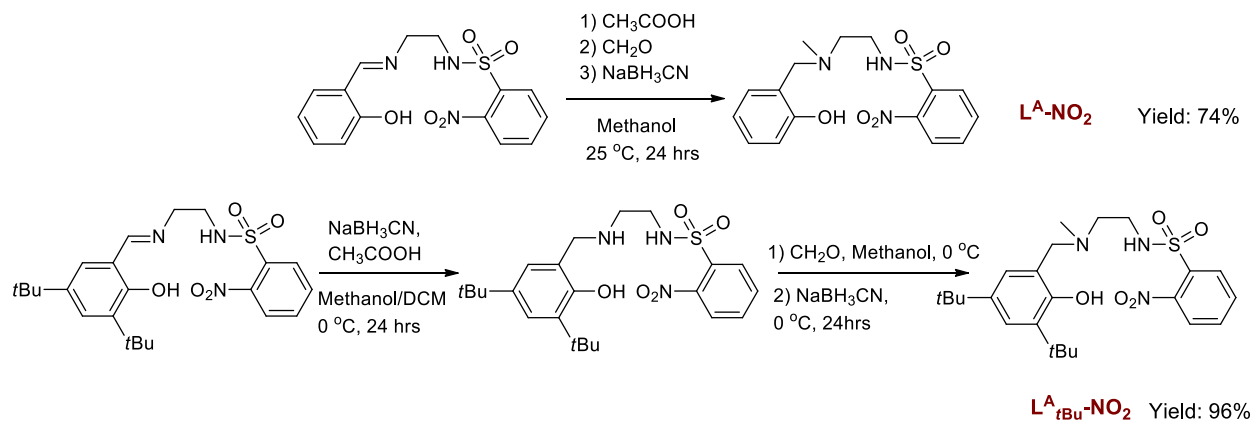
Figure 2.4. General synthesis of $L^A$-$NO_2$ (top) and $L^A_{tBu}$-$NO_2$ (bottom).

In previous work, MSc student Maryam Habibian synthesized a pentadentate ligand ($Lpy_2$-$NO_2$) by replacing the salicylimine moiety with a bis(2-pyridylmethyl)amine (also called bis(picolyl)amine) moiety (Figure 2.5). Sulfonamide deprotonation affords a mono-anionic ligand. This ligand is also readily reduced to its hydroxylamine version, $Lpy_2$-$NHOH$, under standard hydrogenation conditions. Because of the lack of success in isolating well-defined complexes with the aforementioned $L^{A/I}_R$-$NHOH$ ligands, Chapter 3 will focus on the reaction of this $Lpy_2$-$NHOH$ with Cu(II), since it provided an isolable complex amenable to electronic structure elucidation.
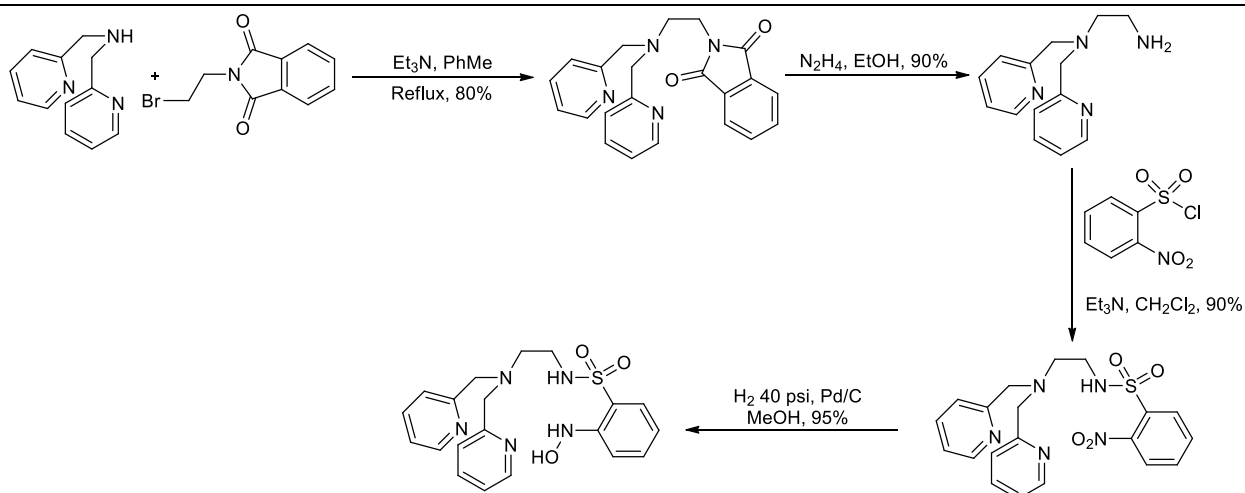


Figure 2.5. Synthesis of $Lpy_2$-$NO_2$ and reduction to $Lpy_2$-$NHOH$.

32

## 2.2  PARTIAL REDUCTION OF NITRO-CONTAINING LIGANDS TO HYDROXYLAMINE MOIETIES

Upon partial reduction, the non-coordinating nitro group becomes a coordinating hydroxylamine group, thereby increasing the ligand denticity by one. Traditional reduction methods including metal-catalyzed hydrogenation or activated zinc with ammonium formate/ammonium chloride were used to reduce these nitro groups to hydroxylamine. Reduction with either of these methods cannot be stopped at the nitroso intermediate since further reduction to hydroxylamine is a faster process than the reduction of the nitro to the nitroso. Our strategy to obtain the nitroso moiety is whether via oxidation or disproportionation of the hydroxylamine moiety upon complexation with a transition metal (Figure 2.6).
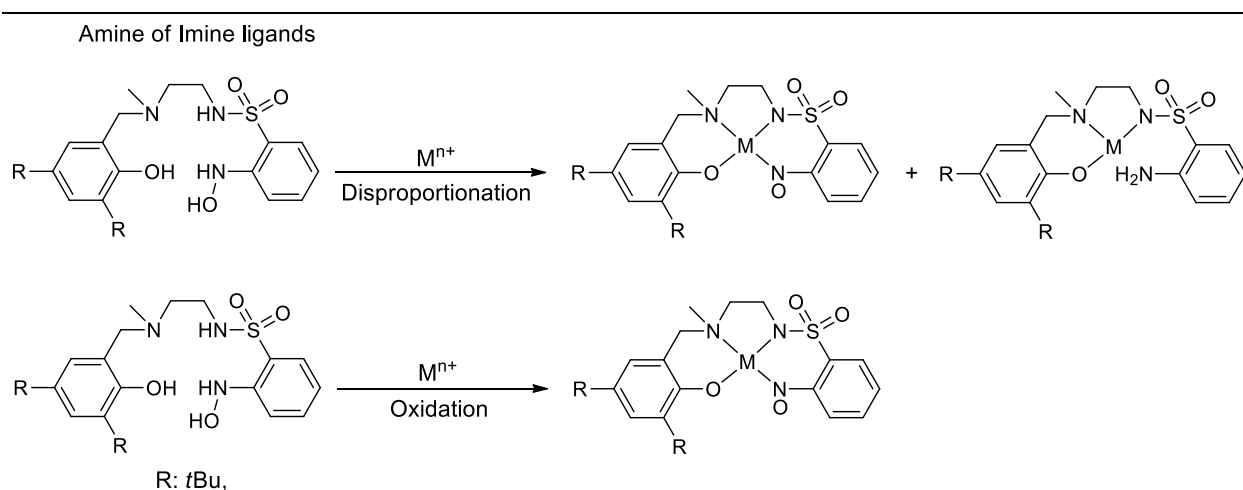


Figure 2.6. Disproportionation of $L^{A/I}$-NHOH ligands in complexation with metal to create nitroso moieties.

Previous work in the XoRG on the reduction of imine ligands ($L^I_{tBu}$-NO$_2$ and $L^I$-NO$_2$) was carried out by catalytic hydrogenation using Pd/C catalyst poisoned by *tert*-butylphenyl sulfide. This led, however, to mixtures comprising leftover starting material, $L^I_R$-NO$_2$ (R = H or *t*Bu), the desired $L^I_R$-NHOH **2**, as well as $L^I_R$-NH$_2$ **3**, and the fully reduced ligand **4**, in which the imine is also reduced (Table 2.1). Best results were obtained with 2 mol% Pd/C per substrate, 5 mol% additive per catalyst and for a reaction time of 30 minutes under 20 psi of hydrogen pressure. The solubility of the products is similar, making their separation from reaction mixture challenging. However, the nitro starting material is insoluble in ether and is easily recovered by filtration. Therefore, the optimized conditions correspond to an incomplete conversion that is designed to minimize the over-reduction to $L^I_R$-NH$_2$. Thus, $L^I$-NHOH was obtained in 95% purity and $L^I_{tBu}$-NHOH in 85% purity, the only contaminant detected by $^1$H-NMR being the

corresponding $L^I_R$-NH$_2$ ligand. Purification by column chromatography failed due to decomposition on the column. In addition, reduction using milder conditions such as zinc and ammonium formate or ammonium chloride (see section 2.3.1 below) failed due to the ligand breaking down during the reduction process, as shown by intractable $^1$H-NMR spectra.

Table 2.1. Hydrogenation of $L^I_{tBu}$-NO$_2$ and $L^I$-NO$_2$.[a]
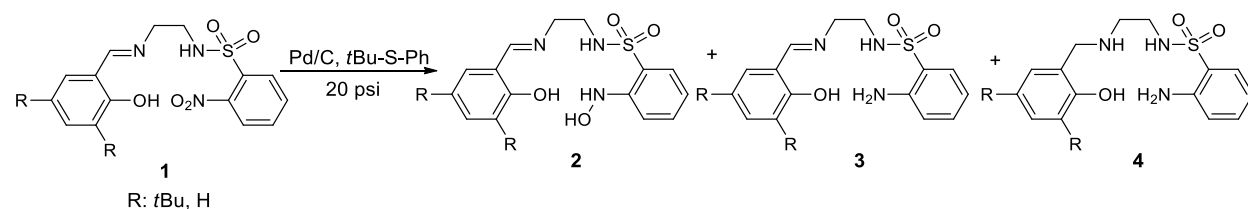


| Ligand (R) | Time (h) | Additive (mol%) | 1 (%) | 2 (%) | 3 (%) | 4 (%) |
|---|---|---|---|---|---|---|
| H | 0.5 | 5 | 29 | 69 | 2 | 0 |
| tBu | 0.5 | 5 | 8 | 83 | 9 | 0 |

[a] Optimization using 5 mol% additive (per mole of catalyst), 2 mol% catalyst (per mole of the substrate), the H$_2$ pressure of 20 psi. Table gives NMR ratios of the four compounds.

With $L^A_{tBu}$-NO$_2$, the same catalytic hydrogenation conditions led to a crude mixture containing 18% residual $L^A_{tBu}$-NO$_2$, 70% $L^A_{tBu}$-NHOH and 12% $L^A_{tBu}$-NH$_2$. Contrary to the $L^I_R$-NHOH examples above, $L^A_{tBu}$-NHOH was stable on the column chromatography but was recovered with a low yield of 38%. Similar conclusions were found for the reduction of $L^A$-NO$_2$ with this method and the quantity of pure $L^A$-NHOH afforded by column chromatography was not sufficient enough for further studies. Therefore, milder reduction conditions were examined (section 2.3.1 below)

## 2.3  OPTIMIZATION PROCEDURES FOR THE PARTIAL REDUCTION OF $L^A_{tBu}$-NO$_2$ AND $L^A$-NO$_2$

### 2.3.1  Development of mild reduction conditions

In section 2.3, we will focus on describing optimization procedures for the partial reduction of the two $L^A_{tBu}$-NO$_2$ and $L^A$-NO$_2$ ligands, using activated zinc and ammonium formate. Imine ligands, $L^I_{tBu}$-NO$_2$ and $L^I$-NO$_2$, are omitted because the reaction conditions yielded a mixture of $L^I_R$-NHOH and $L^I_R$-NH$_2$ products that could not be further purified by column chromatography. The goal is to achieve the highest amount of desired hydroxylamine product ideally by stopping the reaction after the complete consumption of nitro ligand and prior to the formation of the

amine product. Reduction using zinc dust is straightforward as zinc powder is cheap, commercially available and non-toxic.[49] This system operates easily and therefore reduces the challenge of using a hydrogenator (Parr shaker), especially in the preparation of the catalyst, separation and work up sections. Zinc dust/ammonium chloride is used for reduction of nitrobenzene to aniline in presence of water at 80 °C and short reaction time. Reduction of nitroarenes to aromatic amine compounds with $Zn/NH_3$, $Zn/HCl$ or $Zn/NaOH/Et_2O$ are not environmentally benign as mostly high concentration of HCl or NaOH, and organic solvents are consumed. Increased reaction time (24 h) in case of $Zn/NH_3$ or high quantity consumption of Zn in some of these reactions are important synthetic issues.[44] Even with optimization, these methods produce large amounts of waste and are not sustainable pathways due to by-products to final products high ratio and an excess usage of reducing agents.[20,39,40]

Maëlle Mosser's conditions, employing one equivalent of $L^A{}_{tBu}$-NHOH, nine equivalents of activated Zn powder and 16 equivalents of ammonium chloride, in water for 22 h at room temperature, led to a crude mixture composed of 59% residual $L^A{}_{tBu}$-NO$_2$, 38% $L^A{}_{tBu}$-NHOH and 3% $L^A{}_{tBu}$-NH$_2$ (Figure 2.7).
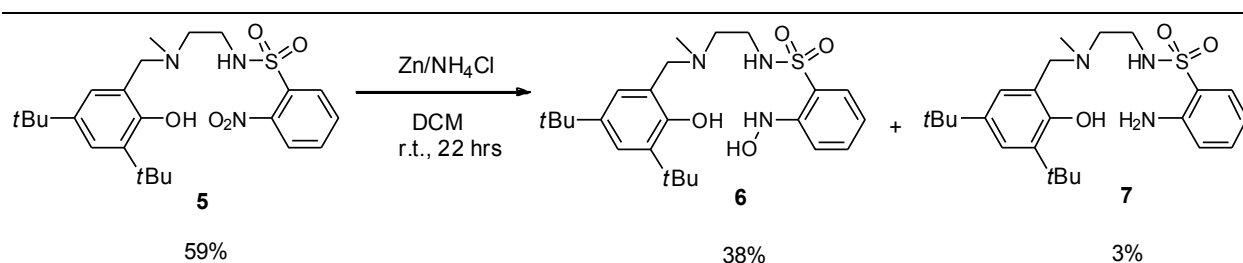


Figure 2.7. Reduction trial of $L^A{}_{tBu}$-NO$_2$ with zinc and ammonium chloride.

Zinc power can be activated by dilute hydrochloric acid to eliminate oxide passivation of the metal surface that occurred when zinc is stored in the air. We activated zinc using 6 M hydrochloric acid (HCl) with vigorous stirring for 10-15 minutes, resulting in a very shiny surface of the zinc. The mixture is then immediately filtered and washed with portions of distilled water, ethanol, and anhydrous diethyl ether and dried in the vacuum oven overnight. Because the reduction conditions are composed of a solid-liquid heterogeneous system, mechanical stirring helps to transport mass from the liquid phase to the surface of the metal. Therefore, attention is required on the efficiency of stirring during the reaction. The main goal of stirring is to keep the solution turbulent throughout the reaction time.[48] In the introduction, we

briefly discussed some examples of advances in selective reduction methods of nitroarene to arylhydroxylamine applying ultrasonic irradiation using zinc in the presence of ammonium chloride,[49] or free of ammonium chloride in the $CO_2/H_2O$ system.[48] In our case we wanted a simple, adaptable procedure, and performed the optimization using conventional stir plates.

## 2.3.2  Reduction of $L^A$-NO$_2$ using zinc and ammonium formate

The general reduction procedure is the addition of ammonium formate dissolved in methanol (1-3 mL) to a vigorously stirring solution of ligand in dichloromethane (2-4 mL) (Figure 2.8). Zinc is then added in portions during the course of the reaction. Ammonium formate shows better solubility in methanol than ammonium chloride, and was therefore used preferentially. At the end of each reaction, the mixture was filtered over Celite[®] 545. The filtrate was then extracted with portions of DCM, washed with a saturated EDTA solution to remove traces of zinc products if any. The organic layer was then dried over sodium sulfate and evaporated in vacuo, yielding a foam-shaped yellow product that was stored in an inert atmosphere (glovebox) to avoid deterioration.
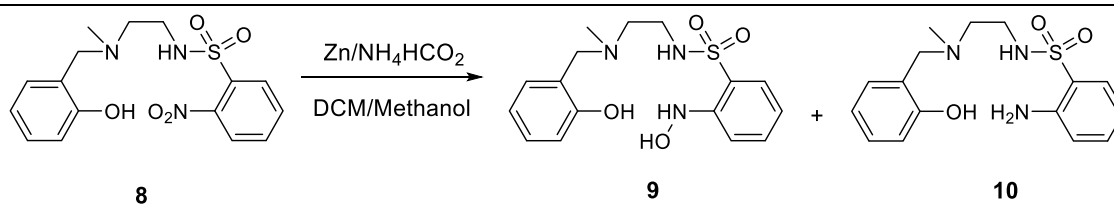


Figure 2.8. Reduction of $L^A$-NO$_2$ with zinc and ammonium formate.

The ratio of the various compounds in the final reaction mixture was assessed by ^{1}H-NMR by using the signals of the backbone methylene ($-CH_2-$) and knowing the characteristic signals for the nitro, hydroxylamine and amine ligands. Figure 2.9 shows an example of the measured ^{1}H-NMR for entry 1 from Table 2.2 below.
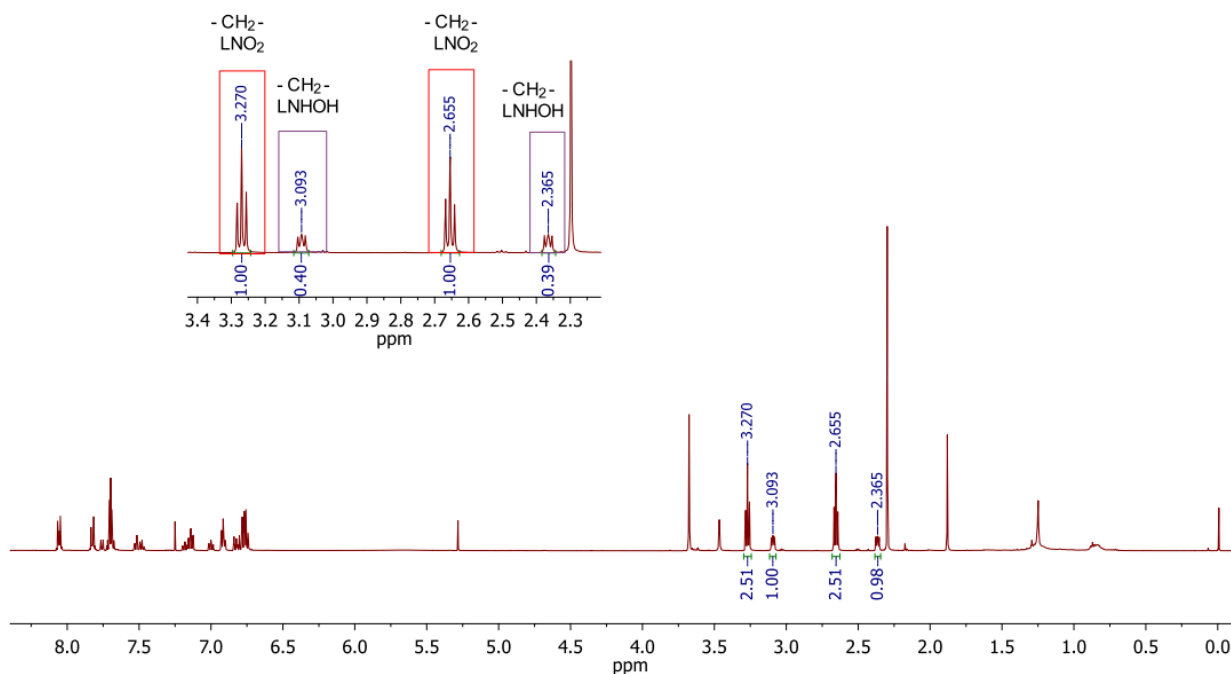
Figure 2.9. $^1$H-NMR of crude L$^A$-NHOH product.

In the optimization stage, we tried to observe the consequences of changing the amount of zinc, reaction time and temperature in the conversion of L$^A$-NO$_2$ to L$^A$-NHOH. Our optimization starting point was using the same mole ratios set up used previously in our group for reducing L$^A$-NO$_2$ with zinc (added in one shot) and ammonium formate. We observed that the reduction reaction at room temperature for 30 minutes (entry 1, Table 2.2) did not lead to total consumption of the nitro ligand while formation of hydroxylamine is accompanied with the production of a small amount of amine. Extending the reaction time to 1 h (entry 2, Table 2.2) did not lead to significantly more reduction of the hydroxylamine to the amine.

Table 2.2. Reduction of L$^A$-NO$_2$ at room temperature using zinc and ammonium formate.[a]

| Entry | DCM (mL) | Methanol (mL) | Zinc (eq.) | NH$_4$HCO$_2$ (eq.) | T (°C) | Time (min) | $^1$H-NMR Ratios[b] | | |
|---|---|---|---|---|---|---|---|---|---|
| | | | | | | | 8 (%) | 9 (%) | 10 (%) |
| 1 | 2 | 1 | 1.2 | 1.6 | 25 | 30 | 67 | 29 | 4 |
| 2 | 2 | 1 | 1.2 | 1.6 | 25 | 60 | 65 | 30 | 5 |

[a] Conditions: Reaction done in methanol and dichloromethane. Ligand used as one equivalent in this reaction. The yield of crude product for entry 1 and entry 2 obtained as and respectively.[b] purity assessed by $^1$H-NMR

Table 2.3. Reduction of $L^A$-$NO_2$ on ice bath using zinc and ammonium formate.[a]

| Entry | DCM (mL) | MeOH (mL) | Zinc (eq.) init. | Zinc (eq.) total | NH₄HCO₂ (eq.) | T (°C) | Time (h) | ¹H-NMR Ratios[b] | | |
|---|---|---|---|---|---|---|---|---|---|---|
| | | | | | | | | 8 (%) | 9 (%) | 10 (%) |
| **1** | 2 | 1 | 1.2 | 2 | 1.6 | 0 | 2 | 45 | 55 | 0 |
| **2** | 2 | 1 | 2 | 5 | 1.6 | 0 | 3 | 0 | 95 | 5 |
| **3** | 4 | 3 | 2 | 5 | 1.6 | 0 | 3 | 0 | 96 | 4 |
| **4** | 2 | 1 | 2 | 5 | 1.6 | 0 | 3.5 | 0 | 92 | 8 |
| **5** | 4 | 3 | 2 | 5 | 1.6 | 0 | 2.5 | | 98-100 | |

[a] Conditions: Reaction done in methanol and dichloromethane. Ligand used as one equivalent in this reaction
[b] purity assessed by ¹H-NMR

To prevent over-reduction of the hydroxylamine to the amine, we lowered the reaction temperature, while at the same time increased the amount of zinc in order to increase the rate of reduction from the nitro to the hydroxylamine. We initiated the reaction from 1.2 equivalents of zinc and reached the total of 2 equivalents in portion-wise addition during the course of the experiment (0.5 eq. every 15-20 min). Increasing the amount of Zn along while reducing the temperature to 0 °C increased hydroxylamine production and decreased the quantity of overly reduced amine (entry 1, Table 2.3). Increasing the total amount of zinc to 5 equivalent and the reaction time of 3 hours leads to 100% conversion with only a small amount of $L^A$-$NH_2$ **10** present (entry 2, Table 2.3). Increasing the amount of solvent, to ensure a more vigorous stirring and better mass transfer, did not affect the yield of $L^A$-NHOH **9** significantly (entry 3, Table 2.3). Extending the reaction time led to a larger quantity of over-reduced $L^A$-$NH_2$ **10** present (entry 4, Table 2.3). Therefore, in order to obtain $L^A$-NHOH **9** as pure as possible, we decreased the reaction time while monitoring the disappearance of $L^A$-$NO_2$ by TLC. Once no sign of remaining nitro is obvious by TLC, the reaction mixture was immediately filtered to remove solids and halt the reduction process. Several trials for best reaction result revealed that with a 2.5 h reaction time, we can obtain $L^A$-NHOH reproducibly with >98 % purity and in 80% yield. In conclusion, the optimized procedure entails: 2.5 h, 2 equivalents of initial Zn, and reaching total of 5 equivalents by aliquot addition (0.5 eq. Zn every 15-20 min) with this procedure, typically 154 mg (0.446 mmol) of $L^A$-$NO_2$ can be converted to $L^A$-NHOH that is sufficiently pure for complexation studies. We note, however, that scaling up the reaction requires consistent

monitoring for $L^A$-$NO_2$ consumption by TLC during the course of reaction. In case of the presence of starting material 0.5 eq. of zinc should be added at a time to the reaction and be monitored by TLC after 15 minutes. The $L^A$-NHOH should be used or stored in the inert atmosphere right away.

### 2.3.3   Reduction of $L^A_{tBu}$-$NO_2$ using zinc and ammonium formate

For the reduction of $L^A_{tBu}$-$NO_2$, we anticipated that larger quantities of zinc would be required to compensate for the steric hindrance imparted by the *tert*-butyl substituents. Still, we started the reaction with using the same reaction mol ratios set up for the optimized reduction of previous ligand, $L^A$-$NO_2$ (Figure 2.10).
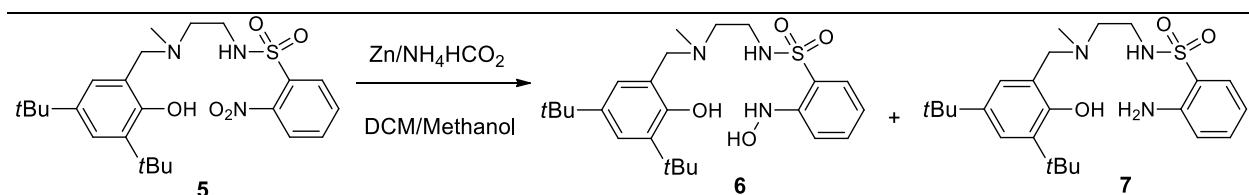


Figure 2.10. Reduction of $L^A_{tBu}$-$NO_2$ with zinc and ammonium formate.

We initiated the screening with 2 eq. of zinc and with portion-wise addition reached to 5 eq. For reaction time of 3.5 h (entry 1, Table 2.4), we observed the presence of nitro **5** and hydroxylamine **6** ligands without any formation of amine product **7**. Indeed, comparing with $L^A$-$NO_2$ ligand under the same conditions the nitro ligand is not completely consumed and trials in giving more reaction time did not increase the amount of hydroxylamine. Thus, to push conversion, we increased zinc up to 6 equivalent and carried out the reaction longer.

Table 2.4. Reduction of $L^A_{tBu}$-$NO_2$ on ice bath using zinc and ammonium formate.[a]

| Entry | DCM (mL) | MeOH (mL) | Zinc (eq.) init. | Zinc (eq.) total | $NH_4HCO_2$ (eq.) | Temperature (°C) | Time (h) | $^1$H NMR ratio [b] 6 (%) |
|-------|------|------|---|---|-----|---|-----|-------|
| 1 [c] | 4 | 3 | 2 | 5 | 1.6 | 0 | 3.5 | 76 |
| 2 [c] | 4 | 3 | 2 | 6 | 1.6 | 0 | 4 | 85-91 |
| 3 [d] | 4 | 3 | 2 | 6 | 1.6 | 0 | 4 | >99 |

[a] Conditions: Reaction done in methanol and dichloromethane. Ligand used as one equivalent in this reaction [b] purity assessed by $^1$H-NMR. [c] On 200 mg of **5**. [d] On 50 mg of **5**.

For larger quantities, around 200 mg of $L^A_{tBu}$-NO$_2$ **5**, several attempts showed production of hydroxylamine with respect to the nitro compounds with purities between 85-91% (entry 2, Table 2.4). However, smaller quantities (~50 mg) normally yield great purities of the hydroxylamine products (entry 3, Table 2.4). Reproducibility of the reaction for smaller quantities made us change the protocol for the synthesis of hydroxylamine in larger quantities. In the case of larger quantities after 4 h, the reaction should be monitored by TLC for any presence of nitro ligand. If observed, 0.5 equivalents of zinc along with 0.5 equivalent of ammonium formate should be added and reaction should be given more time to proceed. Monitoring should be made every 15 min and, if needed, the same amount of zinc should be added to the reaction mixture. The reason for the absence of a definite procedure for the reduction of $L^A_{tBu}$-NO$_2$ can be attributed to several factors. Even if with vigorously stirring, zinc dust sometimes does not properly mix, as some may stick to walls of the reaction flask, oxidation of zinc during the procedure is also possible. These physical issues thus result in more zinc consumption compared to the requirement of having two equivalents of the metal established for formal reduction mechanism of nitro ligand to hydroxylamine with zinc and ammonium formate. Hindrance of the bulky *tert*-butyl groups on the ligand may show more effect in reduction of large quantities nitro groups to reduce to hydroxylamine, by lowering accessibility environment for these moieties with metal surface. We also have tried the reaction at room temperature to check temperature effect on the formation and reactivity of hydroxylamine. In this case at 25 °C, $L^A$-NO$_2$ **8** gets reduced to the amine ligand (though in small quantities), while $L^A_{tBu}$-NO$_2$ **5** did not. Noteworthy, the yield of $L^A_{tBu}$-NHOH is not improved at 25 °C.

## 2.4 CONCLUSION

As a summary, the amine-based ligands, $L^A_R$-NO$_2$ (R = H, *t*Bu), show greater stability toward reduction using zinc and ammonium formate than the $L^I_R$-NO$_2$ ligands. The optimization methods enabled us to obtain $L^A$-NHOH and $L^A_{tBu}$-NHOH ligands with more than 85% yield and great purity. These procedures can be manipulated based on the quantities of under reducing nitro ligands. Even with high quantity the ease of the procedure give a plausible way to obtain NHOH ligands using zinc non-toxic compound, less solvent waste, ease of separation method and work-up and eventually a more green synthesis.

# Chapter 3.   Complexation of synthesized ligands with copper ions

**3.1  COMPLEXATION OF NITRO COMPOUNDS WITH COPPER(II)**

Previously synthesized $NO_2$ ligands structurally assure us that this functional group will not participate in the complexation with a transition metal (Figure 3.1). The X-ray structure of synthesized $L^I$-$NO_2$ by our past member, Fei Chen shows the formation of a square-pyramidal complex with a Cu(II) source in a 1:1 ligand-metal stoichiometry. The coordination to the Cu(II) centre happens via deprotonated phenol oxygen and deprotonated sulfonamide nitrogen, imine nitrogen and a water molecule at the equatorial position.[58] Following this result, we would like to understand the influence of ligand aromatic ring substitutions (R = $t$Bu or H), backbone structure (imine vs. amine moieties) and presence/absence of a base such as triethylamine (in order to facilitate the deprotonation of phenol and sulfonamide moieties) on complexation. We chose to work with Cu(II) sources due to its stability and lability. Performing UV-Vis (Ultraviolet-Visible) titrations contribute to a better understanding of how ligand structure and reaction conditions impact stoichiometry and binding constant in the complexation with a copper centre.
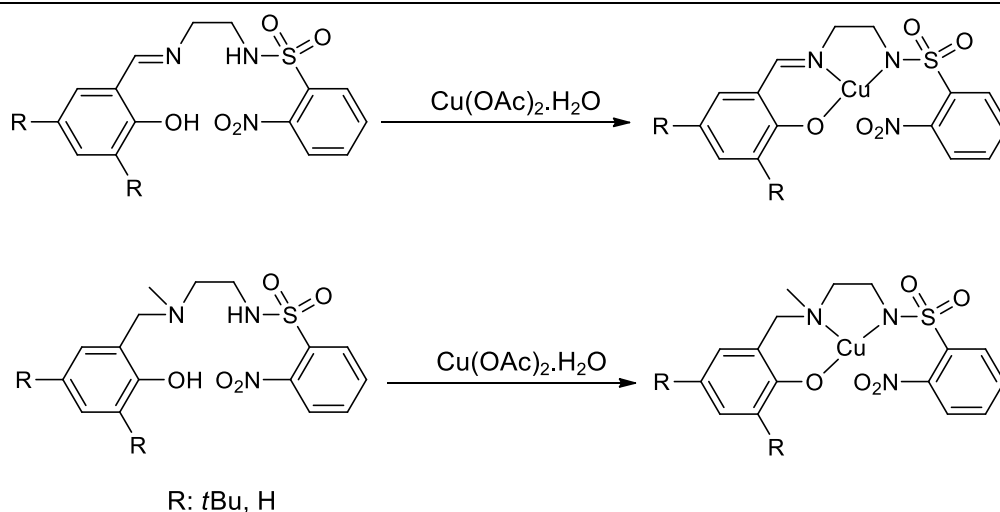


Figure 3.1. Complexation of $L^{A/I}{}_R$-$NO_2$ ligands with a copper(II) acetate.

UV-Vis titrations proceed by addition of a copper solution in aliquots of known concentration (in acetonitrile) to a known concentration of the ligand (in acetonitrile in which

ligand is soluble) in the UV-Vis quartz cell under stirring. Spectra are recorded after each addition (giving enough time for the band to form and stabilize). Figure 3.2 depicts the titration of $L^I_{tBu}$-NO$_2$ with copper(II) acetate (Cu(OAc)$_2$.H$_2$O). As shown in the spectrum, a band around 600 nm rises upon addition of the Cu(II) solution to the ligand solution, representing the formation of a complex. This band is later followed by a shift and growth at higher wavelengths (around 700 nm) due to the excess Cu(II).
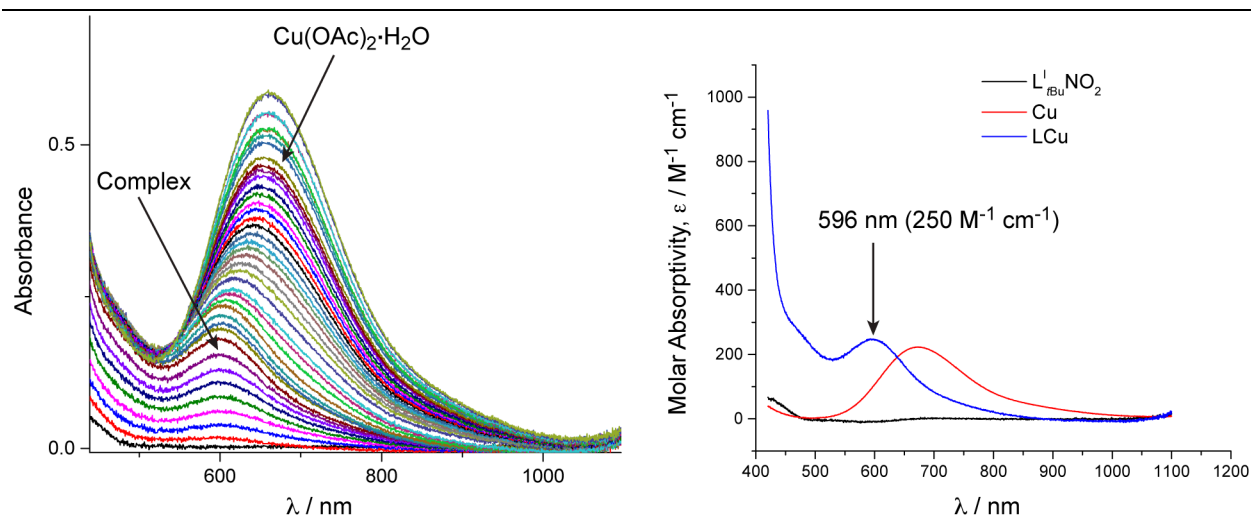


Figure 3.2. Titration of 1 mM $L^I_{tBu}$-NO$_2$ with 0-1 eq. Cu(OAc)$_2$.H$_2$O (left). Molar absorptivity and $\lambda_{max}$ of the complex (right).

Performing multivariate fitting of the data with a 1:1 L:M model led to a fit with small residuals, confirming a 1:1 stoichiometry for the complex. The software also extracts the spectrum for the pure complex, which exhibits a $\lambda_{max}$ of 596 nm with a molar absorptivity of 250 M$^{-1}$ cm$^{-1}$. Figure 3.3 shows the equivalence point of the complex formed based on the 1:1 stoichiometry of ligand to copper. At the beginning where no copper is added the concentration of the ligand is 1 mM (0.001 M). Upon addition of 0.1 equivalent Cu(II), we observed a decrease and increase in concentration of free ligand and free copper, respectively. Where two lines coincide is the stoichiometry point. In the case of $L^I_{tBu}$-NO$_2$ we see that this happens at a stoichiometry of 1 ligand per 1 copper ion. Therefore, the complex has 1:1 L:Cu ratio structure. After this point, there will be a slight deviation from a straight line for complex concentration due to the dilution effect.
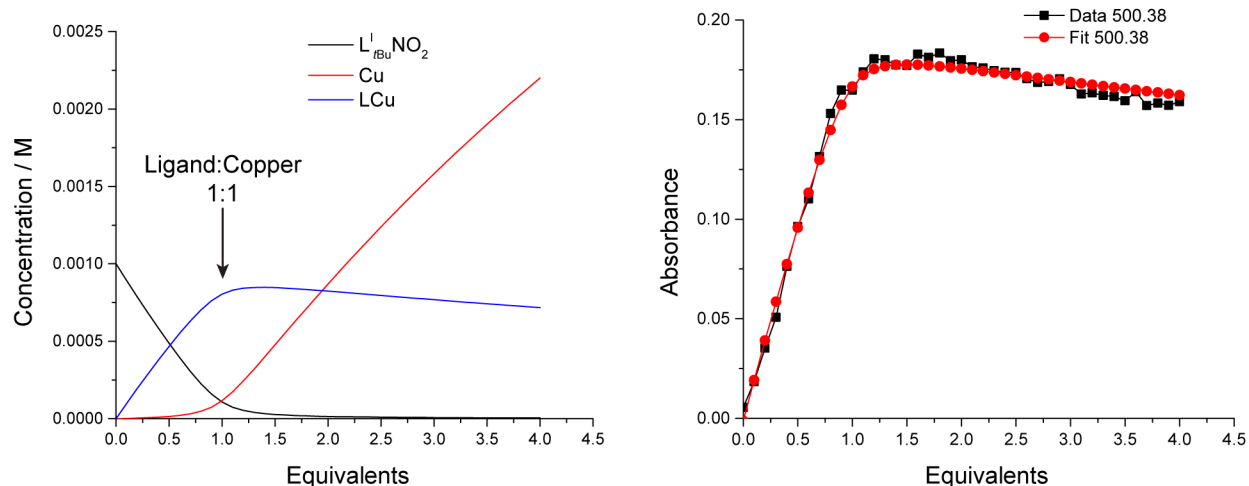
Figure 3.3. Stoichiometry of the complex formed based on $L^I_{tBu}$-$NO_2$ to copper ratio (left). Accuracy of the multivariate 1:1 fitting.

This titration was also performed in the presence of one equivalent of triethylamine as base. For each titration, we can obtain formation constants that are useful to account for which of these ligands form complexes with greater affinity. For comparison purposes, we here also show the titration of $L^A_{tBu}$-$NO_2$ with copper acetate without a base as shown in Figure 3.4. The titration of the ligand with Cu(II) forms two bands attributed to complex one in $\lambda_{max} = 478$ nm ($\varepsilon = 780$ M$^{-1}$ cm$^{-1}$) charge-transfer band and the other at $\lambda_{max}$ 632 nm ($\varepsilon = 425$ M$^{-1}$ cm$^{-1}$) for the complex d-d transition (Figure 3.4). The stoichiometry of the reaction is similar to that of $L^A_{tBu}$-$NO_2$ ligand with Cu(II) with 1:1 L:Cu ratio as shown in Figure 3.5.
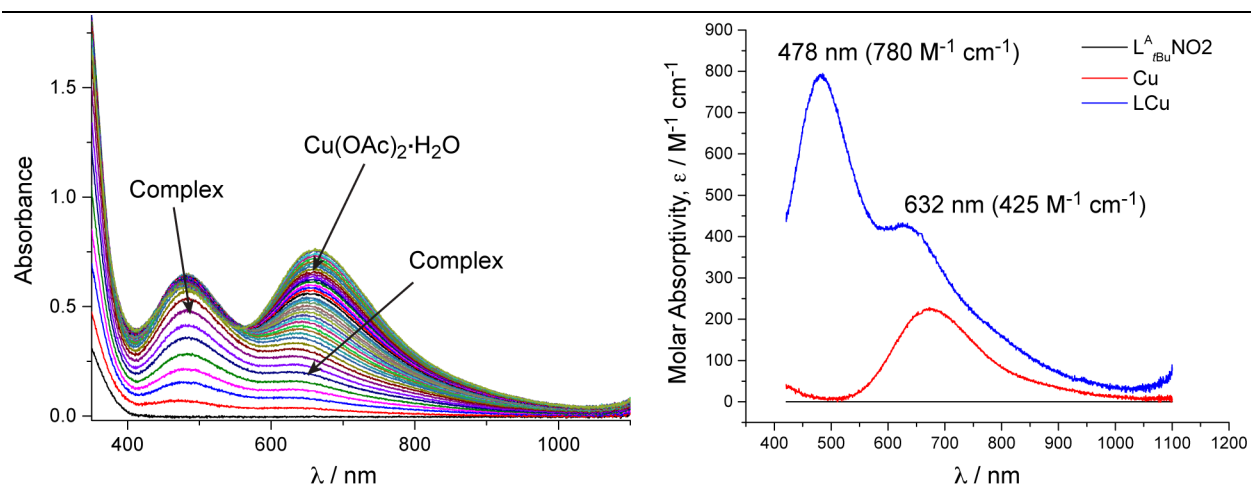
Figure 3.4. Titration of 1 mM $L^A_{tBu}$-$NO_2$ with 0-1 eq. $Cu(OAc)_2 \cdot H_2O$ (left). Molar absorptivity and $\lambda_{max}$ of the complex (right).
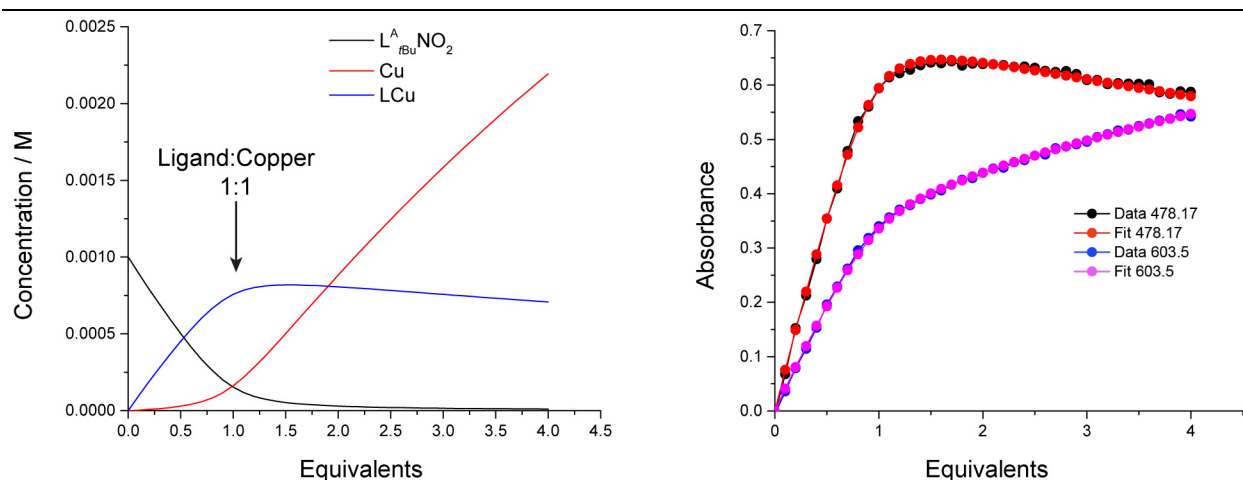


Figure 3.5. The stoichiometry of the complex formed based on $L^A_{tBu}$-$NO_2$ to copper ratio (left). Accuracy of the multivariate 1:1 fitting (right).

Table 3.1 comprises all the formation constants (log $K_f$) in the production of the complexes upon titration of ligands with Cu(II). $L^I_{tBu}$-$NO_2$ and $L^A_{tBu}$-$NO_2$ compared to ligands without *tert*-butyl substituents show relatively higher formation constants. In the presence of a base, they show slightly higher formation constants upon complexation with Cu compared with titrations performed without a base as it was expected for the ability of the base to ease the deprotonation of the ligand and drive the coordination to form stable complexes. As was expected, ligand structures with amine moieties relatively have higher formation constants than the imine moieties.

44

Table 3.1. Formation constants, maximum wavelength of absorption and molar absorptivity for the complexes formed with all synthesized four nitro ligands and copper centre.



| | $L^I_{tBu}$-NO$_2$ | $L^A_{tBu}$-NO$_2$ | $L^I$-NO$_2$ | $L^A$-NO$_2$ |
|---|---|---|---|---|
| log $K_f$ (without base) | 4.799 ± 0.006 | 4.487 ± 0.001 | 4.194 ± 0.008 | 4.695 ± 0.006 |
| log $K_f$ (with base) | 4.920 ± 0.013 | 4.916 ± 0.002 | 4.133 ± 0.014 | 4.250 ± 0.027 |
| $\lambda_{max}$ (nm) (without base) | 596 | 623 / 478 | 588 | 653 |
| $\varepsilon$ ( M$^{-1}$ cm$^{-1}$) (without base) | 246 | 426 / 781 | 143 | 111 |
| $\lambda_{max}$ (nm) (with base) | 600 | 636 / 472 | 616 | 655 |
| $\varepsilon$ ( M$^{-1}$ cm$^{-1}$) (with base) | 230 | 376 / 931 | 73 | 116 |

## 3.2 Reaction of Copper(II) with Lpy$_2$-NHOH

Aforementioned reduction of Lpy$_2$-NO$_2$ to Lpy$_2$-NHOH by hydrogenation using Pd/C provided the advantage of having a single hydroxylamine product without any further reduced amine product. This ligand is relatively stable and can be stored in the glovebox without degradation, making it ideal to work with compared to previously synthesized hydroxylamine ligands which are non-stable in the air and last only for a few weeks in the glovebox.

Titration of Lpy$_2$-NHOH with copper(II) acetate, without the addition of a base, gave the following results in Figure 3.6. Titration proceeds by addition of 0.1 mM aliquots of Cu(II) (in

acetonitrile) to a 1 mM solution of Lpy$_2$-NHOH (in dichloromethane, for solubility) under stirring. Results of the titration with triethylamine are similar to those without the base.
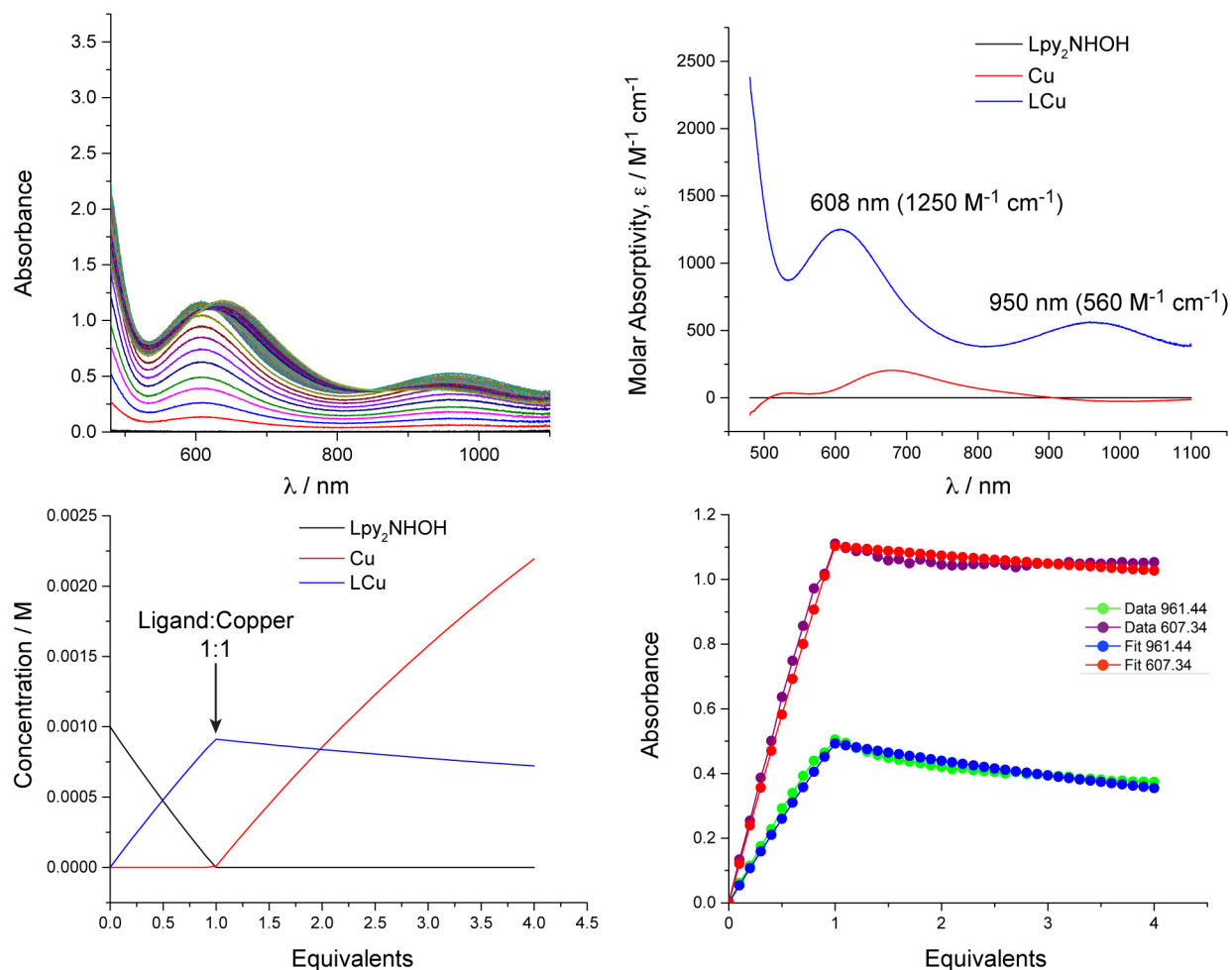


Figure 3.6. Titration of Lpy$_2$-NHOH with copper(II) acetate and multivariate fitting with a 1:1 ligand-to-Cu ratio.

The data is consistent with a 1:1 stoichiometry, i.e. formation of a complex incorporating one ligand for one Cu ion. Formation constants of the complexes are $8.811 \pm 0.398$ and $8.402 \pm 0.194$, respectively, for titration conditions with consumption of 1 equivalent base and without it. These high formation constants are consistent with the sharp "angle" at 1.0 equivalent in the titration profile (Figure 3.6 bottom). Despite dissimilarities in coordination environments, much higher formation constants than their NO$_2$ counterparts, this suggests that the NHOH function is involved in another event than mere coordination.

Obtaining an isolable complex was carried out reproducibly by reaction of Lpy$_2$-NHOH and Cu(OAc)$_2$.H$_2$O in 1:1 ratio (Figure 3.7). The main method of complex synthesis is to dissolve copper(II) acetate in acetonitrile (heating is required for solubilizing), which is then added dropwise to a stirring suspension of ligand in acetonitrile. While Lpy$_2$-NHOH is not completely soluble in acetonitrile, the addition of copper leads to an instantaneous colour change from yellow (ligand) to deep dark green. A dark green powder also precipitates, and the solution too is the same dark green, which suggests that the complex is partially soluble in acetonitrile. ESI-MS of the solid, re-dissolved in acetonitrile (dilute conditions), exhibits a single signal at $m/z = 474.1$ for [M+H]$^+$ with the expected isotopic pattern for $^{63/65}$Cu (Figure 3.8), corresponding to a formulation Lpy$_2$-NO-CuH$^+$, where the NHOH has formally been converted into a NO moiety. This result is confirmed by the elemental analysis of the solid (Table 3.2), which is in perfect agreement with the Lpy$_2$-NO-Cu formulation.
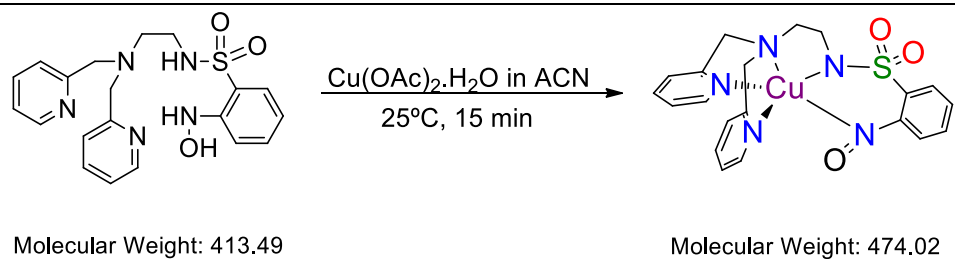


Figure 3.7. General synthesis procedure for the synthesis of Lpy$_2$-NO-Cu complex.
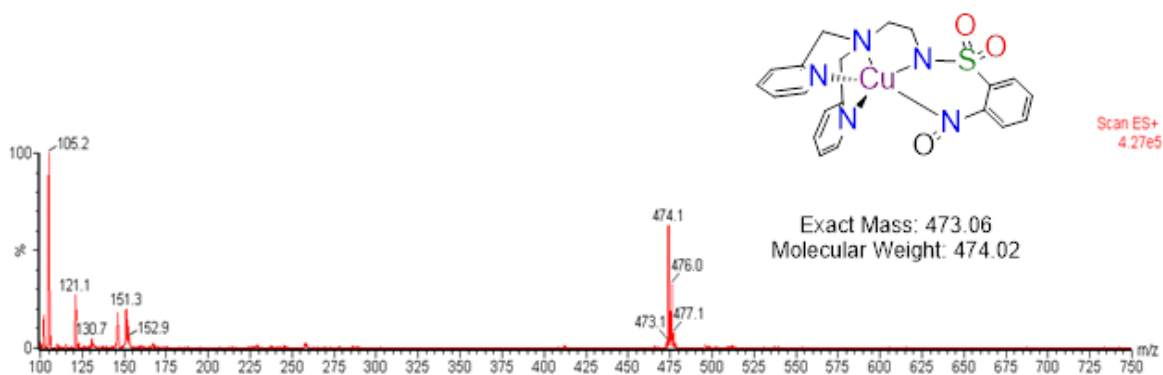


Figure 3.8. ESI-MS data of Lpy$_2$-NO-Cu.

Table 3.2. CHN analysis of Lpy$_2$-NO-Cu.

| | % Nitrogen | % Carbon | % Hydrogen | % Sulphur |
|---|---|---|---|---|
| Theoretical | 14.72 | 50.47 | 4.24 | 6.74 |
| Experimental | 14.77 | 50.68 | 4.25 | 6.76 |

Different methods of synthesis were tried, including using a different source of copper(II) (e.g. Cu(OAc)$_2$.MeCN), lower temperature (-30 °C) and various addition methods (drop-wise addition of ligand to copper, portion-wise addition of solid copper to ligand solution in acetonitrile or vice-versa), and all gave the same Lpy$_2$-NO-Cu product. The appearance of lone peak $m/z$ = 474, [M+H]$^+$ for all of the reaction conditions proved the reproducibility of this complex under numerous conditions. A good yield of 65-85 % is obtained for all reaction conditions. The reaction of the Lpy$_2$-NO-Cu ligand with a copper(I) source led to the formation of amine and nitroso products, which we believe stems from the disproportion of the hydroxylamine moiety. Using a 1:1 ratio of ligand and tetrakis(acetonitrile)copper(I) hexafluorophosphate in acetonitrile resulted in the formation of dark green solution after a few minutes, the product was tested by ESI-MS and data showed the peaks for $m/z$ = 474, [M+H]$^+$ of Lpy$_2$-NO-Cu complex as well as $m/z$= 459, [M] for the complex of Lpy$_2$-NH$_2$Cu (Figure 3.9).
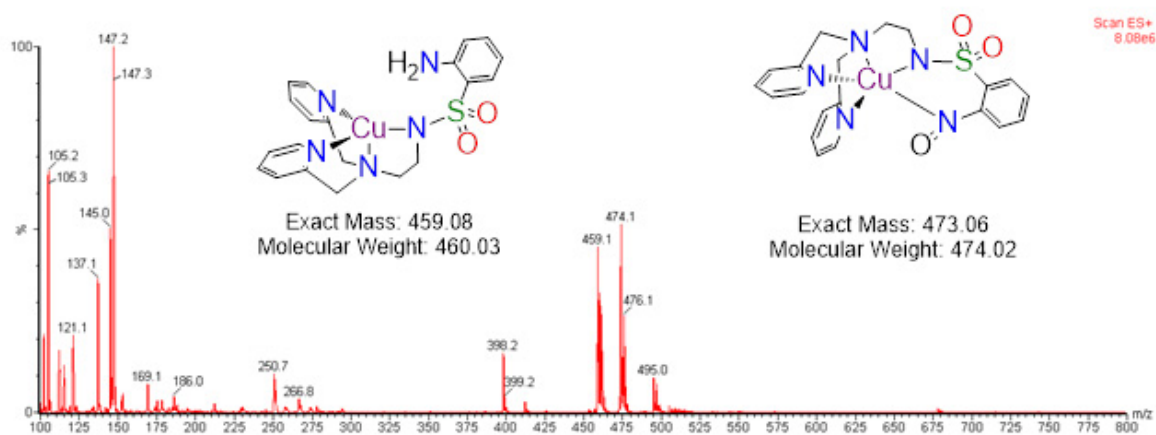


Figure 3.9. ESI-MS data of the reaction of Lpy$_2$-NHOH with [Cu(CH$_3$CN)$_4$](PF$_6$) after a few minutes in acetonitrile.

Crystals of the Lpy$_2$-NO-Cu complex were grown by placing solid ligand in a vial, covering it with a small quantity of acetonitrile, then layering with an acetonitrile solution of copper(II) acetate. We then added a layer of ether and placed the vial at −30 °C in the glovebox freezer. X-ray crystallography data obtained for the Lpy$_2$-NO-Cu complex crystal showed a neutral complex in distorted trigonal bi-pyramidal (TBP) geometry (Figure 3.10). Since the sulfonamide is deprotonated, two hypotheses are possible for the electronic structure of the complex. On one hand, the copper ion is Cu(I) and the NO moiety is a nitroso ($C$−N=O), on the other hand, the copper ion is Cu(II) and the NO moiety is a one-electron reduced aminoxyl anion, $C$−NO$^{•/−}$. With N3−Cu−N1 and N3−Cu−N5 bond angles of 178.1(2)° and 80.1(12)°, respectively, Cu is exhibiting a distorted TBP geometry, which is generally favoured for the Cu(II) oxidation state. The NO bond length, N1−O1 = 1.300(6) Å is quite near the far end for monomeric N-bonded nitroso molecules: 1.209(3)-1.31(2) Å and longer than in monomeric nitrosoarenes (1.13-1.29 Å)[23]. This suggests a reduced bond order of the NO moiety and is in favour of a Cu(II)-aminoxyl formulation.
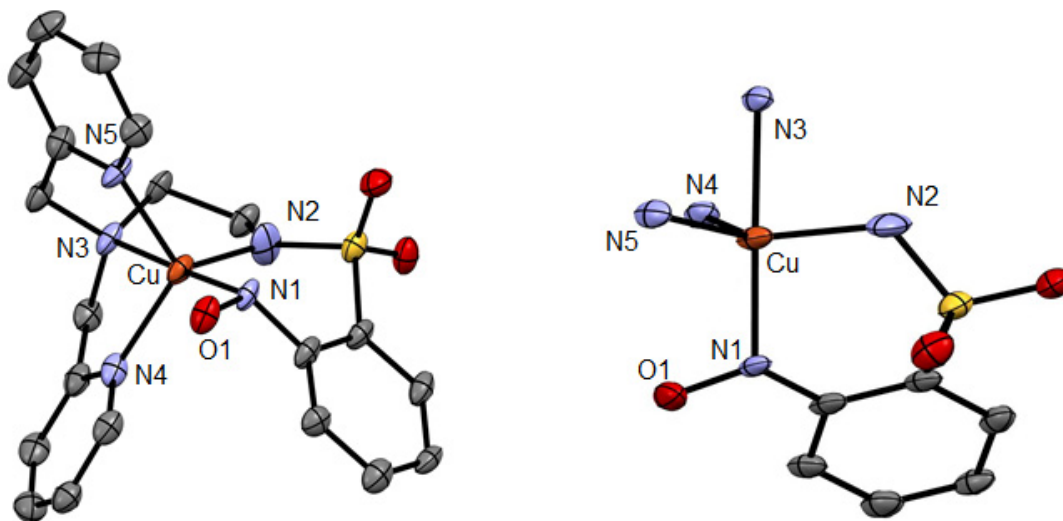


Figure 3.10. ORTEP representation of Lpy$_2$-NO-Cu.$^a$
$^a$ 50% ellipsoid probability. Hydrogen atoms are omitted for clarity. Selected bond lengths (Å) and angles (°): O1-N1 1.300(6), Cu1-N1,1.949(5); Cu1-N5, 2.121(4); N3-Cu1, 2.110(5); Cu1-N4, 2.036(5); Cu1-N2, 1.935(6); N2-Cu1, 1.935(6); N5-Cu1-N4, 112.7(2); N4-Cu1-N3, 81.5(2); N3-Cu1-N2, 83.0(2); N2-Cu1-N5, 116.8(2); N2-Cu1-N4, 124.1(2); N2-Cu1-N1, 95.7(2); N5-Cu1-N1, 99.4(2); N3-Cu1-N1, 178.1(2); N3-Cu1-N5, 80.1(2).

$^1$H-NMR spectra of the Lpy$_2$-NO-Cu complex, in CDCl$_3$ (Figure 3.11) or DMSO-d$_6$, are clearly paramagnetic, with signals extending from −75 to +45 ppm. The Cu(I)-nitroso species would be completely diamagnetic therefore the NMR data is clear evidence that the complex is a Cu(II)-aminoxyl species. The hypothesis of a Cu(II)-aminoxyl $==$ Cu(I)-nitroso valence tautomerism was also discarded based on fact that all signals for a single species are accounted for. Specifically, total integration leads to 20 H, as expected. However, the two CH$_2$ groups in the CH$_2$−py arms do not integrate to a single 4H signal, but rather appear as two signals of 2H integration each. This is consistent with a semi-rigid molecule whereby one C-H bond in each CH$_2$-py is in an "axial" conformation and the other in an "equatorial" conformation, as can be seen in the X-ray structure. The signals do not coalesce even at +90 °C, indicating a very slow exchange between these positions (see VT-NMR section below).
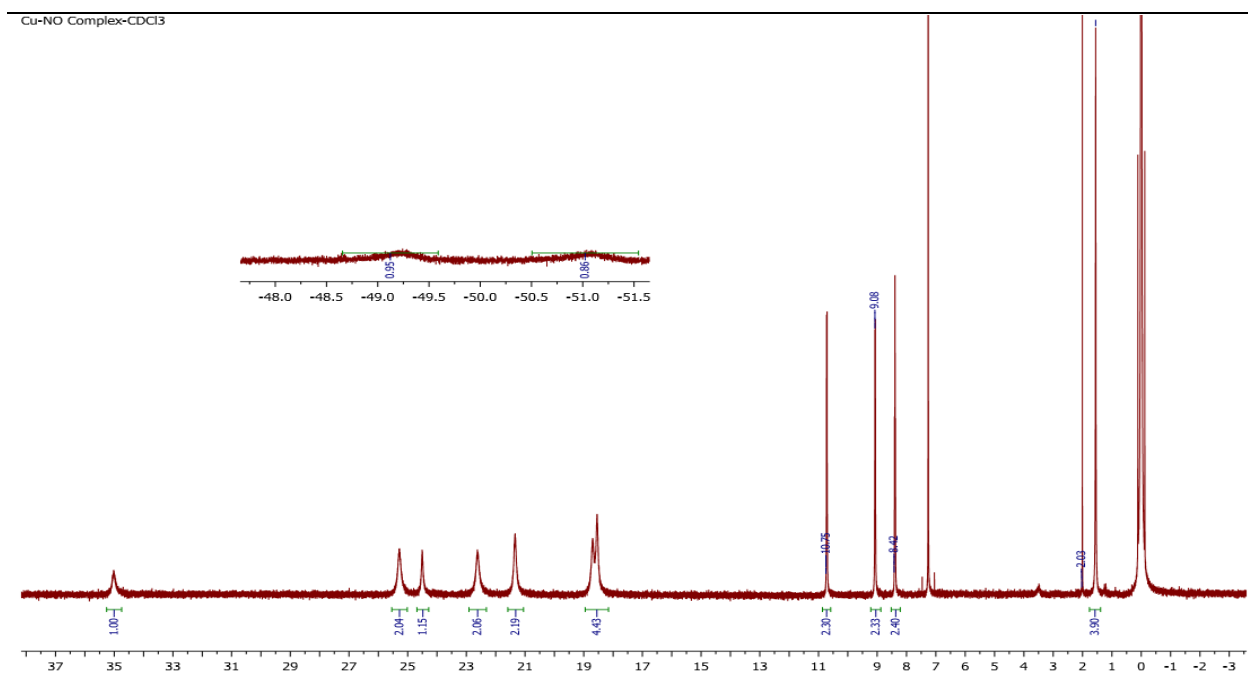


Figure 3.11. $^1$H-NMR (500 MHz) of Lpy$_2$-NO-Cu in CDCl$_3$.

## 3.3 MAGNETIC STUDIES ON LPY$_2$-NO-CU

Because Lpy$_2$-NO-Cu contains two paramagnetic centres, Cu(II) with a $S = \frac{1}{2}$ and the radical with a $S = \frac{1}{2}$, it is expected to exhibit interesting magnetic properties. The coupling of unpaired electrons emerges from the interaction of their spin angular momentums or spin-spin

coupling. Antiferromagnetic ($S = 0$) vs. ferromagnetic ($S = 1$) coupling of spins of two unpaired electrons results in decrease and increase in spin angular momentum, respectively.

Paramagnetic compounds having a non-zero spin or orbital angular momentum are attracted to the applied magnetic field ($H$).[59] Paramagnetism is a characteristic of salts, certain complexes of transition metals, odd-electron molecules and free radicals bearing an unpaired electron in their structure.[60] In contrast, diamagnetic compounds having no unpaired electrons are repelled by external magnetic field. Induced magnetic moment (magnetization) $M$, of the compound, is related to the applied magnetic field $H$ with a proportionality constant $\chi$ ($M = \chi.H$).[1] Magnetic susceptibility, $\chi$, is the measurement of the strength of attraction or repulsion of the studied compound to the magnetic field. Paramagnetic and diamagnetic compounds have positive and negative $\chi$, respectively.[1,59] In magnetochemistry, we use the molar susceptibility, $\chi_M$, expressed in emu mol$^{-1}$ units. Electron Paramagnetic Resonance (EPR) spectroscopy, which is commonly used to probe the electronic structure of paramagnetic species, did not exhibit any signal for Lpy$_2$-NO-Cu. This is not surprising because diamagnetic species are EPR-silent, and $S = 1$ (triplet) species are effectively EPR silent in a perpendicular cavity mode, as was the case on the instrument we used.

To understand the magnetic properties (magnetic moment) of the complex in the solid state, Superconducting Quantum Interference Device (SQUID) measurements were performed by expert collaborators, Prof. Muralee Murugusu and his PhD student Katie Harriman at the University of Ottawa. The measurements on different batches of Lpy$_2$-NO-Cu solid conclusively provided no signal. This is consistent with either a diamagnetic Cu(I)-nitroso formulation or a Cu(II)-NO$^{\bullet/-}$ species with two very strongly antiferromagnetically coupled spin centres, Cu(II) and NO$^{\bullet/-}$. Because of the X-ray data, in the solid state too, showing a TBP Cu ion and an elongated NO bond, the Cu(II)-NO$^{\bullet/-}$ formulation is the most plausible.

Solution $^1$H-NMR recorded at room temperature of the complex showed paramagnetically shifted wide peaks which require the existence of paramagnetic Lpy$_2$-NO$^{\bullet/-}$-Cu(II) in solution. Evans NMR method was therefore used to estimate the molar paramagnetic susceptibility ($\chi_P$) of the complex in solution.[61,62,63] The Evans method measures the influence of paramagnetic solute on the change in the chemical shift of an inert reference compound (e.g. TMS or residual solvent peak) in pure solvent vs. in the paramagnetic solution.[63] Lpy$_2$-NO-Cu complex was thus dissolved in d$_6$-dimethyl sulfoxide (DMSO-d$_6$ with TMS) under N$_2$ in an Evans tube containing a

capillary filled with the DMSO-d$_6$/TMS solvent. A $^1$H NMR spectrum was recorded at room temperature. Paramagnetic susceptibility can be calculated with the following equation:

$$\chi_P = \frac{1000\ \delta v}{v0\ Sf\ C} - \chi_D$$

where:

$\delta v$ is the difference in frequency of the reference (TMS) signal, in Hz;

$v_0$ is the frequency of the NMR spectrometer in Hz,

$C$ is the sample concentration (mol L$^{-1}$)

$S_f$ is a structure factor equal to $4\pi/3$.

Diamagnetic susceptibility ($\chi_D$) is an intrinsic characteristic of all atoms in a molecule and this hidden diamagnetism in a paramagnetic compound can be calculated by summing up all tabulated empirical Pascal's constants for atoms ($\chi_{Di}$) and bonds ($\lambda_i$) in the complex.[59] The calculated paramagnetic susceptibility ($\chi_P = 8.211277 \times 10^{-4}$ emu mol$^{-1}$) is then converted the $\chi_P T$ product, expressed in emu K mol$^{-1}$. For Lpy$_2$-NO-Cu, a value of $\chi_P T = 0.2448$ emu K mol$^{-1}$ was estimated.

The expected $\chi T$ value for a single $S = \frac{1}{2}$ centre is 0.375 emu K mol$^{-1}$ (Curie law). Therefore, for a complex such as Lpy$_2$-NO-Cu with two $S = \frac{1}{2}$ centres, a value of 0.75 emu K mol$^{-1}$ is expected if the two spin centres were not interacting. Hence, the low $\chi T$ product of 0.2448 emu K mol$^{-1}$ for Lpy$_2$-NO-Cu indicates that the two spin centres are antiferromagnetically coupled, i.e. that the complex has a $S = 0$ spin ground state resulting from the antiparallel alignment of the two coupled individual $S = \frac{1}{2}$ momenta, and a $S = 1$ spin excited state resulting from the parallel alignment of the two coupled $S = \frac{1}{2}$ momenta (Figure 3.12).
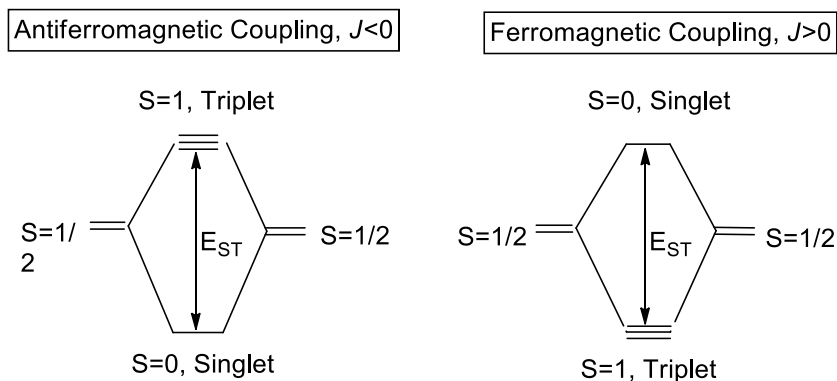


Figure 3.12. Energy level diagram of antiferromagnetic and ferromagnetic coupled systems.

In this case, the singlet-triplet energy difference, $E_{ST}$, is equal to the coupling constant, $J$ expressed in the Heisenberg-Dirac-Van Vleck (HDVV) Hamiltonian operator in an empirical description for spin-spin coupling of two unpaired electrons:[64]

$$\hat{H}_{12} = -J\,\hat{S}_1 \cdot \hat{S}_2$$

Derivatizing this equation on two interacting $S = \frac{1}{2}$ centres leads to the behaviour indicated on Figure 3.13, representing the $\chi T$ value as a function of temperature $T$ for different value of $J$, either positive (ferromagnetic coupling) or negative (antiferromagnetic coupling).[64] The $\chi T$ value for Lpy$_2$-NO-Cu at 298 K gives an estimate of $J \sim -300$ cm$^{-1}$, but this value is highly imprecise due to the lack of precision in measuring the chemical shift difference (0.07 ppm in this case).
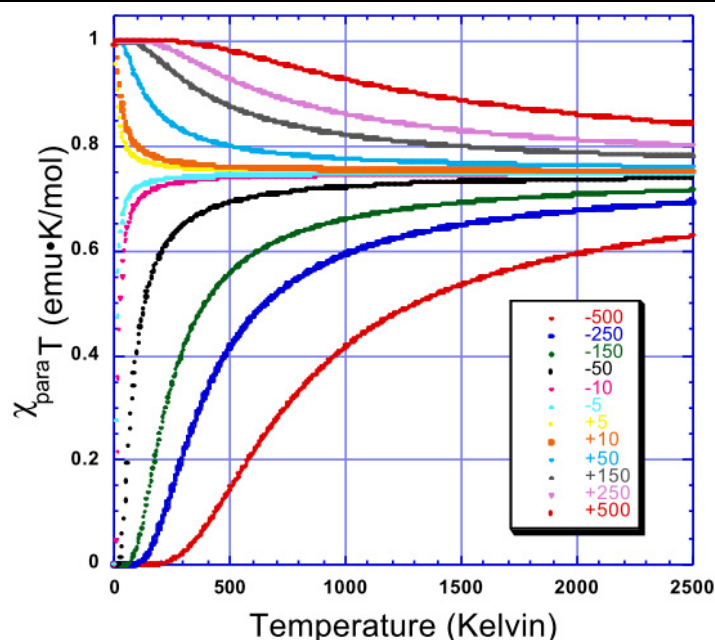


Figure 3.13. $\chi T$ vs. T plot at different values of the coupling constant for two $S = \frac{1}{2}$ centres.[64]

To get a more precise value for the exchange parameter $J$ in Lpy$_2$-NO-Cu, we performed variable-temperature $^1$H-NMR (VT-NMR) in the range 25-90 °C in DMSO-d$_6$ under nitrogen gas (Figure 3.14 and Figure 3.15). The complex shows complete stability towards increasing the temperature: the same NMR spectrum was obtained by reversing the temperature back to 25 °C. with paramagnetically shifted peaks from $\sim -72$ to $+45$ ppm and no extra peaks that would come from a decomposition product.

53
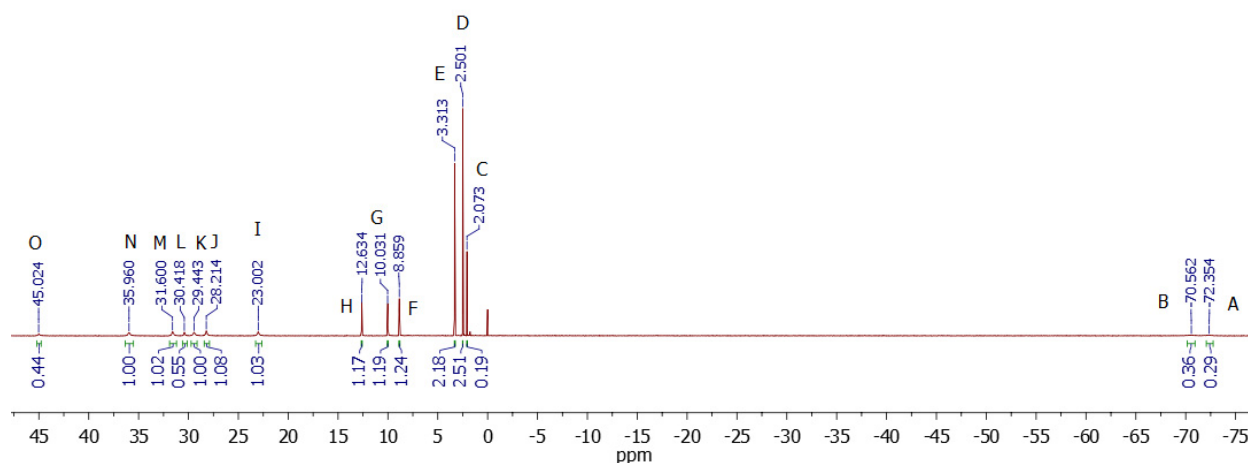
Figure 3.14. $^1$H NMR of Lpy$_2$-NO-Cu in DMSO-d$_6$ under N$_2$ at 25 °C.
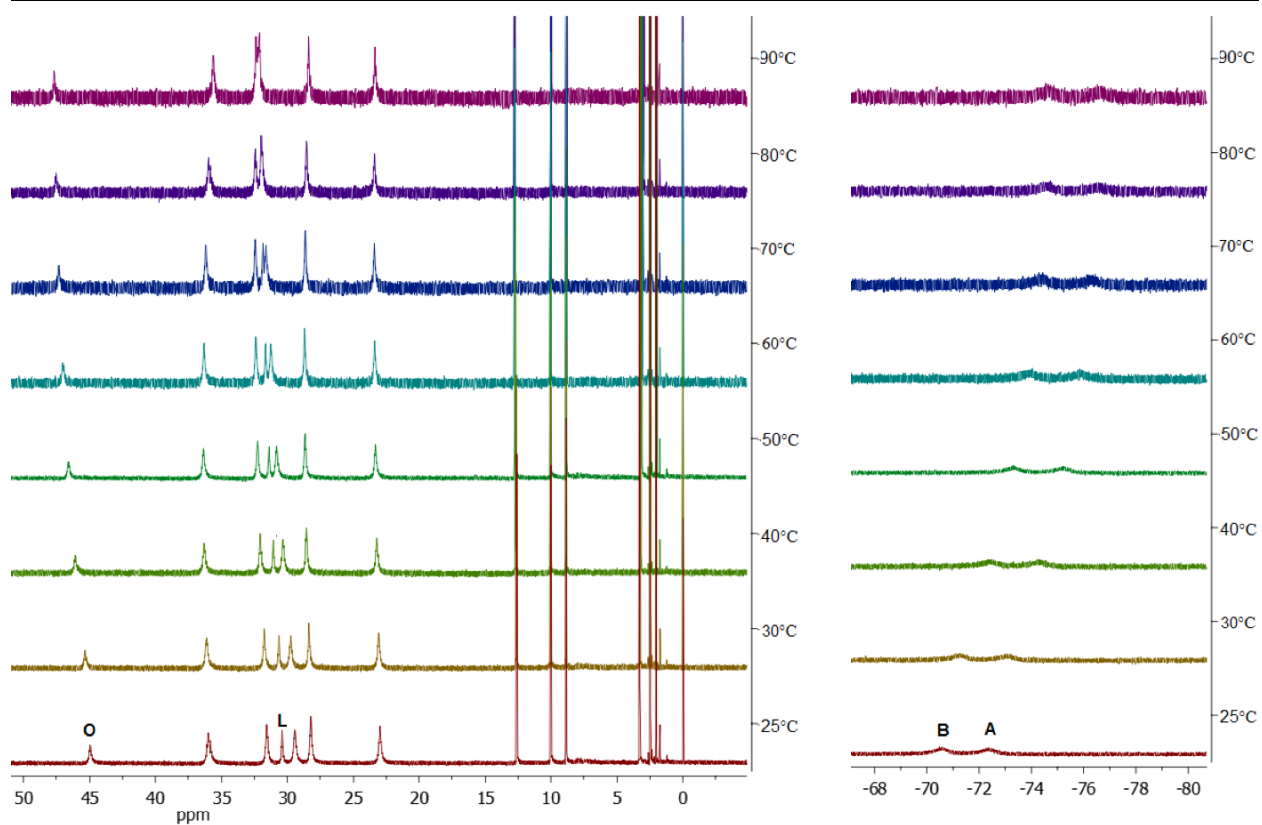


Figure 3.15. $^1$H VT-NMR of Lpy$_2$-NO-Cu in DMSO-d$_6$ under N$_2$ at 25-90 °C.

To calculate exchange parameter $J$, the VT-NMR data four signals of integration 1H corresponding to the radical ring (peaks A, B, L and O in all temperatures) were fitted based on a global fit by assigning one $J$ value for all signals: [65]

54

$$\Delta\delta= \frac{g\beta A}{\left(\frac{\gamma}{2\pi}\right)KT}(3 + e^{-J/KT})^{-1}$$

They show plausible fitting with $J \sim -420$ cm$^{-1}$ for the triplet-singlet state which also is a sign of a very strong antiferromagnetically coupling between two spins. The fitted data are demonstrated with lines; other signals were not fitted are presented by dots in Figure 3.16. Due to the fluxional behavior of the CH$_2$−py moieties, all other signals do not fit this equation.
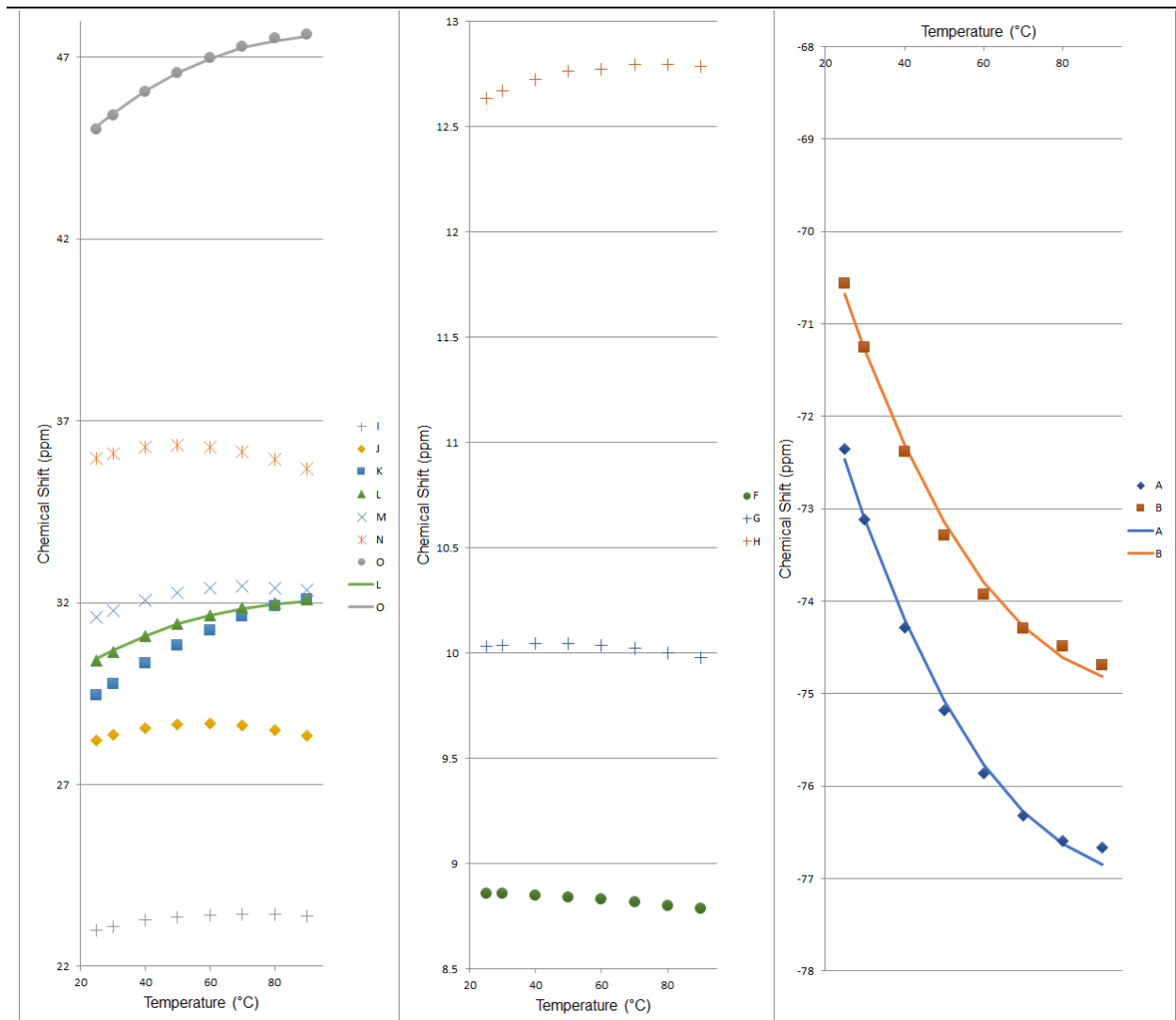


Figure 3.16. Temperature dependence of the individual chemical shifts of Lpy2-NO-Cu, with line, fits for the protons on the aromatic radical moiety.

Preliminary DFT calculations on the triplet state and broken symmetry singlet state were performed by Mohammad Askari, which suggested close energy gap between triplet vs. singlet

state with triplet state with $J$ of $-400$ cm$^{-1}$, close to the value estimated by VT-NMR. The Yamaguchi formula was applied for this calculation:[66,67]

$$J = \frac{E^{BS} - E^T}{<S^2>^T - <S^2>^{BS}}$$

The DFT optimized structures for the singlet and triplet states of the Lpy$_2$-NO-Cu are shown in Figure 3.17. The small structural variation between the two structures is indicative of the proximity of the energies of the two states. The Cu−N bond lengths in the singlet molecule range from 2.011 to 2.325 Å and in the triplet, is in the 1.959-2.206 Å. The shortening of the C−N bonds in the triplet state indicates the presence of Cu(II) oxidation state. In comparison to the crystal structure where the Cu−N bonds range from 1.935-2.121 Å, the singlet state seems to be closer geometrically to experimental data. However, the possibility of Cu(II) with a radical anion coupled antiferromagnetically cannot be overruled. The N-O bond length is the most sensitive parameter to the spin state of the molecule and in the crystal, structure the N-O bond is found to be 1.301(6) Å. In the DFT optimized structures, the N-O bond lengths are 1.252 Å and 1.284 Å for the singlet and the triplet states, respectively. The close proximity in the N-O bond lengths between the crystal structure and the DFT optimized triplet state is indicative of a reduction in N-O bond order in this complex thus supporting the broken symmetry singlet formalism and an antiferromagnetically coupled system.



DFT optimized structures

Singlet state                    Triplet state
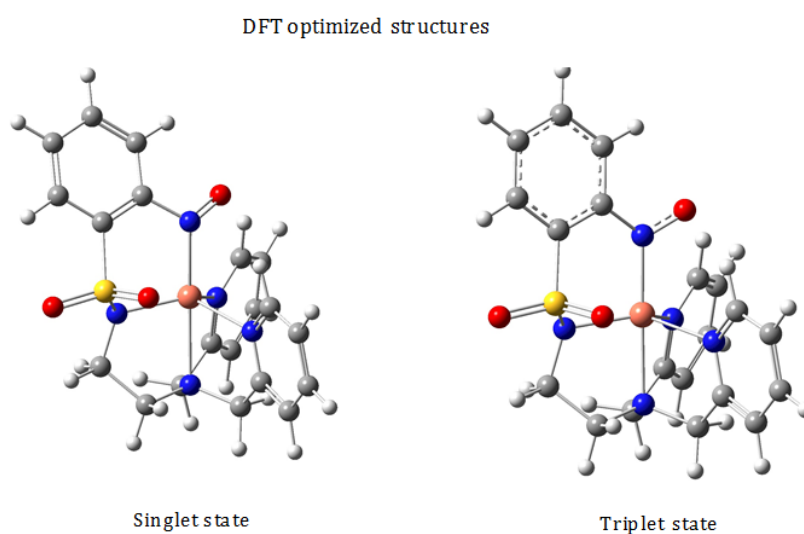
Figure 3.17. DFT-calculated triplet and singlet states for Lpy$_2$-NO-Cu.

The redox chemistry of Lpy$_2$-NO-Cu was more analyzed by cyclic voltammetry (Figure 3.18), which shows an oxidation process at low potential (−187 mV vs. Fc). It also shows a reversible reduction at very low potential (−1.5 V vs. Fc). The wide gap between the two waves indicates that the complex is thermodynamically stable over a wide range of potential, indicating how coordination of a radical to a metal centre increases its stability.
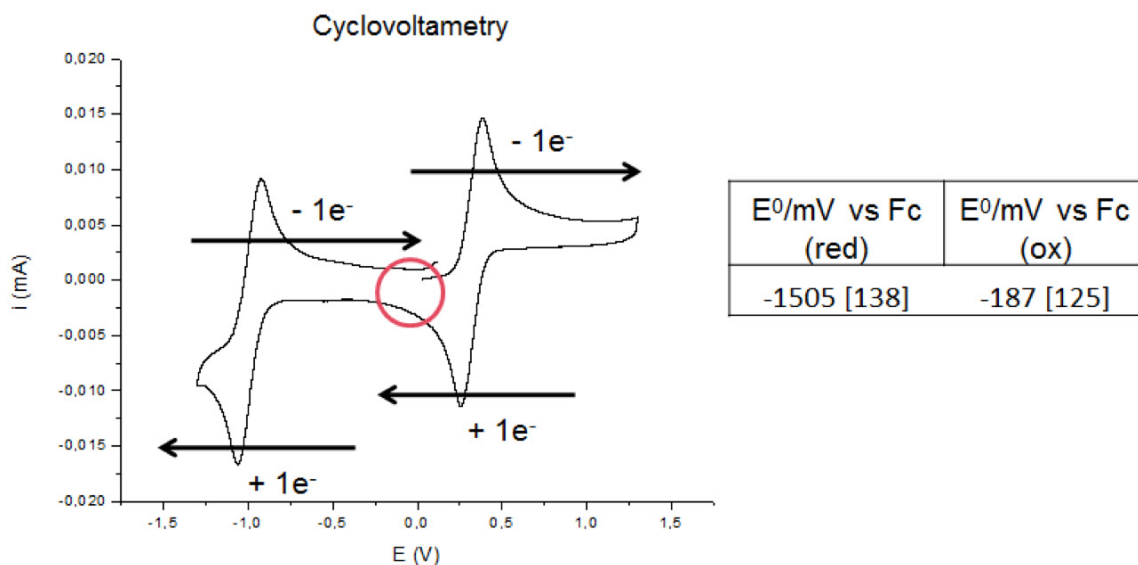


Figure 3.18. Cyclovoltammetry of 1 mM Lpy$_2$-NO-Cu in CH$_2$Cl$_2$ with 0.1 M $n$Bu$_4$PF$_6$ as supporting salt, at 25 °C and a 100 mV/s scan rate. Reference electrode: AgNO$_3$ (1.0 mM)/Ag in 0.1 M $n$Bu$_4$ClO$_4$ in acetonitrile.

Spectroelectrochemistry was performed upon oxidizing a solution of Lpy$_2$-NO-Cu after the first oxidation peak (0.8 V vs. the reference electrode) and following the evolution of the absorption spectrum in situ with fiber optics (Figure 3.19). The 1e$^-$-oxidation of the complex shows the increase one absorption increase around 400 nm and, more importantly, a decrease of the features at the lower energy around 450, 610 nm and in the near-infrared (ca. 1100 nm). This suggests a loss of the radical nature of the ligand, yielding a Cu(II)-nitroso species. We are currently probing this hypothesis with time-dependent DFT calculations, as well as experimental preparation of the oxidized species.
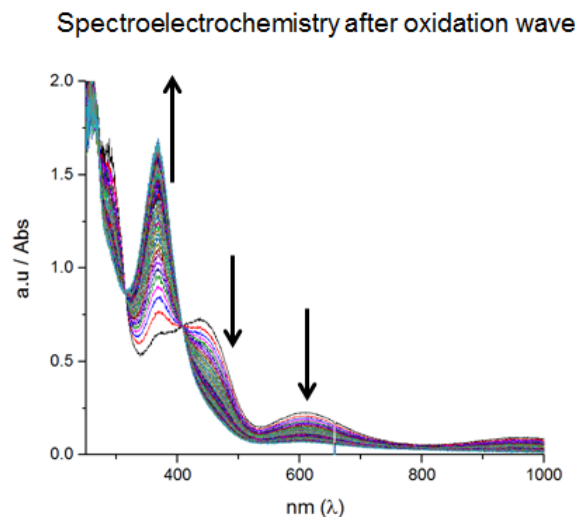
Figure 3.19. Spectral evolution of the Lpy$_2$-NO-Cu solution during spectroelectrolysis upon oxidation beyond the first oxidation wave.[a]

[a] CH$_2$Cl$_2$, 25 °C. Concentration of the complex is 1 mM, but the absorbance in this figure cannot be converted to molar absorptivity because the light is partly absorbed by the platinum grid electrode.

## 3.4 CONCLUSION

The synthesized complex Lpy$_2$-NO-Cu in solution shows strong antiferromagnetic coupling between two spin centres of Cu(II) and NO anion radical. This has been substantiated by calculation of exchange parameter in VT-NMR and DFT calculations. More studies on the complex are underway to fully describe its electronic structure. Preliminary experiments have revealed that the complex, despite containing an accessible radical, is very stable and displays little reactivity in H-atom abstraction reactions (homolytic cleavage of weak C−H bonds) or in reactions with nucleophiles (e.g. phenolates or other Cu(I) species).

# Chapter 4. Conclusion

In conclusion, the possibility to study the redox properties of hydroxylamine (*C*-NHOH) groups near a Cu(II) centre is highly dependent on the availability of stable ligands with a pendant NHOH function. We have shown the synthesis of $L^{I/A}_R$-$NO_2$, R = H, *t*Bu with pendant nitro moieties and have optimized their partial reduction to NHOH-containing ligands. The salen-type ligands containing amine linker ($L^A_R$-$NO_2$, R = H, *t*Bu) backbone were preferred over ligands with imine ($L^I_R$-$NO_2$, R = H, *t*Bu) due to decomposition of these ligands ($L^I_R$-NHOH) in purification methods. The partial reduction of $L^A_R$-$NO_2$ ligands using zinc and ammonium formate were studied and the optimization for this reaction was achieved. The reduction of $L^A$-$NO_2$ to $L^A$-NHOH achieved in high yield 80% and > 98% purity using 5 equivalent of zinc, 1.6 equivalent of ammonium formate at 0 °C in dichloromethane and methanol. The $L^A_{tBu}$-NHOH also were synthesized with 85-91% purity using 6 equivalents of zinc and 1.6 equivalent of ammonium formate at 0 °C in dichloromethane and methanol. The procedure for reduction of large quantities of $L^A_{tBu}$-$NO_2$ was proposed by the addition of half equivalents of zinc in aliquots and monitoring the nitro ligand consumption by TLC. The procedure assures the production of hydroxylamine ligands using least amount of solvents and using non-toxic commercially available zinc dust. The activation of zinc dust before each synthesis is necessary to provide the fresh surface of metal. Although mechanical stirring is present to ensure the efficient mass transfer, sometimes zinc does not enter the reaction mixture because of sticking to the reaction flask. In longer reaction, the formation of zinc oxide is possible. This issue obliges the addition of zinc higher than two equivalent required for formal reduction of nitro groups using metals as reducing agent.

Synthesizing hydroxylamine ligands enabled the study of the interaction of the ligands with Cu(II) ions. UV-Vis titrations of the $NO_2$ ligands with Cu(II) salts provided insight into the ligand-field strength of the ligands and the stoichiometry of complex. Using the multivariate fitting for 1:1 L:Cu model we obtained the formation constant, molar absorptivity and $\lambda_{max}$ for $L^{I/A}_R$-$NO_2$, R = H, *t*Bu. All complexes display similar formation constants, which is not unexpected given their similar structures. The titration of Lpy$_2$-NHOH with Cu(II) showed a

59

much higher formation constant (log $K_f \approx 8.8$), indicating the presence of an additional redox reaction upon Cu(II) coordination.

The $L^A_R$-NHOH ligands do react with Cu(II) salts in a rapid manner. However, we were unable to extract a well-defined complex from these darkly coloured solutions. In the absence of a well-defined procedure that leads to a single or a few separable products, no convincing conclusion can be made on the nature of the reaction. It is certain that redox event occurs, but given the wide redox landscape of NHOH/NO group presented in the introduction, we cannot currently propose a reaction pathway.

Ligand Lpy$_2$-NHOH, which had been reacted with Fe(II) salts in the past, led to a more fruitful outcome. Upon reaction with Cu(II), as delineated above, a single product could be extracted with a Lpy$_2$-NO-Cu formulation. Characterized structure of the Lpy$_2$-NO-Cu using X-ray crystallography suggested the elongated band for N-O 1.300(6) Å is quite near the far end for monomeric N-bonded nitroso molecules: 1.209(3)-1.31(2) Å and longer than in monomeric nitrosoarenes (1.13-1.29 Å). The paramagnetically shifted peaks in ^{1}H-NMR of the complex suggested the presence of a paramagnetic compound Cu(II)-aminoxyl anion. Evans NMR measurements suggest a strong antiferromagnetically coupling between two centres. VT-NMR experiments led to a $J$ value of $-420$ cm$^{-1}$, showing strong antiferromagnetically coupling of two centres. The CH$_2$−py peaks were not globally fitted due to axial fluxional. The DFT calculations suggested ground triplet state with $J$ value of $-400$ cm$^{-1}$ to be a sign of antiferromagnetically coupled centres.

Further work, including advanced electrochemistry, EPR of the oxidized and reduced products, as well as time-dependent DFT calculations, will further highlight the unique properties of this complex and its redox interconversion to other complexes having a NO moiety. From these studies, a more detailed picture will emerge, which will clarify our understanding of the stabilization effect of the Cu ion onto the radical state of the ligand, a state that is extremely reactive on purely organic nitroso species.

# Chapter 5. Experimental Section

## 5.1 SYNTHESIS

All used chemicals were obtained from Alfa Aesar and Sigma-Aldrich. Solvents for air sensitive experiment were obtained from solvent purification system. Air sensitive reactions were performed in the glove box ($O_2$ < 0.1 ppm and $H_2O$ < 0.1 ppm). All hydroxylamine ligands were immediately stored in side the glove box to prevent deterioration. NMR spectra were recorded using Varian-Innova 500 MHz instrument. UV-Vis spectra were recorded using Agilent 8453 spectrometer.

**$N$-(2-((2-hydroxybenzylidene)amino)ethyl)-2-nitrobenzenesulfonamide: $L^1$-NO$_2$**
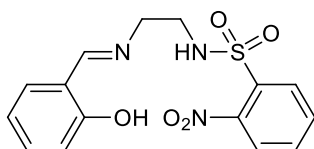


Synthesis of half ligand:

In a 250 mL round bottom flask, ethylenediamine (10 mL, 8.94 g, 148 mmol) was dissolved in 30 mL of anhydrous tetrahydrofuran (THF) and system was cooled down to 0 °C. 2-nitro-benzenesulfonyl chloride (10.98 g, 49.54 mmol) was dissolved in 50 mL of anhydrous THF and was added dropwise to ethylenediamine ($NH_2$-$CH_2$-$CH_2$-$NH_2$) solution while stirring on the ice bath. The solution was warmed to 25 °C upon finishing the addition and the mixture was further stirred for 30 minutes. Using high vacuum the reaction was condensed and an oily yellow residue remained which was then extracted with 50 mL of dichloromethane (DCM) and 50 mL of water. The organic layer was separated and the aqueous layer was further extracted with 3x 50 mL of DCM. Organic layers were mixed and dried over sodium sulfate ($Na_2SO_4$). After filtration solvents were removed under high vacuum remaining a dark yellow oily residue. 50 mL of HCl (12M) was added to this oily residue without stirring and left overnight without disturbance. White precipitation along with the yellow solution was observed. (di-substituted product precipitated as a white powder). After filtration of the mixture over frits, the filtrate was then distilled to remove the hydrochloric acid and left behind a dark brown glue-like residue.

The product was then dissolved in 50 mL of methanol and to this solution, triethylamine (6.91 mL, 5.01 g, 49.54 mmol) and salicylaldehyde (6.40 mL, 7.26 g, 56.45 mmol) were added respectively. The solution was under reflux for 1 hour and then was cooled down to 25 °C and then 0 °C. After 1hr the solution was filtered and further washed with cold methanol. The yellow crystalline solid was recovered. 13.417 g , Yield 77%. $C_{15}H_{15}N_3O_5S$.

**N-(2-((3,5-di-*tert*-butyl-2-hydroxybenzylidene)amino)ethyl)-2-nitrobenzenesulfonamide: $L^I_{tBu}$-NO₂**
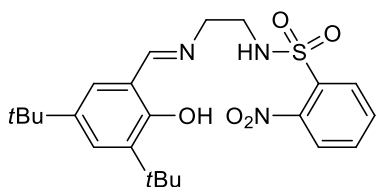


Synthesis of half ligands is similar to that of $L^I$-NO₂ in higher quantities. The half ligand was dissolved in 50 mL of methanol and to this solution, triethylamine (6.91 mL, 5.01 g, 49.54 mmol) and 3,5-Di-tert-buthylsalicyaldehyde (13. 930 g, 56.45 mmol) were added Solution was under reflux for 1 hour and then was cooled down to 25 °C and then 0 °C. After 1hr the solution was filtered and further washed with cold methanol. The bright yellow crystalline solid was recovered. 18.56 g, Yield 81%. $C_{23}H_{31}N_3O_5S$.

**N-(2-((3,5-di-*tert*-butyl-2-hydroxybenzyl)(methyl)amino)ethyl)-2-nitrobenzenesulfonamide: $L^A_{tBu}$-NO₂**
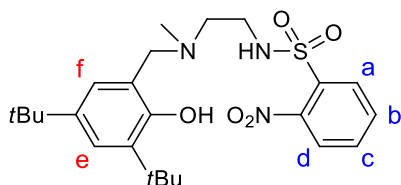


In a 250 mLround bottom flask $L^I_{tBu}$-NO₂ (5 g, 10.83 mmol, 1eq.) was dissolved in 40 mL of DCM on the ice bath. To this solution, NaBH₃CN (748.8 mg, 11.91 mmol, 1.1 eq.) was added slowly and portion-wise while stirring. After 30 minutes 40 mL of methanol was added with further stirring for 30 minutes. Acetic acid (0.681 mL, 11.91 mmol, 1.1 eq.) was then added to the reaction which was then kept for 3hrs in the ice bath, then warmed to room temperature and left stirring overnight. TLC monitoring on alumina (100% DCM) showed an unfinished reaction in this case 0.5 eq. NaBH₃CN was added and the reaction was monitored until completion. After

completion of the reaction verified by TLC, formaldehyde (37%), (487.9 mg, 0.531 mL, 16.2 mmol, 1.5 eq.) and sodium cyanoborohydride (NaBH$_3$CN) (1.02 mg, 16.2 mmol, 1.5 eq.) was added respectively. TLC monitoring after an hour showed the presence of incomplete reaction thus about 0.5 eq. of formaldehyde was added to the mixture. The reaction was complete after an hour verified by TLC (10% Hexane/DCM). Solvents were evaporated and a viscose residue remained to which DCM was added to dissolve. System cooled down on the ice bath and while stirring was added slowly-slowly Na$_2$CO$_3$ in water (10 g Na$_2$CO$_3$ in 100 mL water) with frequent testing for pH of the reaction until an indication of a neutral solution. Then the solution was further stirred for 15 minutes and a suspension of two layers was observed were the product were in the oily yellow layer. The solution was then extracted with 50 mL DCM and 50 mL water. The organic layer was saved and the aqueous layer was extracted with 3x100 mL DCM. It was dried over sodium sulfate, filtered and condensed and dried under vacuum for 48 hours. 5.175 g recovered. Yield 100%.

C$_{24}$H$_{35}$N$_3$O$_5$S, $^1$H NMR (500 MHz, acetone-d$_6$) δ 8.10 (dd, 1H, arom, **d**), 7.95 (dd, 1H, arom, **a**), 7.91 (td, 1H, arom, **b**), 7.85 (td, 1H, arom, **c**), 7.21 (d, 1H, arom, **f**), 6.89 (d, 1H, arom **e**), 3.70 (s, 2H, -C**H$_2$**-N-, linker to aromatic phenol), 3.35 (t, 2H, C**H$_2$**-NHSO$_2$, linker), 2.71 (t, 2H, -N-C**H2**-, linker), 2.29 (s, 3H, -N-C**H$_3$**), 1.38 (s, 9H, *tert*-butyl), 1.26 (s, 9H, *tert*-butyl)
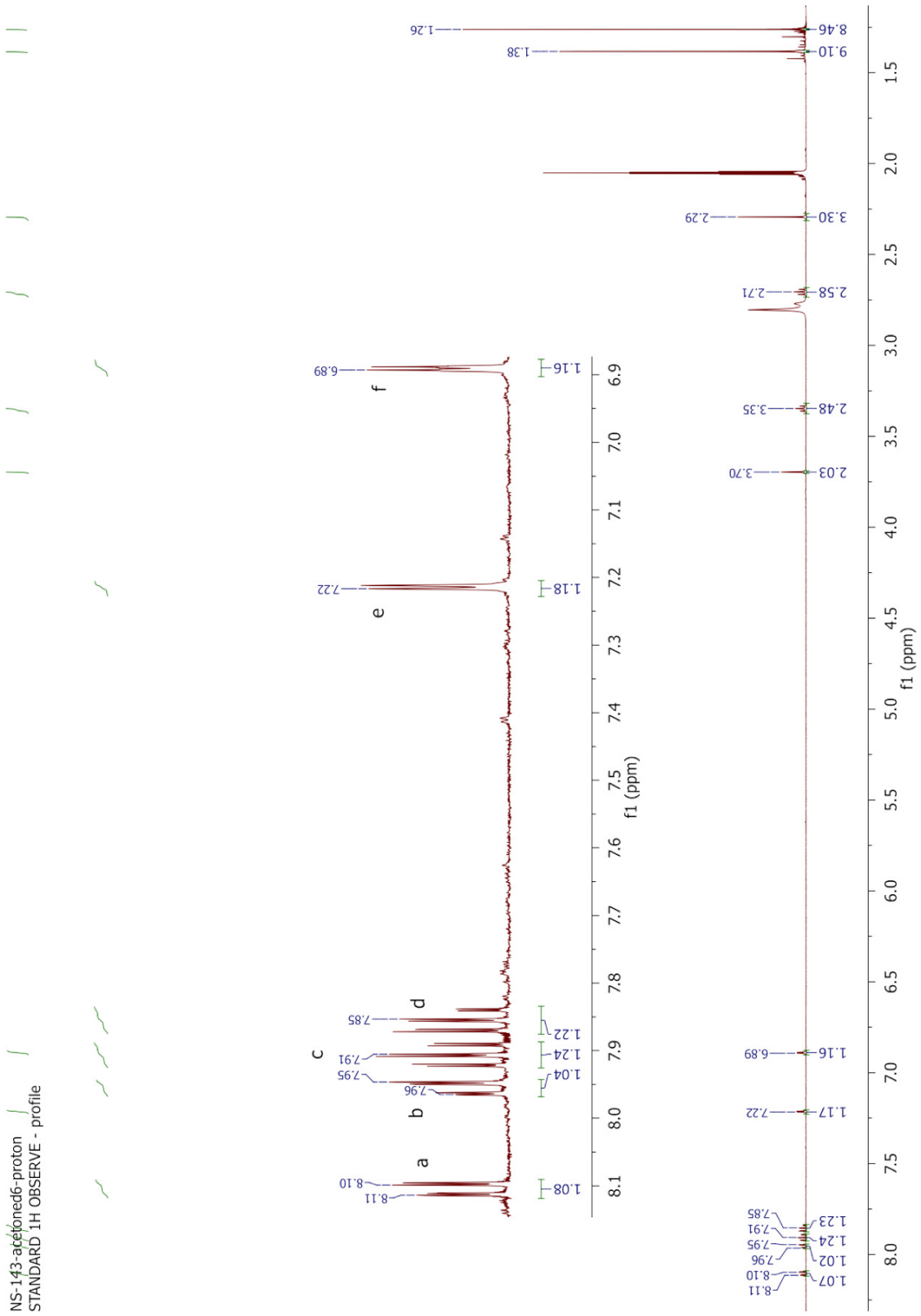
Figure 5.1. $^1$H-NMR of L$^A_{tBu}$-NO$_2$ in acetone-d$_6$

Figure 5.2. gCOSY of $L^A_{t\text{Bu}}$-$NO_2$ in acetone-$d_6$.
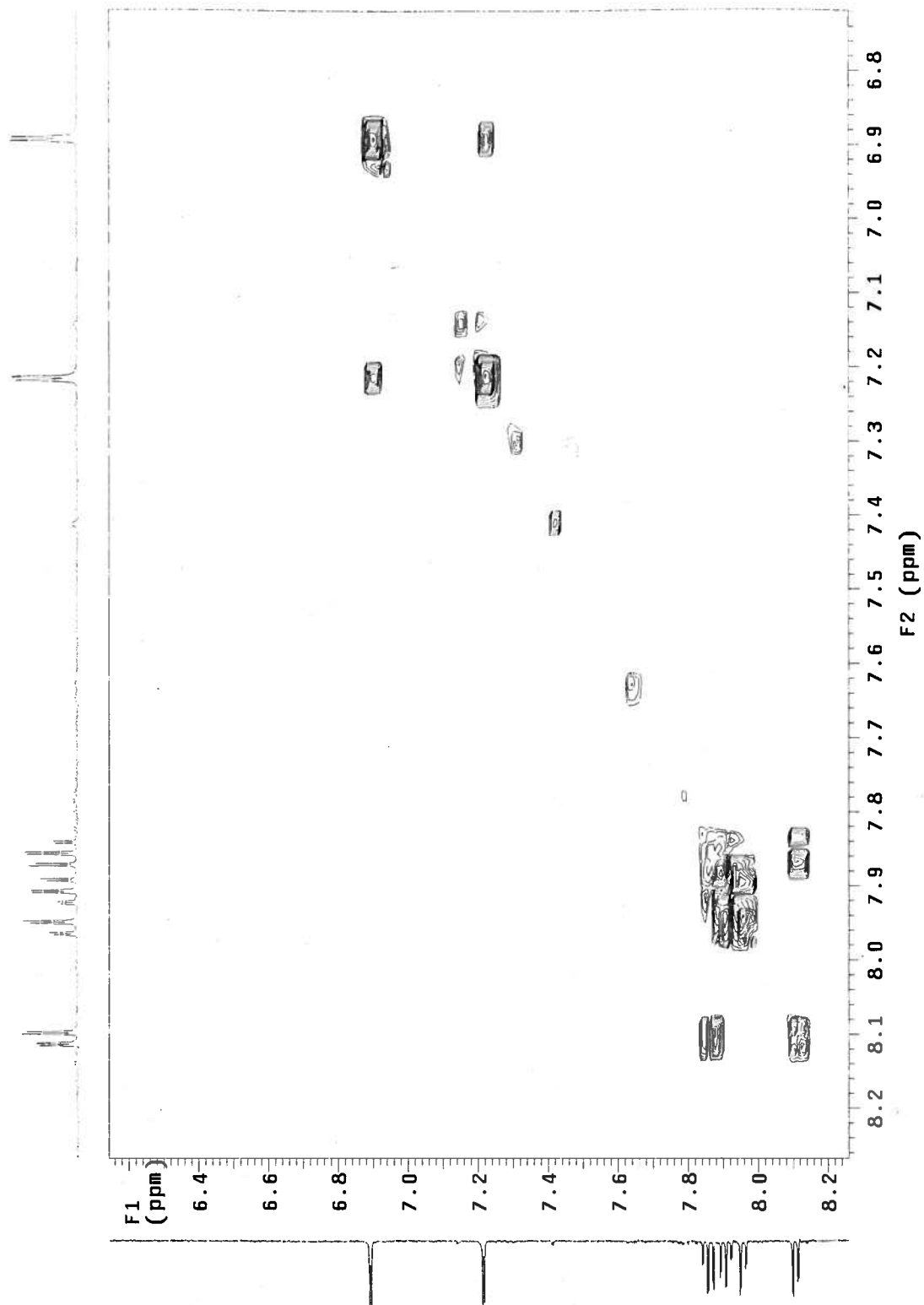
Figure 5.3. gCOSY of L$^A_{tBu}$-NO$_2$ in acetone-d$_6$. Aromatic regions are expanded for clarity.

**Optimized synthetic procedure for *N*-(2-((3,5-di-*tert*-butyl-2-hydroxybenzyl)(methyl)amino)ethyl)-2-(hydroxyamino)benzenesulfonamide: L$^A_{tBu}$-NHOH**
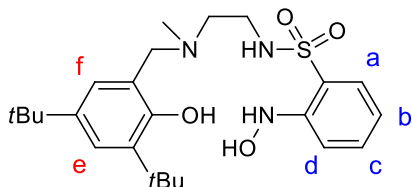


General procedure for higher quantities of **L$^A_{tBu}$-NHOH**: Ammonium formate (1.6 eq.) dissolved in methanol (3 mL) was added to a vigorously stirring solution of L$^A$-NO$_2$ (1eq.) in dichloromethane (4 mL), the solution was placed and kept on the iced bath during the course of the reaction. Initially activated zinc powder (2 eq.) was added to the solution followed by its addition in portions (0.5 eq., 8.94 mg) every 15 minutes up to the total amount of 6 equivalents. The reaction was monitored by TLC and around 4 hours there are still sign of starting material (L$^A$-NO$_2$) remained on the plate, 0.5 equivalents of zinc along with 0.5 equivalent of ammonium formate should be added and reaction should be given more time to proceed. Monitoring should be made every 15 minutes and if needed same amount should be added to the reaction mixture. After completion of the reaction it should then be immediately filtered over celite to prevent further reduction of the desired hydroxylamine ligand. The filtrate was then extracted with portions of DCM, ethylenediaminetetraacetic acid to remove subject to little if any zinc remained and water. The organic layer then combined and dried over sodium sulfate and the solvent was evaporated using a vacuum. A foam shaped yellow product recovered. It was dried under vacuum and was shortly after stored in an inert atmosphere (Glove Box) to avoid deterioration.

C$_{24}$H$_{37}$N$_3$O$_4$S, $^1$H NMR (500 MHz, acetone-d$_6$) δ 8.27 (s, 1H, O**H**), 8.01 (broad s, 1H, SO$_2$N**H**), 7.70 (dd, 1H, aromatic, **a**), 7.53 (td, 1H, aromatic, **c**), 7.47 (dd, 1H, aromatic, **d**), 7.21 (dd, 1H, aromatic, **f**), 6.95 (td, 1H, aromatic, **b**), 6.88 (d, 1H, aromatic, **e**), 6.55 (s, 1H, N**H**OH), 3.66 (s, 2H, -C**H$_2$**-N-, linker to aromatic phenol), 3.09 (t, 2H, C**H$_2$**-NHSO$_2$, linker), 2.58 (t, 2H, -N-C**H2**-, linker), 2.24 (s, 3H, -N-C**H$_3$**), 1.39 (s, 9H, *tert*-butyl), 1.26 (s, 9H, *tert*-butyl)

Figure 5.4. $^1$H-NMR of $L^A_{tBu}$-NHOH in acetone-d$_6$.
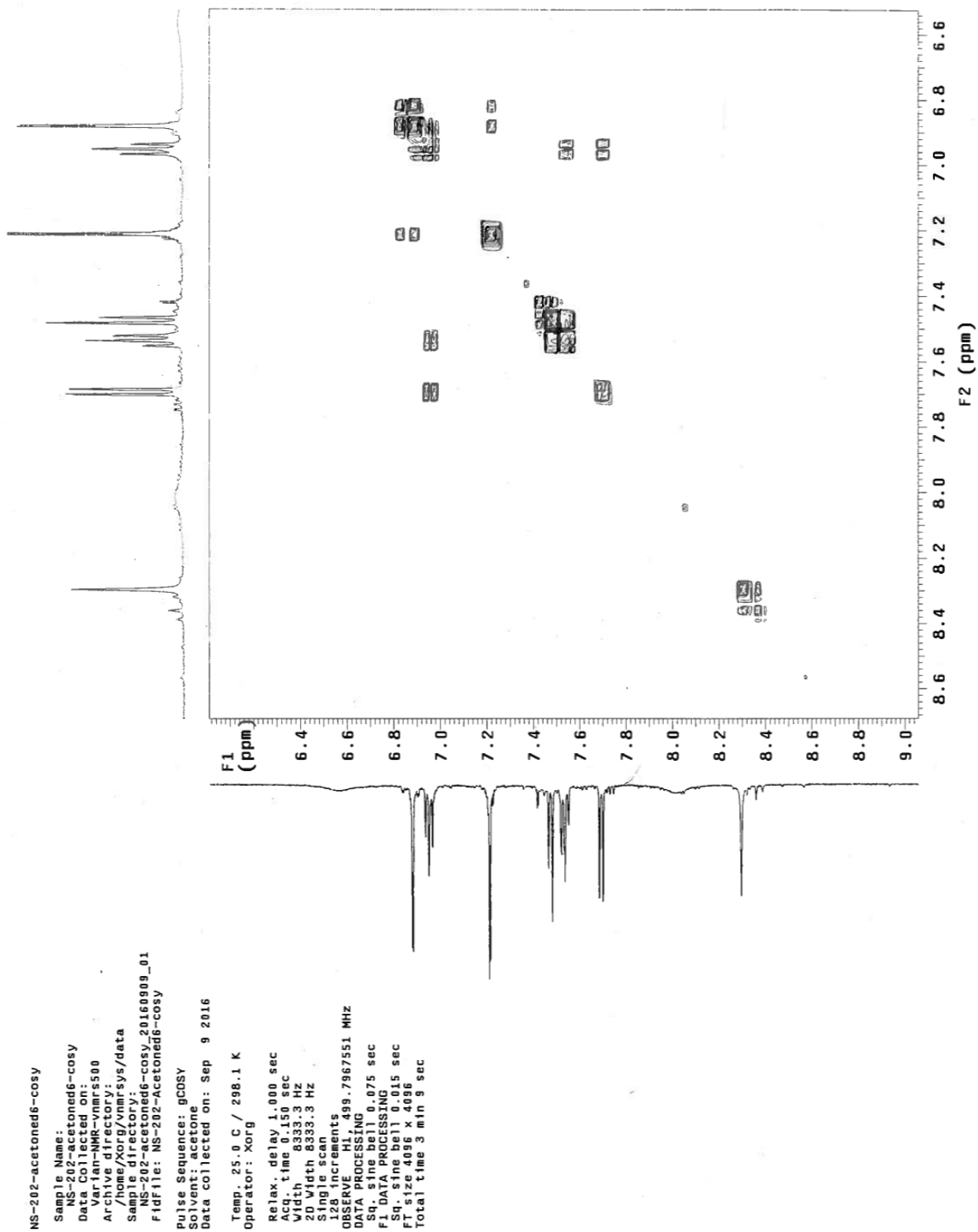
Figure 5.5. gCOSY of L$^A_{tBu}$-NHOH in acetone-d$_6$, aromatic regions.

### *N*-(2-((2-hydroxybenzyl)(methyl)amino)ethyl)-2-nitrobenzenesulfonamide: L$^A$-NO$_2$
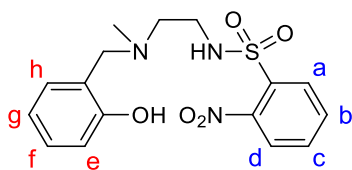


**L$^I$-NO$_2$** (1g, 2.86 mmol, 1eq.) was dissolved in methanol (least amount of methanol to dissolve the ligand). To this solution acetic acid (0.163 mL, 2.86 mmol, 1eq.), formaldehyde (37%) (0.157 mL, 5.72 mmol, 2 eq.) and sodium cyanoborohydride (449 mg, 7.15 mmol, 2.5 eq.) were added respectively. In a few minutes to an hour, pinkish-grey color precipitation observed. The reaction was stirred for 24 hours and was filtered with over frits with portions of cold methanol and ether and dried out in under vacuum overnight. 776 mg recovered. Yield 74%.

C$_{16}$H$_{19}$N$_3$O$_5$S, $^1$H NMR (500 MHz, Acetone-d$_6$) δ 8.11 (dd, 1H, arom, **d**), 7.82-7.96 (m, 3H, arom, **a, b, c**), 7.11 (td, 1H, aromatic, **f**), 6.99 (dd, 1H, arom, **h**), 6.70-6.75 (m, 1H, arom, **e** and **g**), 3.70 (s, 2H, -**CH$_2$**-N-, linker to aromatic phenol), 3.34 (t, 2H, **CH$_2$**-NHSO$_2$, linker), 2.70 (t, 2H, -N-**CH$_2$**-, linker), 2.27 (s, 3H, -N-**CH$_3$**)
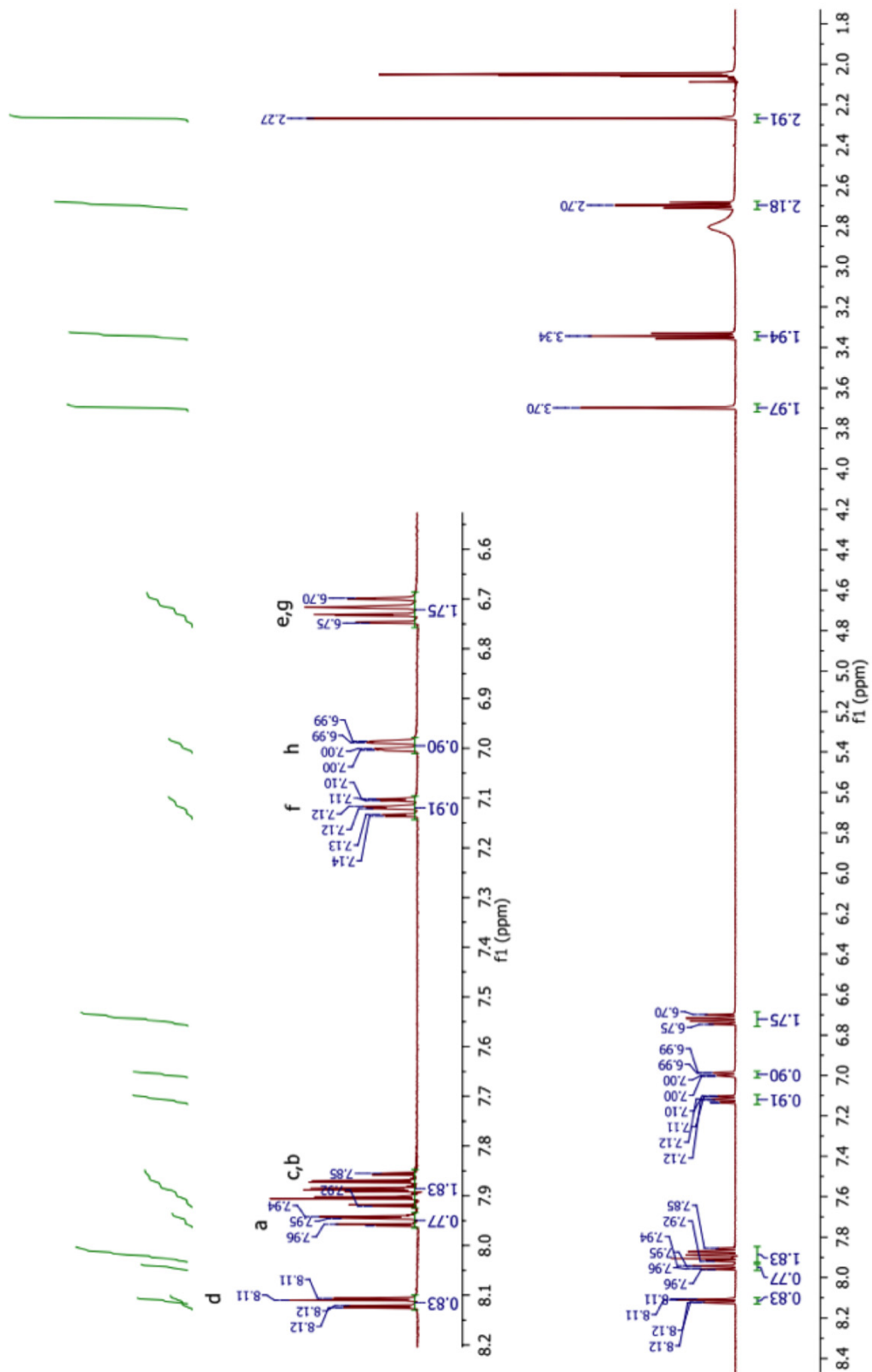
Figure 5.6. $^1$H-NMR of $L^A$-NO$_2$ in acetone-d$_6$.
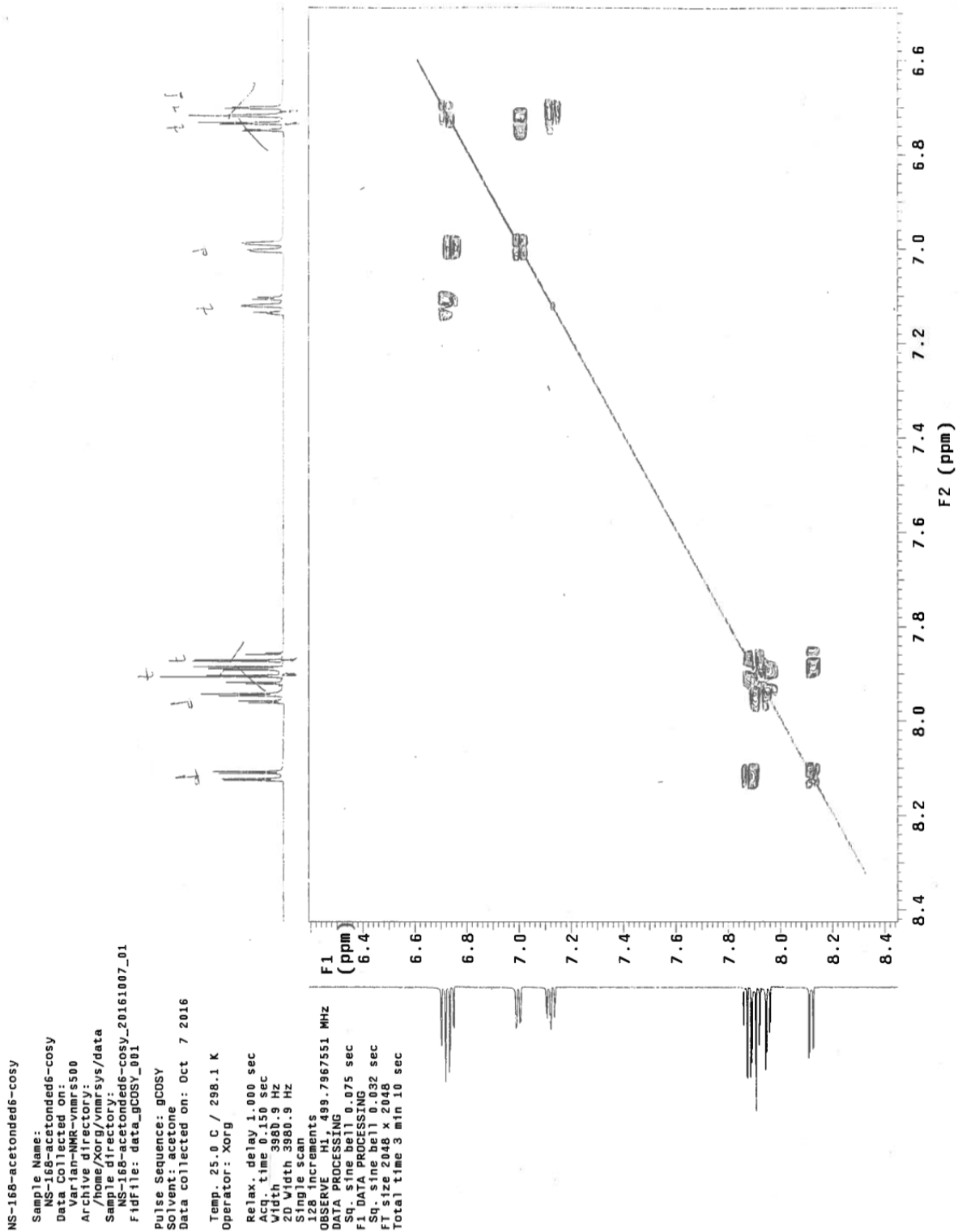
Figure 5.7. gCOSY of $L^A$-$NO_2$ in acetone-$d_6$, aromatic regions.

**Optimized synthetic procedure for 2-(hydroxyamino)-*N*-(2-((2-hydroxybenzyl)(methyl)amino)ethyl)benzenesulfonamide: L^A-NHOH**
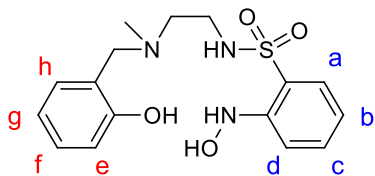


Ammonium formate (20.6 mg, 0.437 mmol, 1.6 eq.) dissolved in methanol (3 mL) was added to a vigorously stirring solution of L^A-NO$_2$ (100 mg, 0.273 mmol, 1eq.) in dichloromethane (4 mL), the solution was placed and kept on the iced bath during the course of the reaction. Initially activated zinc powder (35.89 mg, 0.547 mmol, 2 eq.) was added to the solution followed by its addition in portions (0.5 eq, 8.94 mg) every 15 minutes up to the total amount of 5 equivalents. The reaction was monitored by TLC and around 2.5 hours no sign of starting material (L^A-NO$_2$) remained on the plate. The reaction was immediately filtered over celite to prevent further reduction of the desired hydroxylamine ligand. The filtrate was then extracted with portions of DCM, ethylenediaminetetraacetic acid to remove subject to little if any zinc remained and water. The organic layer then combined and dried over sodium sulfate and the solvent was evaporated using a vacuum. A foam shaped yellow product recovered. It was dried under vacuum and was shortly after stored in an inert atmosphere (glovebox) to avoid deterioration.

C$_{16}$H$_{21}$N$_3$O$_4$S, $^1$H NMR (500 MHz, Acetone-d$_6$) δ 8.28 (sharp s, NHO**H**), 7.98 (broad s, **NH**SO$_2$), 7.70 (dd, aromatic, **a**), 7.53 (td, 1H, arom, **c**), 7.47 (dd, 1H, arom, **h**), 7.12 (t, 1H, arom, **f**), 6.95-6.99 (m, 2H, arom, **b** and **d**), 6.71-6.75 (m, 1H, arom, **e** and **g**), 3.65 (s, 2H, -C**H$_2$**-N-, linker to aromatic phenol), 3.10 (t, 2H, C**H$_2$**-NHSO$_2$, linker), 2.58 (t, 2H, -N-C**H$_2$**-, linker), 2.19 (s, 3H, -N-C**H$_3$**)

Figure 5.8. $^1$H-NMR of L$^A$-NHOH in acetone-d$_6$.
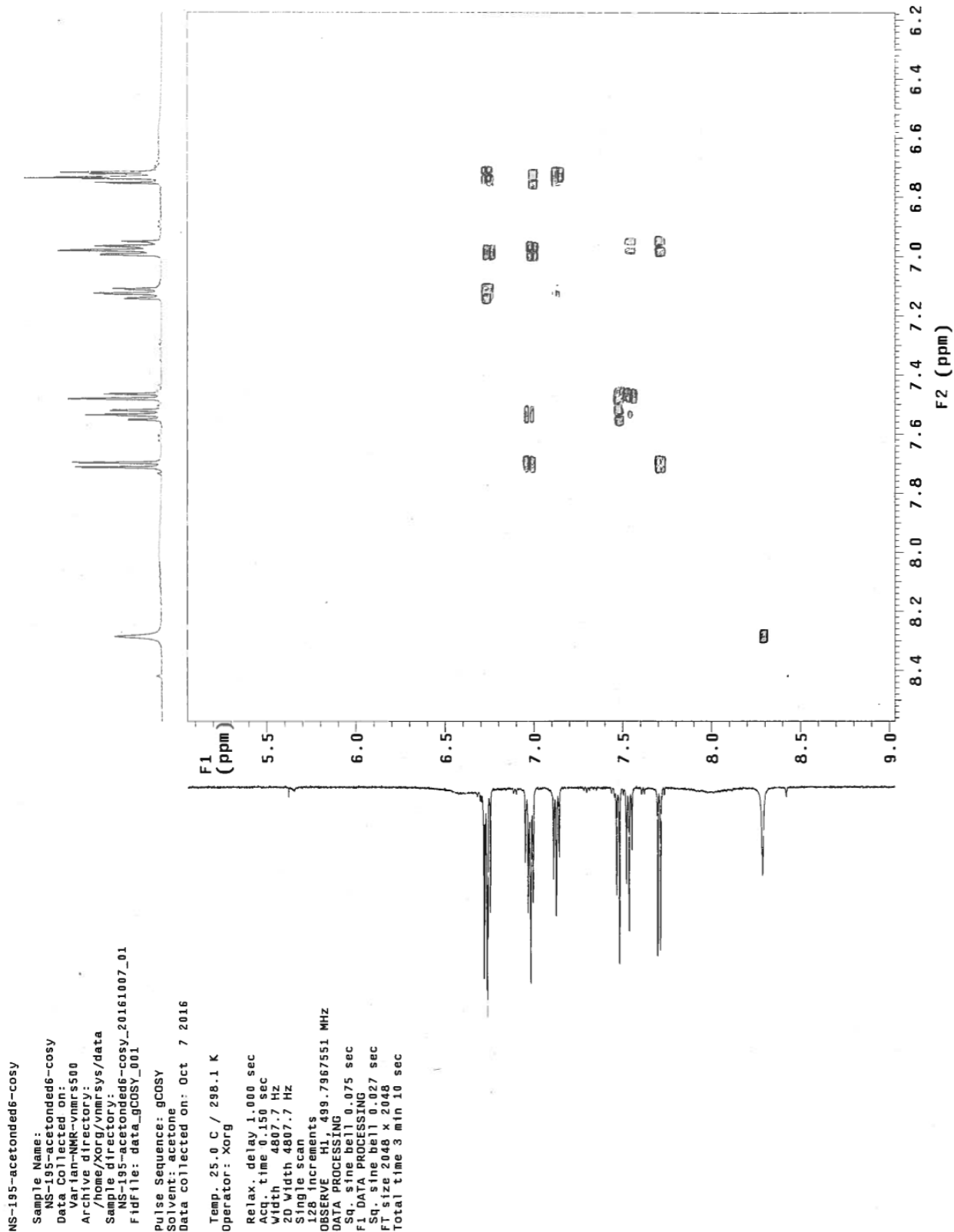
Figure 5.9. gCOSY of the L^A-NHOH in acetone-d$_6$, aromatic regions.

## 5.2 TITRATIONS

## Titration of $L^I_{tBu}$-NO$_2$ with Cu(II) in presence of base (triethylamine)

A 1mM solution of Ligand in Acetonitrile was prepared with 1eq. of the base, triethylamine, Solution was placed in the UV-Vis cuvette and titration was done by adding 0.1 mM solution of copper in acetonitrile each time (0- 4 eq. of copper: Cu(OAc)$_2$.H$_2$O), $K_f$: $4.920 \pm 0.013$.
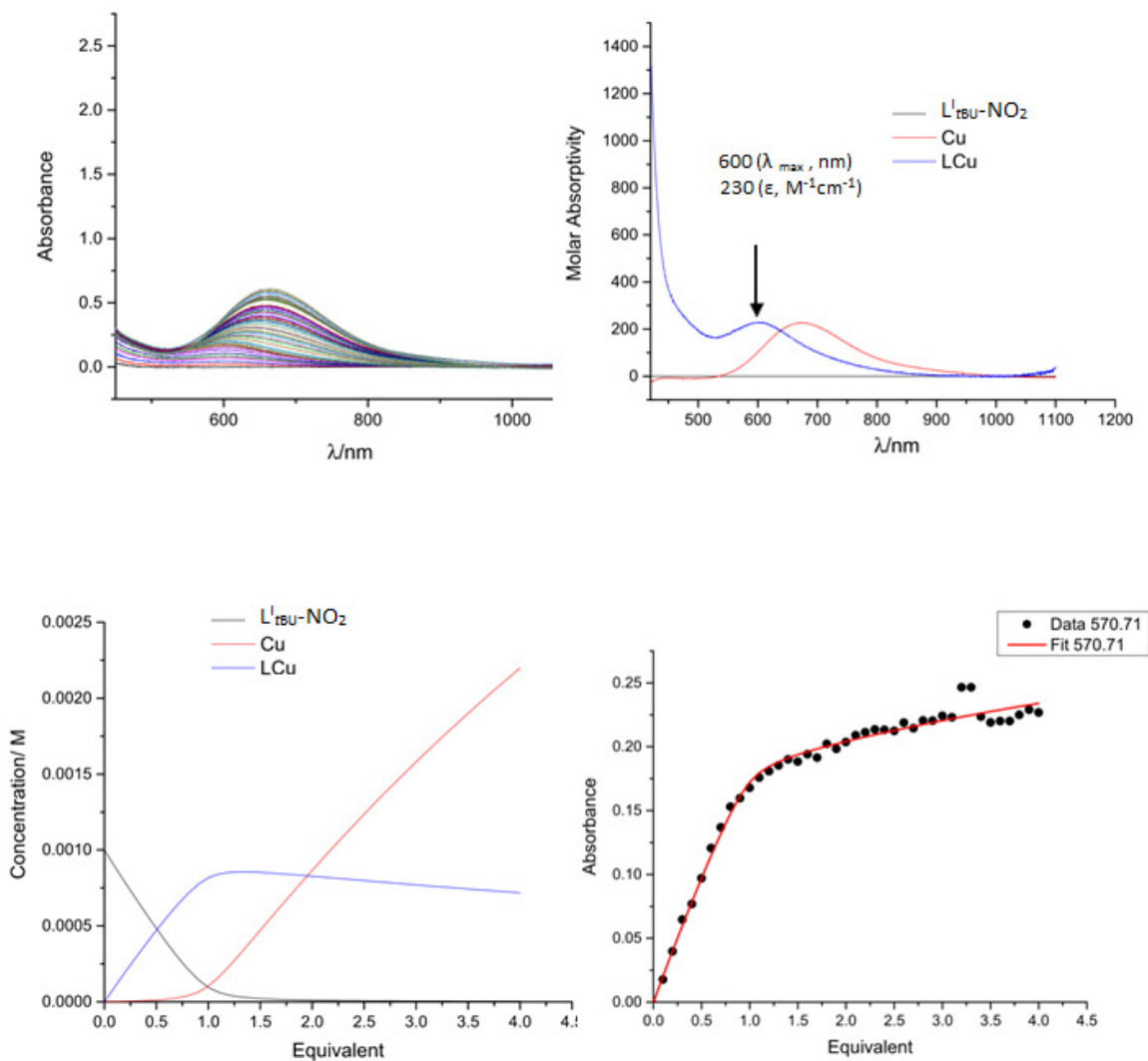


Figure 5.10. Titration of $L^I_{tBu}$-NO$_2$ in with Cu(II) source in the presence of base.

**Titration of L$^A_{tBu}$-NO$_2$ with Cu(II) in presence of base (triethylamine)**

A 1mM solution of Ligand in Acetonitrile was prepared with 1eq. of the base, triethylamine, Solution was placed in the UV-Vis cuvette and titration was done by adding 0.1 mM solution of copper in acetonitrile each time (0- 4 eq. of Copper: Cu(OAc)$_2$.H$_2$O), $K_f$: 4.916 ± 0.002.
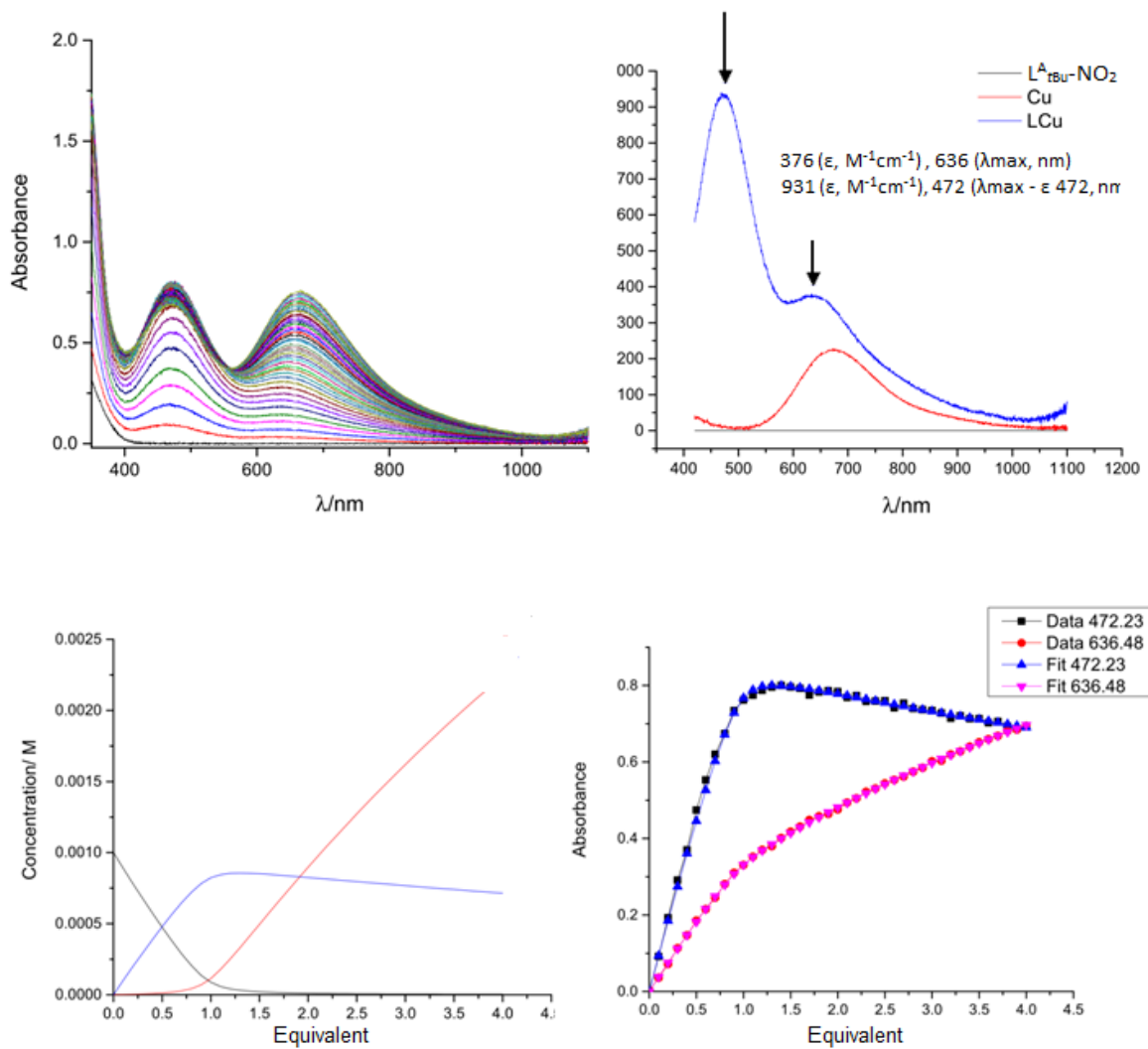


Figure 5.11. Titration of L$^A_{tBu}$-NO$_2$ with Cu(II) source in the presence of base.

### 5.3 MAGNETIC SUSCEPTIBILITY MEASUREMENTS ON LPY$_2$-NO-CU

Magnetic susceptibility is measured using NMR Evans method at room temperature (25 °C, 298.15 K) Paramagnetic susceptibility ($\chi_P$) is measured by the following formula:

$$\chi_P = \frac{1000\ \delta v}{v0\ Sf\ C} - \chi_D$$

$\delta v$: difference in the chemical shift of TMS in Hz: 0.072 ppm × 500 MHz

$v_0$: frequency of the NMR spectrometer in Hz: 500 MHz × $10^6$

$S_f$: $4\pi/3$

$C$: Sample concentration (mol L$^{-1}$): 0.03 M

$$\frac{1000 \times 0.072 \times 500}{500 \times 10^6 \times (\frac{4\pi}{3}) \times 0.03} = 5.729577 \times 10^{-4}\ \text{emu mol}^{-1}$$

Diamagnetic susceptibility ($\chi_D$) can be calculated by summing up all empirical Pascal's constants for atoms ($\chi_{Di}$) and bonds ($\lambda_i$) in the complex.[59] Using the tabulated Pascal's constants for constituent atoms, $\chi_{Di}$ was calculated as follows:

Chemical Formula: $C_{20}H_{20}CuN_5O_3S$

$\chi_D$ = 16 $\chi_D$ (C$_{ring}$) + 4 $\chi_D$ (C) + 20 $\chi_D$ (H) + 2 $\chi_D$ (N$_{ring}$) + 3 $\chi_D$ (N$_{open\text{-}chain}$) + 3 $\chi_D$ (O) + $\chi_D$ (S)
$\quad$ + $\chi_D$ (Cu$^{+2}$)
$\quad$ = [16 (-6.24) + 4 (-6) + 20 (-2.93) + 2 (-4.61) + 3 (-5.57) + 3 (-4.6) + (-15) + (-11)] x $10^{-6}$
$\quad$ = –248.17 × $10^{-6}$ emu mol$^{-1}$

Therefore:

$\chi_P$ = 5.729577 × $10^{-4}$ – ($-248.17 \times 10^{-6}$) emu mol$^{-1}$ = 8.211277 × $10^{-4}$ emu mol$^{-1}$

hence at $T$ = 298 K:

$\chi_P T$ = **0.2447 emu K mol$^{-1}$**

## 5.4 CRYSTALLOGRAPHIC DATA FOR Lpy₂-NO-Cu

|  | Lpy$_2$-NO-Cu |
|---|---|
| Empirical formula | $C_{20}H_{20}CuN_5O_3S$ |
| Formula weight | 474.01 |
| $T$ (K) | 110(2) |
| Wavelength (Å) | 1.54178 |
| Crystal system | Monoclinic |
| Space group | $P2_1/n$ |
| *Unit cell dimensions* | |
| a (Å) | 9.9812(4) |
| b (Å) | 15.7589(5) |
| c (Å) | 12.3836(4) |
| $\alpha$ (°) | 90 |
| $\beta$ (°) | 90.065(3) |
| $\gamma$ (°) | 90 |
| $V$ (Å$^3$) | 1947.85(12) |
| Z | 4 |
| $D_{calc}$ | 1.616 |
| Absorption coefficient | 2.881 |
| F(000) | 976 |
| Crystal size (mm) | 0.080x0.055x0.055 |
| $\theta$ (°) | 2.804 – 68.544 |
| Index ranges | $h = -11 – 12$ |
| | $k = -18 – 18$ |
| | $l = -14 – 14$ |
| Reflections collected | 24949 |
| Independent reflections | 3553 |
| Completeness ($\theta$) | 99.9% |
| Data/restraints/parameters | 3553/0/272 |
| Goodness of fit (GOF) on $F^2$ | 1.048 |
| Final R indices [$I > 2\sigma(I)$] (%) | $R_1 = 5.36$, $wR_2 = 14.18$ |
| R indices (all data) (%) | $R_1 = 6.35$, $wR_2 = 14.85$ |
| Largest difference in peak and hole (e Å$^{-3}$) | 0.899 and -0.815 |

## 5.5 DFT CALCULATIONS

Electronic calculations were performed with the Gaussian 09 package.[68] Geometry optimizations, starting from the crystal structure of the $Lpy_2$-NO-Cu, were performed using the B3LYP[67,68] functional with TZVP[71] basis set on all atoms and tight convergence criteria. Singlet broken symmetry calculation[72–74] was performed through single point energy minimization on the singlet structure using the triplet orbitals as initial guess. The magnetic-exchange coupling constant based on the Heisenberg–Dirac–van Vleck Hamiltonian[75–77] was evaluated using the Yamaguchi formula.[66,67]

# Chapter 6.  References

1. Atkins, P. W., Overton, T. L., Rourke, J. P., Weller, M. T. & Armstrong, F. A. *Shriver and Atkins' Inorganic Chemistry, Fifth Edition*. (W. H. Freeman and Company, 2010).

2. Miessler, G. L., Fischer, P. J. & Tarr, D. A. *Inorganic Chemistry, Fifth Edition*. (Pearson, 2014).

3. Weight, S. & Density, S. H. Nitrogen (N2) Properties , Uses and Applications Nitrogen Gas and Liquid Nitrogen. *Universal Industrial Gases, Inc.* (2016). Available at: http://www.uigi.com/nitrogen.html. (Accessed: 24th June 2016)

4. Morrell, C. & Manning, P. P. An automatic liquid-nitrogen filling system for use with solid-state X-ray detectors. *Nucl. Instruments Methods Phys. Res. Sect. A Accel. Spectrometers, Detect. Assoc. Equip.* **381,** 560–566 (1996).

5. Thiemann, M., Scheibler, E. & Wiegand, K. W. Nitric Acid , Nitrous Acid , and Nitrogen Oxides. *Ullmann's Encycl. Ind. Chem.* **24,** 177–223 (2000).

6. MacMicking, J., Xie, Q. W. & Nathan, C. Nitric oxide and macrophage function. *Annu. Rev. Immunol.* **15,** 323–50 (1997).

7. Faddy, S. C. & Garlick, S. R. A systematic review of the safety of analgesia with 50% nitrous oxide: can lay responders use analgesic gases in the prehospital setting? *Emerg. Med. J.* **22,** 901–908 (2005).

8. Shaver, M. P. & Fryzuk, M. D. Activation of Molecular Nitrogen: Coordination, Cleavage and Functionalization of N2 Mediated By Metal Complexes. *Adv. Synth. Catal.* **345,** 1061–1076 (2003).

9. Fryzuk, M. D. Activation and functionalization of molecular nitrogen by metal complexes. *Chem. Rec.* **3,** 2–11 (2003).

10. Shilov, A. E. Catalytic reduction of molecular nitrogen in solutions. *Russ. Chem. Bull.* **52,** 2555–2562 (2003).

11. Mylona, P., Pawlowski, K. & Bisseling, T. Symbiotic Nitrogen Fixation. *Plant Cell* **7,** 869–885 (1995).

12. Seefeldt, L. C., Hoffman, B. M. & Dean, D. R. Mechanism of Mo-Dependent Nitrogenase. *Annu. Rev. Biochem.* **78,** 701–722 (2009).

13.  Fryzuk, M. D. & Johnson, S. A. The continuing story of dinitrogen activation. *Coord. Chem. Rev.* **200–202,** 379–409 (2000).

14.  Hoffman, B. M., Lukoyanov, D., Dean, D. R. & Seefeldt, L. C. Nitrogenase: a draft mechanism. *Acc. Chem. Res.* **46,** 587–95 (2013).

15.  Gowenlock, B. G. & Richter-Addo, G. B. Preparations of C-nitroso compounds. *Chem. Rev.* **104,** 3315–3340 (2004).

16.  Adam, W. & Krebs, O. The Nitroso Ene Reaction: A Regioselective and Stereoselective Allylic Nitrogen Functionalization of Mechanistic Delight and Synthetic Potential. *Chem. Rev.* **103,** 4131–4146 (2003).

17.  Zuman, P. & Shah, B. Addition, Reduction, and Oxidation Reactions of Nitrosobenzene. *Chem. Rev.* **94,** 1621–1641 (1994).

18.  Gowenlock, B. G. Structure and properties of C-nitroso-compounds. *Q. Rev. Chem. Soc.* **12,** 321–340 (1958).

19.  Beaudoin, D. & Wuest, J. D. Dimerization of Aromatic C -Nitroso Compounds. *Chem. Rev.* **116,** 258–286 (2016).

20.  Blaser, H.-U. A golden Boost to an Old Reaction. *Science (80-. ).* **312,** 312–313 (2006).

21.  Momiyama, N. & Yamamoto, H. Simple synthesis of alpha-hydroxyamino carbonyl compounds: new scope of the nitroso aldol reaction. *Org. Lett.* **4,** 3579–3582 (2002).

22.  Hawkins, C. L. & Davies, M. J. Detection and characterisation of radicals in biological materials using EPR methodology. *Biochim. Biophys. Acta - Gen. Subj.* **1840,** 708–721 (2014).

23.  Lee, J., Chen, L., West, A. H. & Richter-Addo, G. B. Interactions of Organic Nitroso Compound with Metals. *Chem. Rev.* **102,** 1019–1065 (2002).

24.  Wiese, S., Kapoor, P., Williams, K. D. & Warren, T. H. Nitric Oxide Oxidatively Nitrosylates Ni (I) and Cu (I) C-Organonitroso Adducts. *J. Am. Chem. Soc.* **131,** 18105–18111 (2009).

25.  Richter-Addo, G. B. Binding of organic nitroso compounds to metalloporphyrins. *Acc. Chem. Res.* **32,** 529–536 (1999).

26.  Williams, K. D., Cardenas, A. J. P., Oliva, J. D. & Warren, T. H. Copper c-nitroso compounds: Activation of hydroxylamines and NO reactivity. *Eur. J. Inorg. Chem.* **2,** 3812–3816 (2013).

27. Shoeman, D. W. & Nagasawa, H. T. The reaction of nitroxyl (HNO) with nitrosobenzene gives cupferron (N-nitrosophenylhydroxylamine). *Nitric Oxide* **2,** 66–72 (1998).

28. Kundu, S. *et al.* Redox Non-Innocence of Nitrosobenzene at Nickel. *Angew. Chem. Int. Ed.* **55,** 10321–10325 (2016).

29. Jørgensen, K. A. & Møller, E. R. Chemistry of Molybdenaoxaziridines. A Study of Oxo(N-phen ylh ydroxylamido- O,N)(pyridine- 2,6-dicarboxylato)(hexamethylphosphortriamide)molybdenum(VI) and its Catalytic Properties. *J. Am. Chem. Soc.* **115,** 11814–11822 (1993).

30. Ho, C.-M. & Lau, T.-C. Copper-catalyzed amination of alkenes and ketones by phenylhydroxylamine. *New J. Chem.* **24,** 859–863 (2000).

31. Srivastava, R. S. & Nicholas, K. M. On the Mechanism of Allylic Amination Catalyzed by Iron Salts. *J. Am. Chem. Soc.* **119,** 3302–3310 (1997).

32. Johannsen, M. & Jørgensen, K. A. Mechanistic Aspects of Iron-Catalyzed Allylic Amination. *J. Org. Chem.* **60,** 5979–5982 (1995).

33. Srivastava, R. S., Khan, M. A. & Nicholas, K. M. Nitrosoarene-Cu(I) Complexes are Intermediates in Copper-Catalyzed Allylic Amination. *J. Am. Chem. Soc.* **127,** 7278–7279 (2005).

34. Srivastava, R. S., Tarver, N. R. & Nicholas, K. M. Mechanistic Studies of Copper (I)-Catalyzed Allylic Amination. *J. Am. Chem. Soc.* **129,** 15250–15258 (2007).

35. Cenini, S., Ragaini, F., Tollari, S. & Paone, D. Allylic amination of cyclohexene catalyzed by ruthenium complexes. A new reaction involving an intermolecular C-H functionalization. *J. Am. Chem. Soc.* **118,** 11964–11965 (1996).

36. Srivastava, R. S. & Nicholas, K. M. Iron-catalyzed Allylic Amination by Nitroorganics. *Chem. Commun.* 2705–2706 (1998).

37. Kolel-Veetil, M. K., Khan, M. A. & Nicholas, K. M. A Cyclic Carbamoyl Complex Is a Resting State in Allylic Aminations Catalyzed by [Cp*Fe(CO)2]2. *Organometallics* **19,** 3754–3756 (2000).

38. Askari, M. S., Orio, M. & Ottenwaelder, X. Controlled nitrene transfer from a tyrosinase-like arylnitroso–copper complex. *Chem. Commun.* **51,** 11206–11209 (2015).

39. Corma, A., Concepción, P. & Serna, P. A different Reaction Pathway for the Reduction of Aromatic Nitro Compounds on Gold Catalysts. *Angew. Chemie - Int. Ed.* **46,** 7266–7269

(2007).

40. Siegrist, U., Baumeister, P., Blaser, H.-U. & Studer, M. *The Selective Hydrogenation of Functionalized Nitroarenes: New Catalytic Systems*. *Catalysis of Organic Reactions* (MARCEL DEEKER, INC., 1998).

41. Smith, M. B. *Organic Synthesis, Second Edition*. (Mc Graw Hill, 2002).

42. Dorda, G. *et al.* Chemoselective Hydrogenation of Nitro Compounds with Supported Gold Catalysts. *Science (80-. )*. **313,** 332–334 (2006).

43. Channe Gowda, D., Mahesh, B. & Gowda, S. Zinc-catalyzed ammonium formate reductions: Rapid and selective reduction of aliphatic and aromatic nitro compounds. *Indian J. Chem. - Sect. B Org. Med. Chem.* **40,** 75–77 (2001).

44. Tsukinoki, T. & Tsuzuki, H. Organic reaction in water. Part 5.1 Novel synthesis of anilines by zinc metal-mediated chemoselective reduction of nitroarenes. *Green Chem.* **3,** 37–38 (2001).

45. Rong, Z., Du, W., Wang, Y. & Lu, L. Carbon supported Pt colloid as effective catalyst for selective hydrogenation of nitroarenes to arylhydroxylamines. *Chem. Commun. (Camb).* **46,** 1559–61 (2010).

46. Takenaka, Y., Kiyosu, T., Choi, J. C., Sakakura, T. & Yasuda, H. Selective Synthesis of N-Alkyl Hydroxylamines by Hydrogenation of Nitroalkanes using Supported Palladium Catalysts. *ChemSusChem* **3,** 1166–1168 (2010).

47. Kamm, O. β-PHENYLHYDROXYLAMINE. *Org. Synth.* **4,** 57 (1925).

48. Liu, S., Wang, Y., Yang, X. & Jiang, J. Selective reduction of nitroarenes to N-arylhydroxylamines by use of Zn in a CO2-H2O system, promoted by ultrasound. *Res. Chem. Intermed.* **38,** 2471–2478 (2012).

49. Ung, S., Falguires, A., Guy, A. & Ferroud, C. Ultrasonically activated reduction of substituted nitrobenzenes to corresponding N-arylhydroxylamines. *Tetrahedron Lett.* **46,** 5913–5917 (2005).

50. Yanada, K., Yamaguchi, H., Meguri, H. & Uchida, S. Selenium-catalysed Reduction of Aromatic Nitro Compounds to N-Aryl h ydroxylamines. *J. Chem. Soc., Chem. Commun.* 1655–1656 (1986).

51. Synthesis of N-Arylhydroxylamines by Tellurium-Catalyzed Reduction of Aromatic Nitro Compounds. *Chem. Lett.* **15,** 1069–1070 (1986).

52. Takenaka, Y., Kiyosu, T., Choi, J. C., Sakakura, T. & Yasuda, H. Selective synthesis of N-Aryl hydroxylamines by hydrogenation of nitroalkanes using supported platinum catalysts. *Green Chem.* **11,** 1385–1390 (2009).

53. Lim, D. H. *et al.* Binary-surfactant (Brij 35 + Tween 20) assisted preparation of highly dispersed Pt nanoparticles on carbon. *J. Nanoparticle Res.* **10,** 1215–1220 (2008).

54. Butsch, K. *et al.* Redox chemistry of copper complexes with various salen type ligands. *Inorganica Chim. Acta.* **394,** 237–246 (2013).

55. Venkataramanan, N. S., Kuppuraj, G. & Rajagopal, S. Metal-salen complexes as efficient catalysts for the oxygenation of heteroatom containing organic compounds - Synthetic and mechanistic aspects. *Coord. Chem. Rev.* **249,** 1249–1268 (2005).

56. Jacobsen, E. N., Zhang, W., Muci, A. R., Ecker, J. R. & Deng, L. Highly enantioselective epoxidation catalysts derived from 1,2-diaminocyclohexane. *J. Am. Chem. Soc.* **113,** 7063–7064 (1991).

57. Jacobsen, E. N., Zhang, W. & Guler, M. L. Electronic tuning of asymmetric catalysts. *J. Am. Chem. Soc.* **113,** 6703–6704 (1991).

58. Chen, F., Askari, M. S. & Ottenwaelder, X. Synthesis of a sulfonamide-Schiff base ligand and its Cu(II), Fe(III) and Co(III) complexes. *Inorganica Chim. Acta* **407,** 25–30 (2013).

59. Bain, G. A. & Berry, J. F. Diamagnetic Corrections and Pascal ' s Constants. *J. Chem. Educ.* **85,** 532–536 (2008).

60. Mulay, L. N. *Magnetic Susceptibility*. **4,** (John Wiley and sons, INC., 1963).

61. Cohen, I. A. & Ostfeld, D. A Cautionary Note on the Use of the Evans Method for Magnetic Measurements. *J. Chem. Educ.* **49,** 829 (1972).

62. Piguet, C. Paramagnetic Susceptibility by NMR : The ' Solvent Correction ' Removed for Large Paramagnetic Molecules. *J. Chem. Educ.* **74,** 815–816 (1997).

63. Ralph, K. & Florida, W. Utilizing the Evans Method with a Superconducting NMR Spectrometer in the Undergraduate Laboratory. *J. Chem. Educ.* **69,** 62 (1992).

64. Among, I., Determines, S., Type, T. H. E. & Magnetism, O. F. MAGNETISM — A Few Basics. Available at: http://gr.xjtu.edu.cn/c/document_library/get_file?folderId=2064504&name=DLFE-39605.pdf. (Accessed: 11th November 2017)

65. Verma, P., Weir, J., Mirica, L. & Stack, T. D. P. Tale of a Twist : Magnetic and Optical

Switching in Copper ( II ) Semiquinone Complexes. *inorg. Chem.* **50,** 9816–9825 (2011).

66. Yamaguchi, K., Takahara, Y. & Fueno, T. Ab-Initio Molecular Orbital Studies of Structure and Reactivity of Transition Metal-OXO Compounds. *Appl. Quantum Chem.* **Smith, V.,** 155–184 (1986).

67. Soda, T. *et al.* Ab initio computations of effective exchange integrals for H–H, H–He–H and Mn2O2 complex: comparison of broken-symmetry approaches. *Chem. Phys. Lett.* **319,** 223–230 (2000).

68. Frisch, M. J. *et al.* Gaussian 09, Revision B.01. *Gaussian, Inc. Wallingford CT* (2010).

69. Becke, A. D. A new mixing of Hartree–Fock and local density-functional theories. *J. Chem. Phys.* **98,** 1372–1377 (1993).

70. Lee, C., Yang, W. & Parr, R. G. Development of the Colle-Salvetti correlation-energy formula into a functional of the electron density. *Phys. Rev. B Condens. Matter Mater. Phys.* **37,** 785–789 (1988).

71. Schafer, A., Huber, C. & Ahlrichs, R. Fully optimized contracted Gaussian basis sets of triple zeta valence quality for atoms Li to Kr. *J. Chem. Phys* **100,** 5829–5835 (1994).

72. Noodleman, L. Valence bond description of antiferromagnetic coupling in transition metal dimers. *J. Chem. Phys.* **74,** 5737–5743 (1981).

73. Noodleman, L. & Davidson, E. R. Ligand spin polarization and antiferromagnetic coupling in transition metal dimers. *Chem. Phys.* **109,** 131–143 (1986).

74. Noodleman, L. & Case, D. A. Density-Functional Theory of Spin Polarization and Spin Coupling in Iron — Sulfur Clusters. *Adv. Inorg. Chem.* **38,** 423–470 (1992).

75. Heisenberg, W. Mehrkörperproblem und Resonanz in der Quantenmechanik. *Z. Phys.* **38,** 411–426 (1926).

76. Heisenberg, W. Zur Theorie des Ferromagnetismus. *Z. Phys.* **49,** 619–636 (1928).

77. Van Vleck, J. H. *The Theory of Electronic and Magnetic Susceptibilities . Oxford University: London, 1932.* (Oxford University: London, 1932).